Durham E-Theses

Identification of excited states in conjugated polymers

Hartwell, Lewis John

IDENTIFICATION OF EXCITED STATES IN CONJUGATED POLYMERS

Lewis John Hartwell, submitted for degree of PhD, 2002

ABSTRACT

This thesis reports quasi steady state photoinduced absorption measurements from three conjugated polymers: polypyridine (PPy), polyfluorene (PFO) and the emeraldine base (EB) form of polyaniline. The aim of these experiments was to determine the nature of the photoexcited states existing in these materials in the millisecond time domain, as this has important consequences for the operation of real devices manufactured using these materials. The results from the photoinduced absorption experiments are closely compared with published results from pulse radiolysis experiments. In all cases there is very good correspondence between the two data sets, which has enabled the photoexcited states to be assigned with a high degree of confidence.

Quasi steady-state photoinduced absorption involves the measurement of the change in absorption of a material in response to optical excitation with a laser beam. The changes in absorption are small, so a dedicated instrument was developed and optimised for each different sample. Lock-in techniques were used to recover the small signals from the samples. The samples involved were thin films of the polymer spin coated onto sapphire substrates in the cases of PPy and EB. Solution state experiments were conducted on EB. The experiments on PFO were conducted on aligned and unaligned thin films provided by Sony. In the case of the aligned PFO samples, the photoinduced absorption spectrometer was modified to enable polarisation-sensitive data collection.

In PPy, both triplet excitons and polarons have been shown to be long-lived photoexcitations, with photoinduced absorption features at 2.29 eV (triplet exciton transition), 1.5 eV and 0.8 eV (polaron transitions). In PFO, the one observed photoinduced band at 1.52 eV is assigned to a triplet exciton. Two photoinduced absorption bands are observed in EB, at 1.4 eV and 0.8 eV. These are assigned to a self-trapped CT singlet exciton and triplet exciton, respectively.

IDENTIFICATION OF EXCITED STATES IN
CONJUGATED POLYMERS

By

Lewis John Hartwell

A thesis submitted to the Faculty of Science, Durham University, for the degree of
Doctor of Philosophy.

Department of Physics,
University of Durham,
September 2002

1 8 JUN 2003

TABLE OF CONTENTS

DECLARATION

Except where specific reference is made, all material in this dissertation is the result of my own work. This dissertation has not be submitted in whole or in part for the award of a higher degree at this or any other university.

ACKNOWLEDGEMENTS

Chapter 1. Introduction

This thesis is about conjugated polymers, which are a class of materials with combine the flexibility, processibility and low density of conventional, everyday plastics (saturated polymers) with the ability to emit light and conduct electricity more like inorganic semiconductors or metals. This unusual behaviour is both interesting in itself (in terms of the new physics it exposes) and because of the novel applications that such materials can be put to. The work presented here is principally concerned with the elucidation of the photophysics behind the behaviour of three different types of conjugated polymer and not of the application of such materials into real devices. However reference to real world uses will be given along the way.

1.1. Material Applications

Perhaps the most likely candidate for commercial exploitation of these conjugated polymers comes in the area of light emitting devices. Electroluminescence from a conjugated polymer was first reported in 1990 from a device using thin films of PPV[2]. At the present time, a number of different light emitting polymers are available, and commercial interest is leading to the production of a new generation of displays based upon polymer light emitting diodes (PLED)[3,4,5].

The commercial advantages of PLEDs over conventional inorganic LED systems are easily enumerated. The principle driving factor for this commercial interest is the fact that semiconducting polymers are easy to process, and can be processed from solution, often at room temperature, and patterns can be formed by printing, and not lithography. By contrast inorganic semiconductor production involves large and complex fabrication plants that require extremes of heat and pressure and many processing steps to produce a device that's only capable of generating a point source of light. Additionally, semiconductor devices are built from layers of different materials and polymers are not particularly sensitive to the preparation of these interfaces. By contrast, interface surfaces between inorganic semiconductors must be absolutely regular and lattice matched at the atomic level. Ruptured bonds at the surfaces of inorganic LEDs can have non-bonding orbitals that will prevent the device from working. By contrast the covalent bonds within polymer materials only occur along each molecule, and building up a PLED is simply a matter of adding layer after layer.

2

Finally, by changing the emissive conjugated polymer, and/or by adding side groups to existing materials the emissive wavelength of the device can be tuned.

It should be noted that PLEDs are not going to replace inorganic LEDs in all circumstances. Their emission is relatively broad, and so absolutely pure colours may not be achievable from PLEDs. This is not a problem in display technology, where the conjugated polymers inside the photoreceptors in our eyes have similar broad acceptance ranges.

1.2. Physics, photophysics and photoinduced absorption

The difference in behaviour between saturated and conjugated polymers is due to a difference in their bonding arrangements. Carbon atoms in saturated polymers are attached to four other atoms by σ bonds. These σ bonds are strong, requiring large amounts of energy to excite to an antibonding (σ^*) state. Such an excitation will generally disrupt the polymer chain since the carbon-carbon σ bonding states are all that holds the chain together. Carbon atoms in conjugated polymers are attached to three other atoms by three σ bonds and a delocalised entity known as a π bond between adjacent carbons (in addition to the σ bond). The π bonds, spread over a larger volume of space, require much less energy to excite to the antibonding π^* state than the σ bond. Importantly, when the π bond state is excited to π^* the σ bond polymer backbone remains in place. Thus energy can be stored or captured on the chain without destroying the polymer. Examples of conjugated polymers are given in Figure 1.

Polyacetylene $(CH)_x$

Polypyrrole (PPy)

Polyparaphenylene (PPP)

Polyparaphenylene vinylene (PPV)
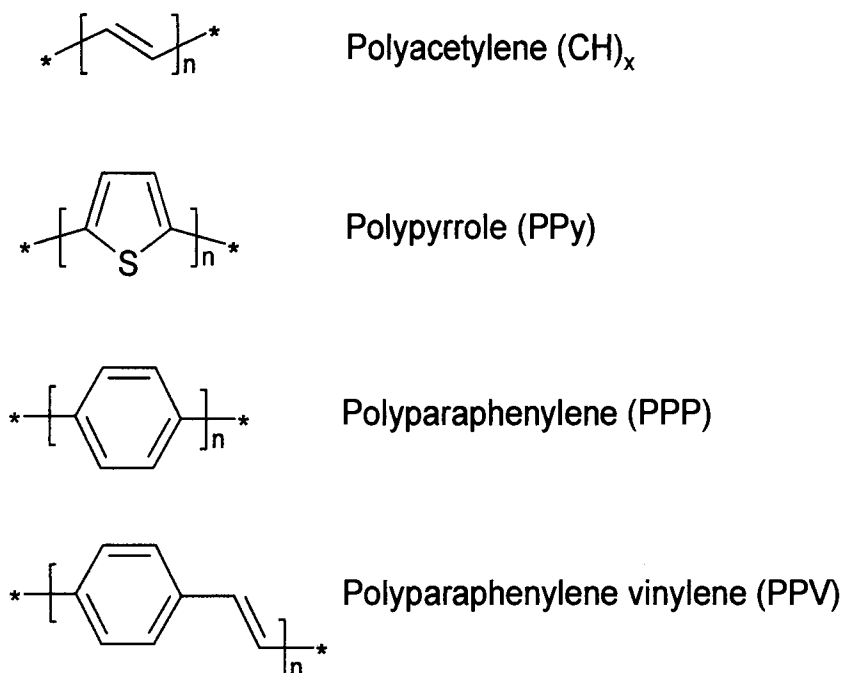
Figure 1. Some conjugated polymers.

Doping

The introduction of charges (doping) into the polymer bands allows for radiative recombination of oppositely charged pairs across the band gap (photoluminescence and phosphorescence) and/or metallic levels of charge transport at sufficiently high doping levels. There are a variety of doping methods, all of which are generally concerned with introducing electronic charge onto the polymer chains. Of particular concern within this work is photodoping; the response of the system to photoexcitation.

Excited states

The photophysics of the polymer excited states is complex, with different excited state species existing at different lifetimes. It is important to understand the excited states of these polymeric materials because only by doing so can we exploit their optical, electronic and physical properties successfully. For example, singlet and triplet excitons are formed on capture of an electron and hole within the interface region of a PLED[6]. The weakly-emissive triplet states limit the quantum efficiency of the device:

in this way it's important to characterise the photophysical response of the polymers so that these triplet states can be identified.

Photoinduced absorption

Some of the excited states that are created on a polymer chain because of doping have new electronic transitions associated with them. These transitions can be detected as new absorption bands using the experimental technique of absorption spectroscopy. The fractional change in transmission caused by the new absorption bands is often of the order of 1 part in $1,000^7$ to 1 part in $1,000,000^8$. Such a change is very difficult to detect experimentally. Photoinduced absorption uses an intense laser beam to excite (photo-dope) the sample. One advantage of using photo-excitation is simply that the doping can be switched on and off rapidly allowing the doped and undoped transmission to be compared. The photoinduced absorption (PIA) bands can then be identified despite the small change in transmission. PIA can identify these new absorption bands and determine the nature and kinetics of the excited state. This information is of vital interest for device applications.

1.3. Thesis Organisation

Chapter 2 describes the nature of bonding in conjugated polymers in more detail, together with the theoretical models that have been developed to explain the behaviour of these systems, including the long-lived excited states that can be detected using the quasi steady-state experimental techniques used in this work that are described in Chapter 3. Chapter 4 is the first of the experimental chapters concerning a luminescent material called poly-p-pyridine. Quasi steady state photoinduced absorption results are presented for this material, together with results from experiments such as Pulse Radiolysis to yield the first comprehensive analysis of the photophysics. Chapter Chapter 5 concerns polyfluorene, which is an efficient luminescent material that has liquid crystalline properties that make it easily processible into aligned films, giving a polarised emission source. Polarisation dependent photoinduced absorption measurements were made on aligned samples of polyfluorene. Chapter 5 introduces a

model to analyse the polarised data. Chapter 6 then investigates one of the forms of polyaniline. Chapter 7 draws general conclusions from the rest of the work.

Chapter 2. Theoretical Principles

2.1. Introduction

This chapter will give a brief introduction to some of the established principles of conjugated polymers that are of relevance to this work. Section 2.2 discusses the nature of conjugated polymers. Based upon this understanding a description of the general absorption, luminescence and phosphorescent properties is developed in section 2.3. It is then necessary to consider the nature of the primary photo-excitations in conjugated polymers, and the models are discussed in section 2.4. The experimental techniques used in this research reveals information about the steady state populations of these excited states. It's therefore important to have a knowledge of the various dynamic mechanisms that can change these populations, and this is covered in sections 2.5 and 2.6.

2.2. Bonding in Conjugated Polymers

Polymers are basically chains built up from many repeats of the same sub-structure (or monomer). Carbon atoms – by definition the main constituent of these organic polymers – can form bonds to other atoms in different ways. Carbon has 4 valence electrons to form electronic bonds with. The orbitals of these electrons can hybridise in different ways leading to the sp^3, sp^2 and sp bonding configurations, as shown in Figure 2.

An important structural difference between conjugated polymers and saturated polymers allows the former to have interesting electronic properties. In a saturated polymer, all of the carbon bonding electrons will be in a sp^3-hybridised state. These bonding orbitals are relatively confined in space and are arranged in a tetrahedral pattern, as shown in Figure 2. The sp^3 bonding orbitals lead to the formation of four σ bonds between the carbon atoms and other atoms in the polymer chain. The polymer is then known as "saturated" because all 4 bonding electrons in every carbon atom are used to form a separate bond to another atom.
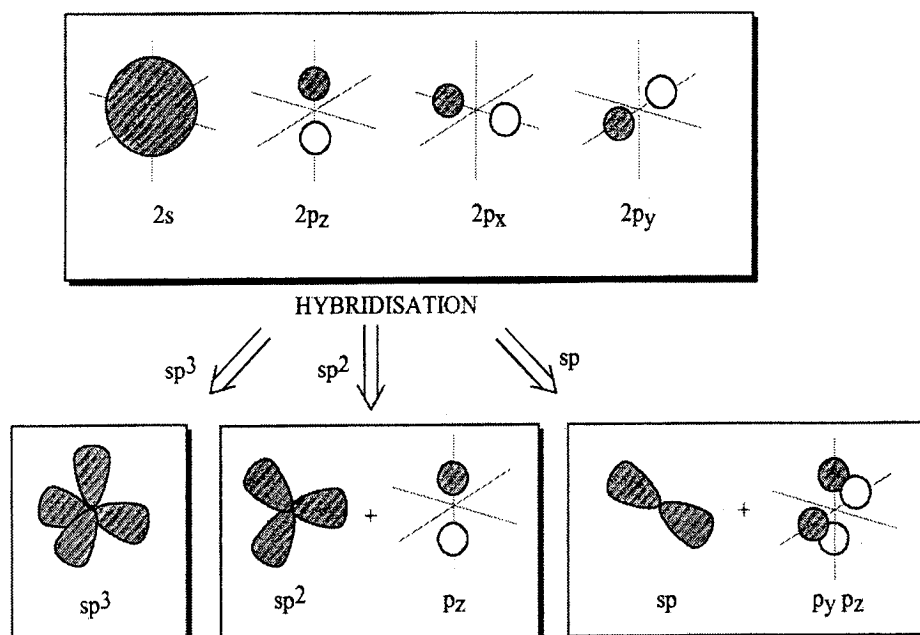
Figure 2. Hybridisation states of the carbon atom[9]

In a conjugated polymer, the carbon bonding electrons can be described as sp^2p_z: each carbon has three valence electrons in the sp^2-hybrid configuration and one in the p_z configuration. Electrons in the sp^2-hybridised state lead to the formation of three σ bonds, arranged at 120° intervals in a plane. The remaining p_z orbital projects out of the plane of the σ bonds.

The three sp^2 hybrid orbitals (three σ bonds) on each carbon join to other atoms; in the case of ethylene (Figure 3) one σ bond joins the other carbon (C-C bond) and two σ bonds join the carbon to hydrogen atoms (C-H bonds). The remaining carbon electron resides in a p_z state that is more spatially extended than the sp^2 hybrid orbitals. These spatially extended p_z states on adjacent carbons can overlap, forming a weaker C-C bond known as a π bond as shown in Figure 3. This π bond allows the conjugated material to absorb energy through the bonding π state to the antibonding π^* state. The carbon-carbon σ bond backbone remains intact in such an excitation process, allowing the polymer to store energy – and thus be optically and electronically active – without being degraded. Such energy storage is not possible in saturated polymers since energy storage through excitation from bonding σ to antibonding σ^* will degrade the polymer.

sp^2 hybrid σ bond

p$_z$ orbital

π bond formed from p$_z$ orbital overlap

C $=$ C   Usually drawn as this
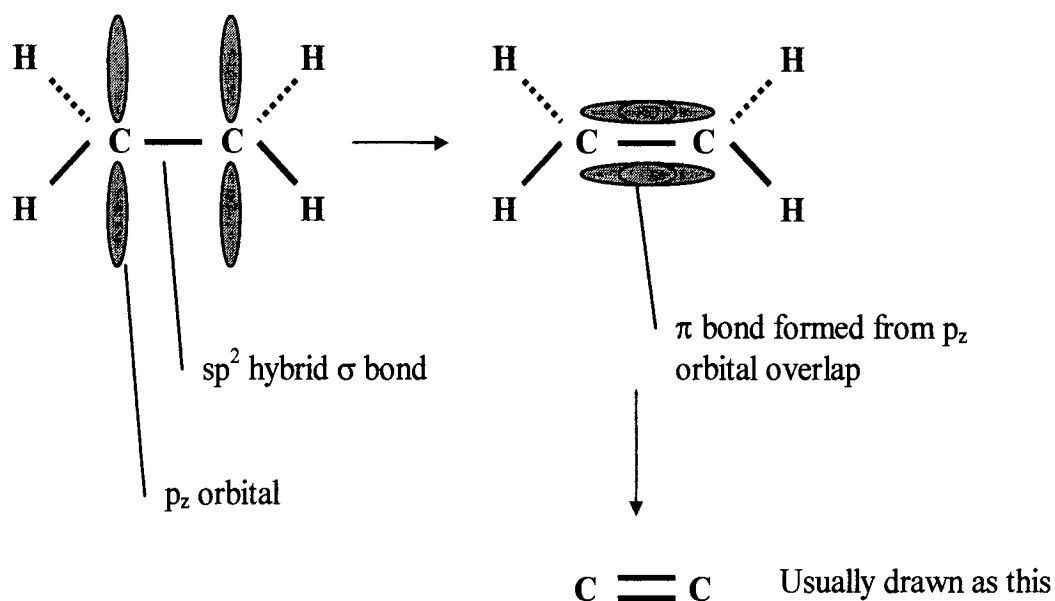
Figure 3. Formation of carbon-carbon bond structure in a simple molecule (ethylene).

In the case of ethylene there is a carbon double bond formed from one σ bond and one π bond. In longer chains of carbon atoms an alternating double and single bond structure is formed, as shown in Figure 4 for the simplest conjugated polymer, *trans -* polyacetylene (PA).
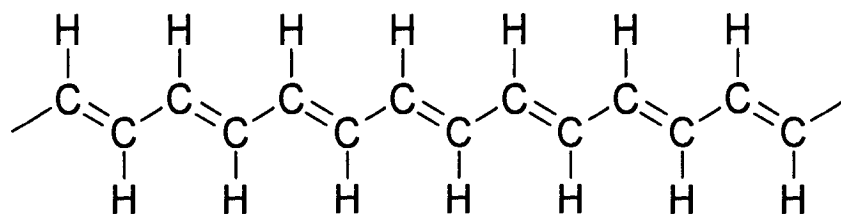
Figure 4. Section of a PA polymer chain showing alternating single (σ bond) and double (σ bond and π bond) structure.

It is of course possible for the carbons to form other bonds besides C-C and C-H; in particular in polymers carbon-nitrogen (C-N) and carbon-oxygen (C-O) bonds are possible.

The σ bonds, formed from sp^2 hybridisation, are strong. Electrons in these bonding states exist in a deep potential well and so a large amount of energy (6 eV or more) is

needed to excite electrons out of this well into anti bonding states. So σ bonds are difficult to disrupt and are considered localised. π bonds result from the overlap of p_z orbitals, which are more extended in space. Electrons in these delocalised π bonding states require less energy (around 2.5 eV) to be promoted to π* antibonding states; these are thus easily photoexcited by visible light. The exact π-π* energy depends on the degree of delocalisation, which is related to effective chain length, which in a real bulk sample is governed by defects and dopants or impurities within the bulk sample. A range of conjugation lengths, and thus broad absorption bands are therefore expected.

The overlap of p_z orbitals on adjacent sites creates π molecular orbitals, and with one electron per site the lower half of these orbitals is occupied (π, bonding orbitals) and the upper half is unoccupied (π*, antibonding orbitals). The occupancy of the π orbitals contributes to the bonding energy, and so carbon-carbon bond lengths are dependent on the electronic state. Promotion of electrons from π to π* states changes the bonding energy, resulting in a change in the equilibrium geometry of the molecule. This is seen experimentally through the coupling of electronic and vibrational transitions.

2.3. Optical Properties of Conjugated Polymers

2.3.1. Optical Absorption and Allowed Transitions

The Beer Lambert Law (Equation 1) describes the fraction of incident light that is transmitted through a material.

$$I(x) = I(0)e^{-\alpha x}$$

Equation 1. Beer Lambert Law

Where:

$I(0)$ Incident intensity

$I(x)$ Intensity at depth of material x

α Frequency dependent absorption coefficient

The absorption coefficient $\alpha(E)$ can vary greatly because the strength of any optical absorption is dependent upon the transition dipole moment between the ground and excited state. The transition dipole moment is an integral involving the ground state wavefunction, the electric dipole moment operator and the complex conjugate of the excited state wavefunction. In free atoms light is absorbed in narrow bands because of the well-defined, discrete set of available ground state and excited states. In polymers these absorption lines become broad absorption bands because of the extra degrees of freedom that the molecule has to store energy in, such as vibronic side bands[10]. In a bulk polymer sample the bands become broader still because of the variations in polymer configuration within the bulk; defects and dopants lead to a variation in the effective conjugation length.

A useful measure of the overall strength of any given absorption band is the dimensionless oscillator strength, f, which is defined[10] as shown in Equation 2.

$$f = \left(\frac{4 m_e c \varepsilon_0}{N_A e^2} \right) A = 6.26 \times 10^{-19} \times A$$

Equation 2. Oscillator strength[10]. The numerical form of the equation shown on the right is for values of A measured in $m^2 mol^{-1} s^{-1}$.

Where:

m_e Electron mass

c Speed of light

ε_0 Vacuum permittivity

N_A Avogadro constant

e Electron charge

A Integrated absorption coefficient

The coefficient A is related[10] to the transition dipole moment such that f evaluates to 1 for an electron bound so that it oscillates harmonically in three dimensions. The observed oscillator strength is therefore the ratio of the intensity of the transition to the intensity of a harmonically oscillating electron in three dimensions. In practice, $f \approx 1$ for electric dipole allowed transitions and $f \ll 1$ for forbidden transitions. In order for a transition to be allowed, the transition dipole moment must be nonzero, which is satisfied when various selection rules are followed. For a conjugated polymer f can be expressed as a product of these factors, as shown in Equation 3.

$$f = p_s p_o p_p p_m f_a$$

Equation 3. Probability factors encoding transition selection rules

Where:

p_s Electron spin factor. A change in electron spin during the excitation is forbidden and so transitions between singlet and triplet initial/final states have[11] p_s values of 10^{-5}. If a heavy atom is present, the rule is no longer valid as the spin-orbit coupling can allow singlet-triplet and triplet-singlet conversions.

p_o Orbital symmetry factor. The wavefunctions for the initial and final states must overlap in space. This is the case for the π-π^* transitions in conjugated polymers as the bonding (π) and antibonding (π^*) transitions lie in the same plane.

p_p Parity factor. Conjugated polymers (and therefore their orbitals) exhibit symmetry. If a wavefunction changes its sign through a point of symmetry it is said to have odd parity, otherwise it has even parity. Allowed transitions involve a change of parity. In the familiar π-π^* transition in conjugated polymers, the π orbital is symmetric, with odd parity whereas the π^* orbital is anti-symmetric, with even parity; π-π^* transitions are therefore parity allowed.

p_m Momentum factor. Transitions that involve large changes in the linear or angular momentum of the molecule are momentum forbidden.

f_a Oscillator strength of a fully allowed π-π^* transition (≈ 1).

2.3.2. The Frank Condon Principle

The absorption and emission from an organic molecule is represented in Figure 5. In this figure, the energies of the ground and first excited states are shown as a function of a generalised co-ordinate of the system, which represents the positions of the atomic nuclei. Each electron state has a set of vibrational energy levels associated with it. In general, the minimum of the excited state potential curve is at a different position to that of the ground state. The reason for this is that the excited state bond strength is less than that of the ground state, and thus the equilibrium length of the bond will be greater.
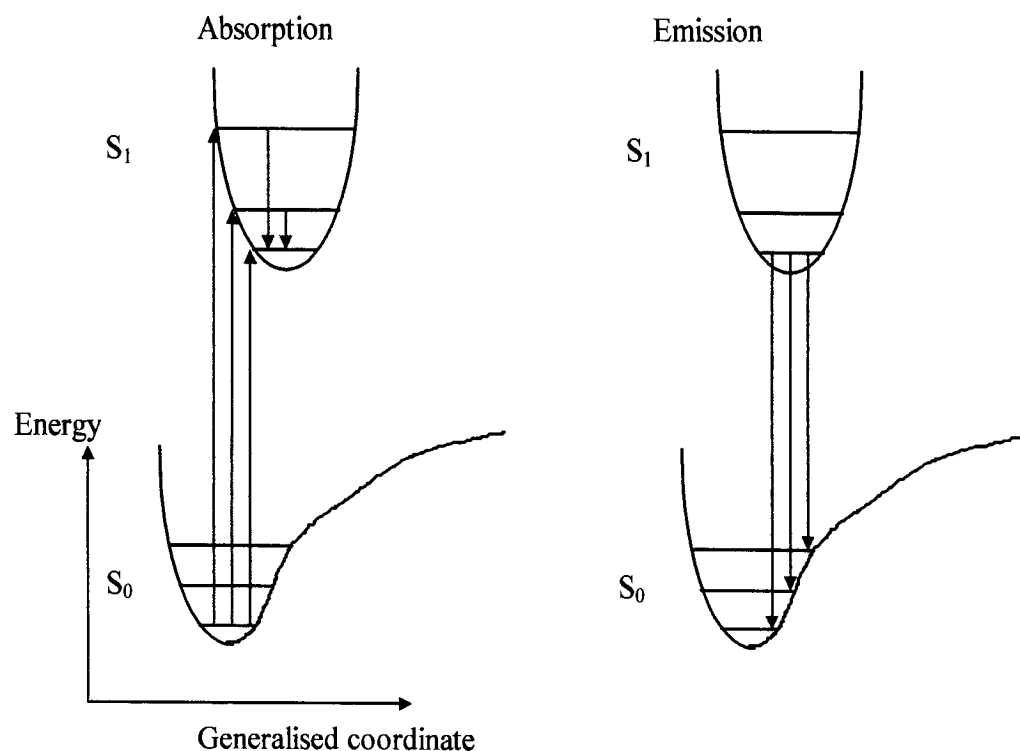
Figure 5. Absorption and emission level changes between the S_0 (π, bonding) and S_1 (π^*, antibonding) electronic states of an organic molecule.

Since electronic transitions take place on a much faster timescale than nuclear motions (less than 10^{-15} s compared to approximately 10^{-13} s), nuclei do not have time to change their position during an electronic transition[10]. Electronic transitions are therefore represented by vertical lines on Figure 5 and are known as vertical or Franck-Condon transitions[10]. The probability of an electronic transition between two states depends on the overlap between the vibrational wavefunctions of the initial and final states.

2.3.3. The Jablonski diagram

Figure 6 is known as the Jablonski diagram, and it is used to describe the processes of absorption and emission in conjugated polymers. Absorption starts from the singlet ground state, S_0 at the vibrational ground state $v = 0$. This creates an excited state S_1, with a range of v' values. A molecule in a vibrationally excited state will undergo nonradiative decay to the lowest vibrational state, S_1, $v' = 0$. This is known as internal conversion (IC). Experimentally this occurs very quickly, on timescales of approximately 10^{-13} s in line with nuclear motion. Emission S_1-S_0 therefore occurs from the lowest vibrational state of the electronic excited state[12], and this is known as fluorescence. Fluorescence too is a fast process, occurring within a few hundred picoseconds[13]. Radiation emitted between states of different multiplicity is known as phosphorescence. The triplet manifold T_1 of the polymer is populated through intersystem crossing[10] (ISC) from S_1, mainly through the mechanism of spin-orbit coupling. Again the excess vibrational energy is lost quickly, as shown in Figure 6. The triplet state can be depopulated radiatively as shown (phosphorescence T_1-S_0) or non-radiatively. As a spin flip is required for phosphorescent emission it is a weak process unless a heavy atom is present to enhance the spin-orbit coupling. The radiative lifetime of the T_1 state can be as long as a second[14,15].
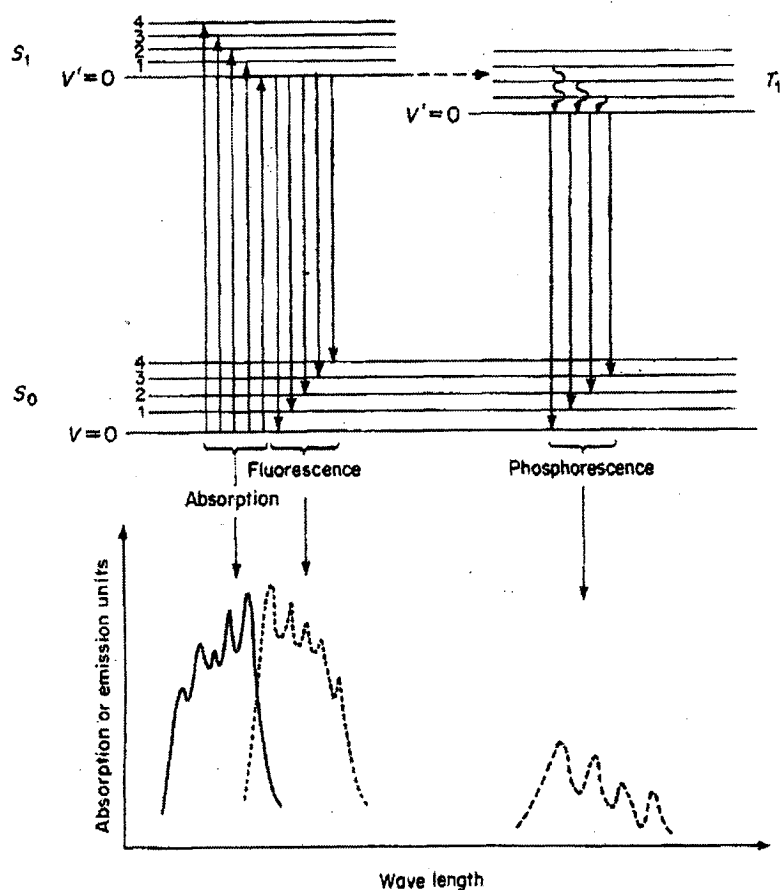
Figure 6. Jablonski diagram showing absorption and emission spectra[12]

It is important to have an understanding of the nature of the type of excitation represented by S_1^0, and this is discussed in the next section.

2.4.   Excited State Models

Different models describing the excited states in conjugated polymers have been proposed over the years, with varying degrees of success. One of the earliest models which was commonly accepted for some time was SSH theory, named after its initial proponents Su, Schrieffer and Heeger[16,17]. The model concentrated on the effects of electron-phonon interactions in the ground and excited states of the conjugated polymer. It was (incorrectly) assumed that electron-electron correlation effects were either negligible or could be accounted for by adjusting parameters in the SSH Hamiltonian. For historical interest the SSH Hamiltonian is reproduced as Equation 4.

$$H = -\sum_n \left[t_o + \alpha\left(u_n - u_{n+1}\right) \right]\left(c_n^+ c_{n+1} + c_{n+1}^+ c_n \right) + \frac{1}{2M}\sum_n p_n^2 + \frac{K}{2}\sum_n \left(u_n - u_{n+1} \right)^2$$

Equation 4. The SSH Hamiltonian.

Where:

t_o	Transfer integral between two uniformly spaced carbon sites
K	Effective spring constant
c_n, c_n^+	Creation and annihilation operators at site n
α	Electron-phonon coupling constant
u_n	Displacement of nth atomic site
p_n	Momentum of atom at site n

The first term gives the kinetic energy of the π electrons, the second term gives the kinetic energy of the lattice and the third term gives the σ bond strain energy. According to SSH theory, photoexcitation produces free carriers that are trapped within structural distortions of the polymer, giving rise to pseudo-particles known variously as solitons[16,17], polarons and bipolarons[18,19]. These pseudo-particles are then free to migrate across the entire length of the polymer chain in conduction and valence bands (i.e. fully delocalised π^* antibonding and π bonding orbitals) very similar to those found in inorganic semiconductors. For quite a while results from photoinduced absorption experiments of the type performed in this work were commonly interpreted as indicating soliton, polaron or bipolaron formation – for an example, see 20.

The SSH model has been superseded in more recent developments by the Exciton model, which was initially proposed by Bassler *et al* [21]. For a time the question of which model was more accurate was debated in the literature[14,22], but more recently it has become commonly accepted that singlet excitons are created upon photoexcitation. Various decay paths are then open to this initial singlet exciton population.

2.4.1. The Exciton Model

Though the description of the excited states of the conjugated polymer chain had been couched in the framework of a non-interacting electron model, with coupling to the lattice, it has already been indicated that electron-electron interactions play an important role in a description of the electronic structure, for both ground and excited states. The effects of electron exchange and correlation are to a considerable extent taken into account in the description of the ground state by the empirical parameterisation of these models. However, this breaks down in the description of the excited states, particularly optically generated excited states that are excitonic in nature. Attempts were made to compensate for electron-electron interactions by adding new terms into the SSH Hamiltonian[23], but discrepancies such as the dependence of Stokes shift on photoexcitation energy[24] and the increase of photoconductivity yield[25] above the band gap still arise.

Within the short chain lengths over which true conjugation and delocalisation exists, optical excitation results not in a free (soliton) or loosely bound (polaron, bipolaron) charge pairs in a valence band or conduction band, but in a bound or correlated electron-hole pair, otherwise known as an exciton. The initially photogenerated π-π* exciton population consists solely of singlet excitons; populations of triplet excitons can then form via intersystem crossing (ISC) from the singlet state. The triplet (S_0-T_1) energy is roughly 1eV smaller than the singlet (S_0-S_1) energy[26], which can be explained as follows. The Pauli exclusion principle forbids 2 electrons with the same spin to occupy the same orbital; in a triplet the electrons exist in separate orbitals which increases their separation and this reduces their Columbic repulsion.

There are different classifications of exciton, based upon the value of the exciton binding energy E_e, which measures the potential well the charge pair resides in; thus the classification of the exciton also relates to its spatial extent. These classifications were originally established for molecular crystals. The classes of excitons are shown in Figure 7.

A Frenkel exciton is one where the bound charge pair are in the same conjugation region. The electron and hole are closely correlated and move together through the

18

bulk as a unit. Recombination of Frenkel excitons is believed to be responsible for the rapid fluorescence observed from some conjugated polymers upon photoexcitation. The low separation of the charge pairs means that the excitation has no permanent dipole moment.

A charge transfer (CT) exciton is formed when the excitation is sufficient to transfer one of the charges to a neighbouring molecule. The electron is considered to be excited to a particular site, rather than being free to orbit the hole, as is the case for the other two classes of exciton. The CT exciton can either be mobile or trapped, depending on the response of the local polymer chain to the charge. A permanent dipole moment is associated with CT excitons due to the increased charge separation over that for Frenkel exciton. CT excitons have also been proposed as the source of delayed fluorescence (DF) in photoexcitation experiments[27,28] because of the relationship between the fluorescence and the applied electric field.

A Mott-Wannier (MW) exciton is weakly correlated and highly separated, with a low value of E_e. In this case the exciton is most like the free carriers in the band model discussed previously. As with the Frenkel exciton there is no permanent dipole moment; the excitons may be stabilised due to their columbic attraction being shielded by the intervening polymer bulk.
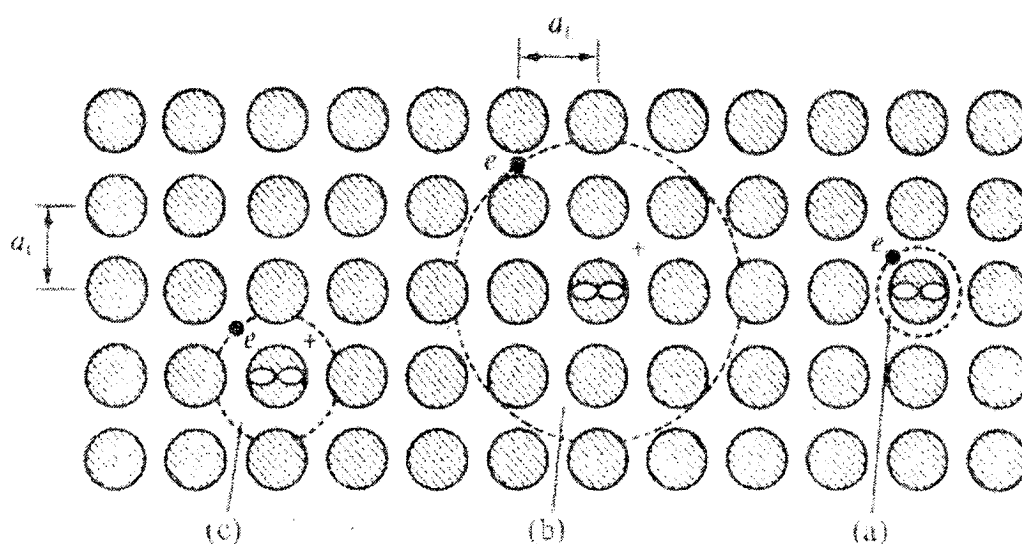
Figure 7. Frenkel (a), Mott-Wannier (b) and Charge transfer (c) excitons in a periodic lattice. From Pope and Swenberg[27]. The diagram was for molecular

crystals where each circle represented a lattice unit; in the polymer case the circles can be considered to be repeat units of the chain.

The value of the exciton binding energy is a key factor in determining what the evolution of the initial singlet exciton population will be. Higher values for E_e ($\geq$ ~0.4 eV) would indicate that charge correlation effects are significant, whereas a low value (~ 0.1 eV) indicates free carriers are easily formed following photoexcitation due to the ionisation of the initially created singlet excitons. In order to determine which model (exciton or band) is dominant, several groups have developed methods to determine the value of E_e. PPV was commonly used for this work, but a variety of results were reported and the issue was unclear for a time[25, 29, 30, 31, 32, 33]. More recently results[22, 34, 35, 36] with other polymers have yielded E_e ~ 0.3-0.4 eV, which supports the exciton model.

2.4.2. Free carriers in conjugated polymers

Conjugated polymers have two phases of bond alteration, and in most cases the two phases are non-degenerate. If an electron is introduced onto a polymer it switches the conjugation phase of the chain, but the chain deformation is restricted in size because the alternate phase comes with an energy cost. Typically the bond deformation is about 20 repeat units in length, and is mobile. The pseudo-particle consisting of the positive or negative charge and bond defect pair is known as a polaron, P^+, P^- respectively. This is illustrated in Figure 8 for the case of poly(p-phenylene) (PPP).
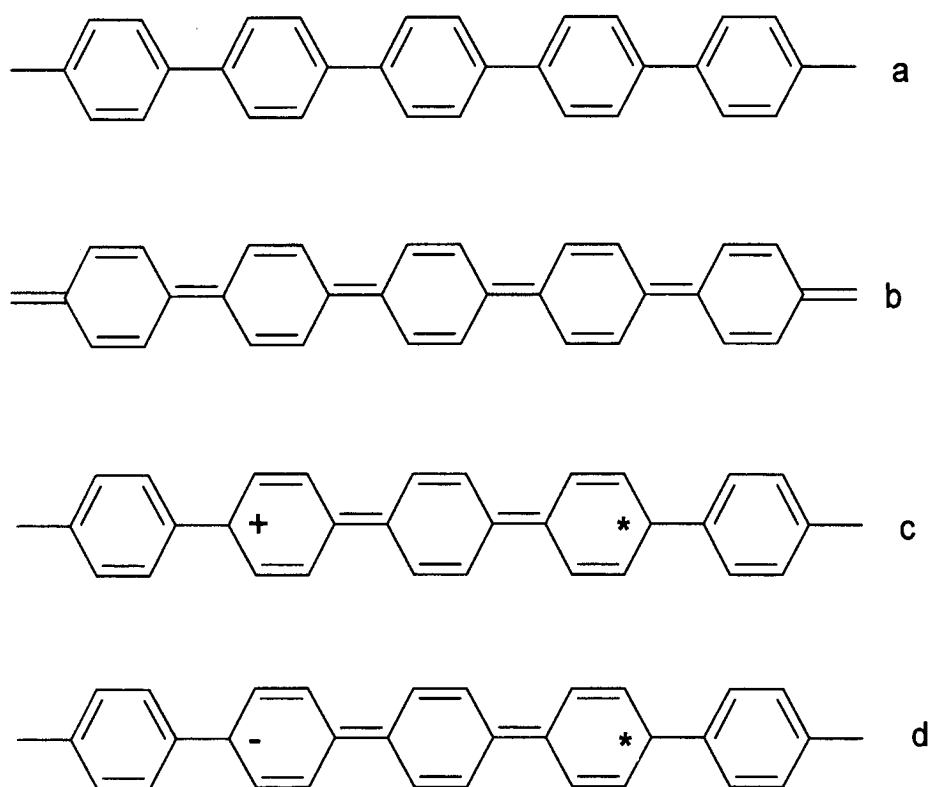
Figure 8. Schematic diagram showing different states of PPP (a) Ground state - Phase A (b) Phase B (c) P^+ pseudo-particle with two phase boundaries (d) P^- pseudo-particle with two phase boundaries[37].

Polarons may be formed directly when charge is injected into the polymer from an external material, such as electron injection from a metal and hole injection from ITO in a polymer LED[38], as shown in Figure 9.

Electrons and holes are injected into the polaron conduction and valence bands[39] and migrate through the device as negative or positive polarons, until they capture[6] each other in the interface region of the device. Polarons decay upon capture into correlated or bound electron-hole pairs – i.e. excitons, some of which can then decay radiatively to emit light. The spin of the polarons is randomly distributed between ±1/2 and hence both singlet and triplet excitons will form upon recombination. Statistically the formation of more triplet excitons than singlet excitons would be expected because there are three triplet spin combinations and only one singlet excited state, as shown in Equation 5.
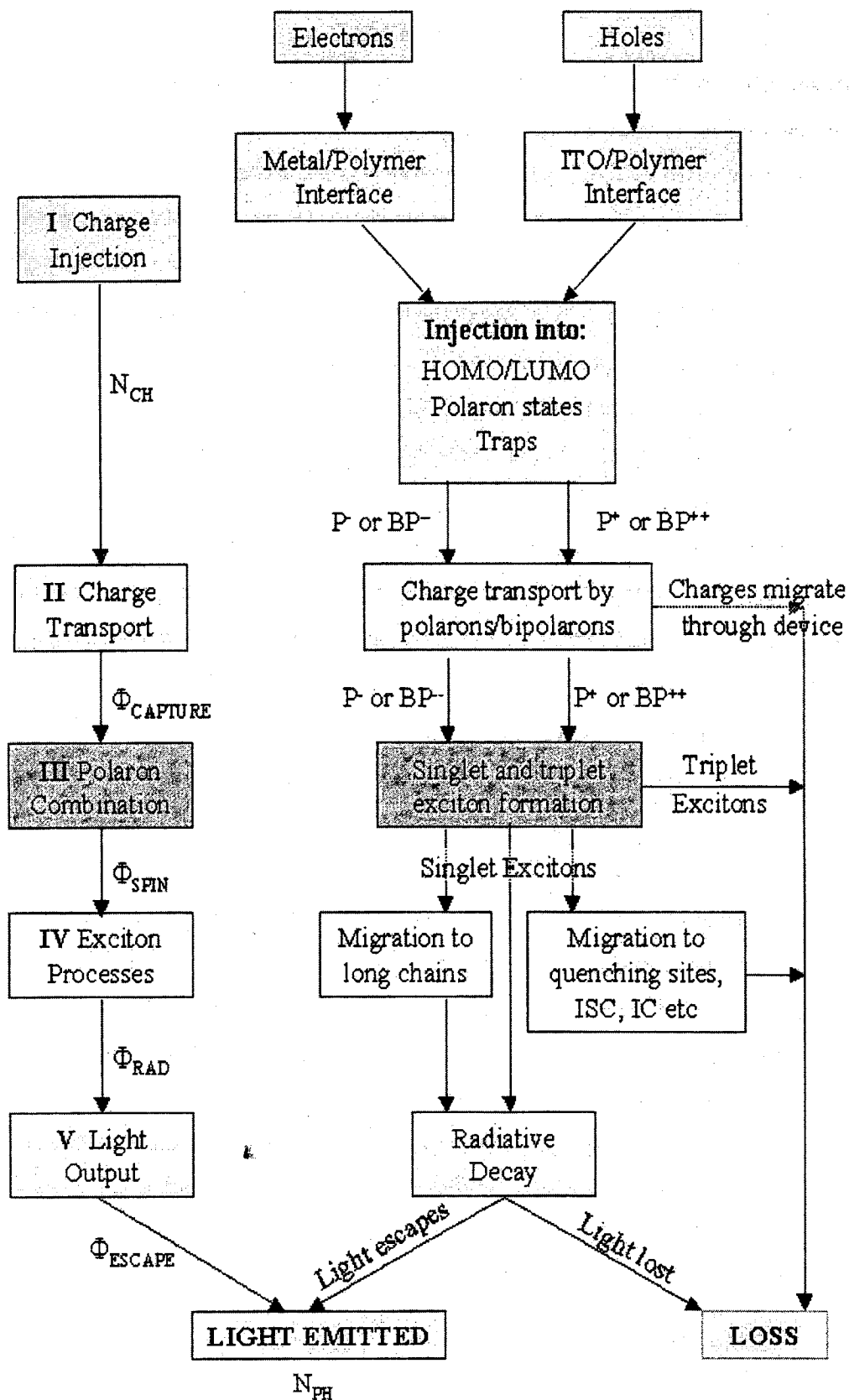
Figure 9. Flow chart of the processes involved in emission from PLEDs[38]

$$S = \frac{1}{\sqrt{2}}[(\uparrow\downarrow)-(\downarrow\uparrow)]$$

$$T = \left\{ \begin{array}{c} (\uparrow\uparrow) \\ \frac{1}{\sqrt{2}}[(\uparrow\downarrow)+(\downarrow\uparrow)] \\ (\downarrow\downarrow) \end{array} \right\}$$

Equation 5. Singlet and triplet electronic states. The up arrow ($\uparrow$) indicates an electron with spin + ½, the down arrow ($\downarrow$) indicates an electron with spin - ½.

Initially it was proposed that only 25% of oppositely charged polaron capture events would lead to singlet exciton formation[2,4]. More recent development have suggested[40,41] that this assumption of spin-independent recombination is invalid. The reasoning is that the wavefunction overlap between the singlet exciton and loosely correlated electron-hole pair is greater than the overlap between the triplet exciton and electron-hole pair. This follows from the more energetic singlet exciton having a greater radius and thus a character more like the ionic nature of the loosely bound electron-hole (P^- and P^+) bound pair. Proportionally then more than 25% singlet excitons would be expected.

Whatever the absolute fraction of triplets generated in the process it is accepted that a considerable number of triplet excitons will be formed, and their presence is generally regarded as a bad thing in polymeric LEDs. The triplet excitons are long lived, because of weak coupling to S^0, and they also can quench singlet excitons through a process known as STA (see section 2.6.3), reducing the performance of the device. Additionally, triplet-triplet absorption is strongly allowed in some materials[42,43,44] as predicted theoretically[45], and this can impact the photoluminescent (PL) and electroluminescent (EL) behaviour of the device. The additional triplet-triplet absorption loss can have a big impact on loss-critical systems such as laser devices. This has lead some groups[46,47] to add phosphorescent triplet harvesting molecules to the active layers of PLEDs: the idea is to harness more of the triplets in light emission or at least reduce the triplet population in order to minimise STA. It is apparent that it is necessary to understand and characterise triplet excitons in these materials in order to manufacture better PLEDs.

Polarons may also be formed by the ionisation of photoexcited excitons, depending on the exciton binding energy.

The basic aim of this research is to try and identify the type of species generated in a set of conjugated polymers upon photoexcitation. However the experiments that have been performed only measure the steady state populations of these excited states that are present in large numbers milliseconds after the initial photoexcitation; essentially the experiment is sensitive only to the long-lived remnants of the initially photoexcited singlet exciton population. In order to analyse these results knowledge of the dynamic processes for the various species is required. Firstly it is necessary have some knowledge of the energy transfer processes that are allowed, since these are the basic mechanisms behind most of the exciton-exciton interactions.

2.5. Energy transfer

There are three basic processes by which energy may be directly transferred between a donor molecule and an acceptor molecule. These molecules or species may be the same (such as in the case of internal energy transfer within a polymer) or different (as in the case of the pulse radiolysis experiments discussed in section 3.4). Perhaps the simplest form of direct energy transfer is the re-absorption by the conjugated polymer of its own emission. In addition to this there are two more subtle mechanisms, known as Forster and Dexter transfer.

2.5.1. Resonant Energy Transfer (Forster Transfer)

This mechanism depends on an overlap between the emission spectrum of an excited donor site and the absorption spectrum of the acceptor site. Energy is then transferred from the one site to the other. The mechanism is driven by the dipole-diople coupling of the two sites. Forster[11,48] developed an expression for the transfer rate from the donor to the acceptor which is given as Equation 6.

$$K_{D \to A} = \frac{1}{\tau_D} \frac{1}{R^6} \frac{1}{n_0^4} \left(\frac{3}{4\pi} \int \frac{c^4}{\varpi^4} F_D(\varpi) \sigma_A(\varpi) d\varpi \right)$$

Equation 6. Rate Equation for Forster transfer

Where:

τ_D	Donor excited state lifetime
R	Donor-acceptor separation distance
n_0	Refractive index
$F_D(\varpi)$	Normalised donor fluorescence emission spectrum
$\sigma_A(\varpi)$	Normalised acceptor absorption cross section

The integral in Equation 6 calculates the overlap between the acceptor absorbance and donor emission spectra; the overlap integral must therefore be non-zero in order that Forster transfer will occur. The process is illustrated in Figure 10.
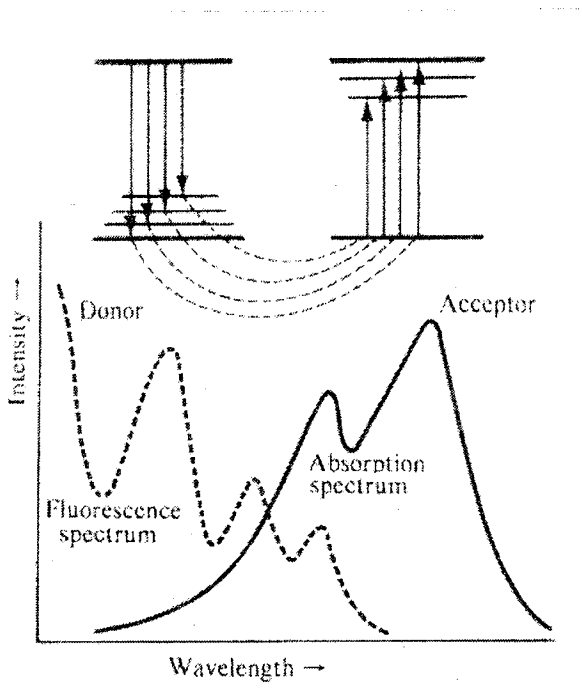
Figure 10. Overlap between acceptor absorption and donor emission required for Forster Transfer[6]

Since the Forster process is based upon a dipole-dipole interaction, only energy, and not spin, can be transferred between the donor and acceptor excited states.

2.5.2. Electron Exchange Energy Transfer (Dexter Transfer)

Dexter extended[49] the theory of resonant transfer to deal with dipole-forbidden transitions involving triplet states. Essentially, if the donor and acceptor species are close enough so that their electronic orbitals overlap, an electron from the donor site may be able to transfer to the acceptor site. Dexter's theory is applicable to triplet energy transfer, and the transfer rate is expressed as Equation 7.

$$K_{D \to A} = \frac{2\pi}{\hbar} |\beta_{DA}|^2 \int F_D(E) F_A(E) dE$$

Equation 7. Rate equation for Dexter transfer

Where:

β_{DA} Exchange energy interaction between donor and acceptor

$F_D(E)$ Normalised phosphorescence spectrum of the donor

$F_A(E)$ Normalised absorption of the acceptor

In the case of triplet energy transfer, two electrons are transferred, thus conserving spin, as shown in Figure 11.
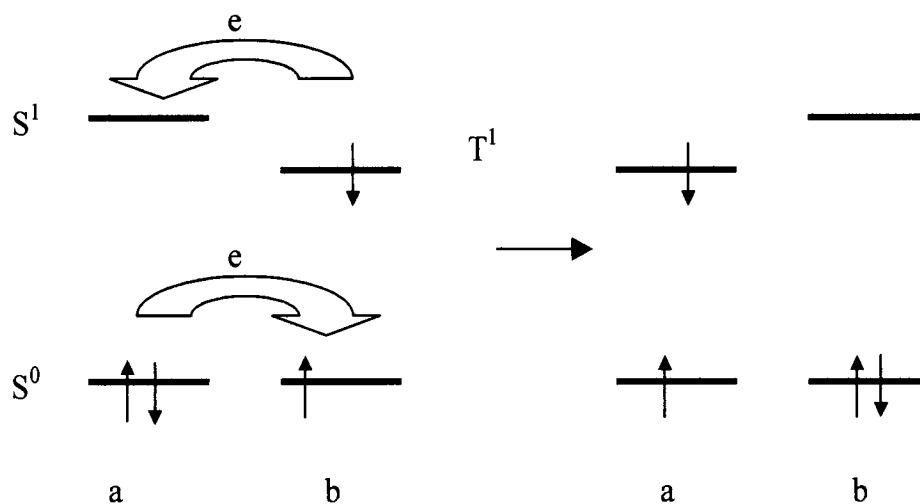
Figure 11. Schematic diagram showing triplet energy transfer between site a (acceptor) and site b (donor).

2.6. Exciton Processes

In this section we consider the main non-radiative process that the singlet and triplet exciton population can undergo. These processes are categorised into monomolecular and bimolecular processes as the technique of steady state photoinduced absorption can distinguish between these two classifications (see section 3.2).

2.6.1. Impurities and imperfections

Classic monomolecular non-radiative decay processes include the interaction of the exciton with a chain defect or an impurity. Fluorescence or phosphorescence from singlet and triplet excitons is obviously also a monomolecular process.

2.6.2. Singlet-Singlet annihilation (SSA)

This is a relatively simple process in which energy of a singlet excited state is transferred to an acceptor state through a Forster energy transfer (see section 2.5.1) process. The additional energy promotes the acceptor state into a higher vibronic

energy state. Within the exciton model, two singlet excitons annihilate to form products as follows:

$$S^1 + S^1 \rightarrow S^n + S^0$$
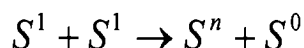
The acceptor exciton can then thermalise, emitting a phonon, Ω:

$$S^n \rightarrow S^1 + \Omega$$
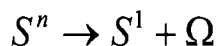
2.6.3. Singlet-Triplet annihilation (STA)

In this process the excited singlet state (S^1) transfers its energy to a triplet state (T^1) instead of another singlet. For this Forster-like process to happen the emission from the singlet exciton (fluorescence) must match to the absorption within the triplet manifold.

This transition is spin-allowed, whereas the reverse process of triplet energy being transferred to a singlet is spin-forbidden since the triplet T^1 must then transition to S^0:

$$S^1 + T^1 \rightarrow T^n + S^0$$
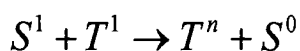
As with the SSA process, the excited triplet T^n then thermalises:

$$T^n \rightarrow T^1 + \Omega$$
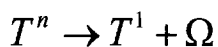
It has been proposed that triplet excitons are efficient singlet quenchers in a polymer LEDs.

2.6.4. Triplet-Triplet annihilation (TTA)

In addition to the energy transfer (Forster) processes described above, triplet-triplet annihilation is possible, although this requires the short-range collision of two triplet

excitons[26] and electron exchange as per the Dexter mechanism (see section 2.5.2). In the solid state, the requirement for proximity means that the interaction is limited to neighbouring triplets on the same polymer chain. The TTA process is shown below:

$$T^1 + T^1 \rightarrow \left(T^1 + T^1\right)^{1,3,5} \rightarrow \left\{ \begin{array}{l} \dfrac{8}{9}(S^0 + T^n) \\ \dfrac{1}{9}(S^0 + S^n) \end{array} \right\}$$
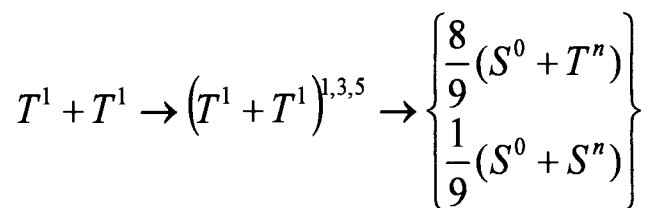
The intermediate pair state[50] can have singlet, triplet or quintuplet spin multiplicity, and so the fraction of excited singlet states produced on decay is 1/9, as shown. Once formed, the excited singlet S^n can then relax to S^1 and then undergo a radiative transition $S^1 \text{-> } S^0$. This is the mechanism behind the phenomenon of delayed fluorescence (DF) [6,42,44,51].

2.7. Summary

The chapter has attempted to give a brief introduction to the different types of long-lived photoexcitations that may exist in conjugated polymers. It is the aim of this work to differentiate between the spectral characteristic signatures of excitons, triplets and charge carriers in an attempt to determine the nature of the long-lived photogenerated states in three conjugated polymers. The nature of the long-lived states impacts the behaviour of devices containing these materials The role of triplet populations in electroluminescent devices is of particular importance: a high steady state triplet population can reduce the efficiency of singlet emission through STA, soak up energy in non-emissive states and reduce the external efficiency by absorbing some of the PL or EL emission in triplet-triplet transitions.

Chapter 3. Experimental Techniques

3.1. Introduction

Chapter 2 demonstrated how photoexcitation of conjugated polymers can lead to the formation of excited state species such as singlet and triplet excitons, polarons & bipolarons. These new states tend to have distinct electron energy levels and are therefore amenable to investigation using transmission spectroscopy. In order to observe transitions between these new states there must be sufficient oscillator strength coupling between the new energy states created by each species or between the new states and some pre-existing energy level (e.g. the global singlet ground state) to absorb a detectable amount of light. The oscillator strength that is required depends on the sensitivity of the instrumentation and the population of excited states that can be generated. Typically the transition must be sub-gap in order to be detected, it being much harder experimentally to detect a small change in absorption in a region of strong absorption rather than in a region of no absorption.

The technique of photoinduced absorption allows information to be gathered on these different excited states; the difficulty comes in unambiguously assigning photoinduced absorption features to particular species. This chapter describes the technique of photoinduced absorption (PIA), particularly quasi steady state PIA[52] (section 3.2), followed by details of the particular experimental implementation of the technique (section 3.3) used in this work. The thesis also makes use of transient absorption data obtained through the technique of pulsed radiolysis, which is a method of directly injecting specific excited states into a target polymer in solution. The technique of pulsed radiolysis is described in section 3.4

3.2. Photoinduced absorption basics

There are two light sources in the photoinduced absorption experiment: the pump beam and the probe beam. The pump will create new electronic states by the variety of possible mechanisms discussed earlier. The probe beam maps out the electronic

states both before and after excitation. This is shown in Figure 12, for the example of a positive polaron excited state.
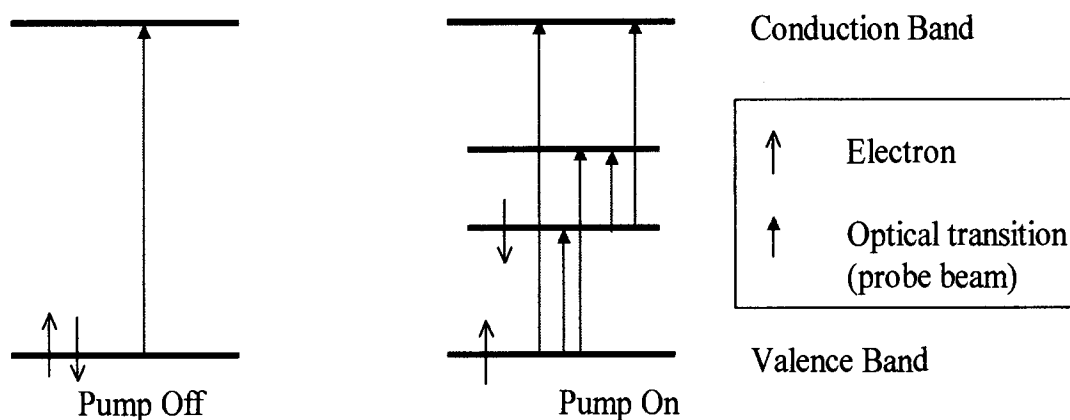
Figure 12. Transitions between ground and photoexcited electron energy levels showing positive polaron (p^+) creation.

There are two changes in the sample absorption spectrum associated with photoexcitation, as can be seen from Figure 12. Firstly there are four possible new absorption bands for the probe beam associated with the photocreated energy levels. Figure 12 shows the example of a positive polaron but solitons, bipolarons, singlet and triplet excitons also produce new absorption bands. Secondly, after photoexcitation there are fewer electrons in the valence band compared to the pump off state since electrons have been transferred to the new states. This reduction in oscillator strength reduces the absorption band in a process known as photobleaching. Associated with the formation of the mid-gap soliton, polaron or exciton absorption band is the loss of π and π^* states and the bleaching of the π-π^* interband transitions. Oscillator strength must be conserved overall.

For the case of triplet excitons, the new activated absorption bands correspond to transitions within the photo-populated triplet manifold, as shown in Figure 13.
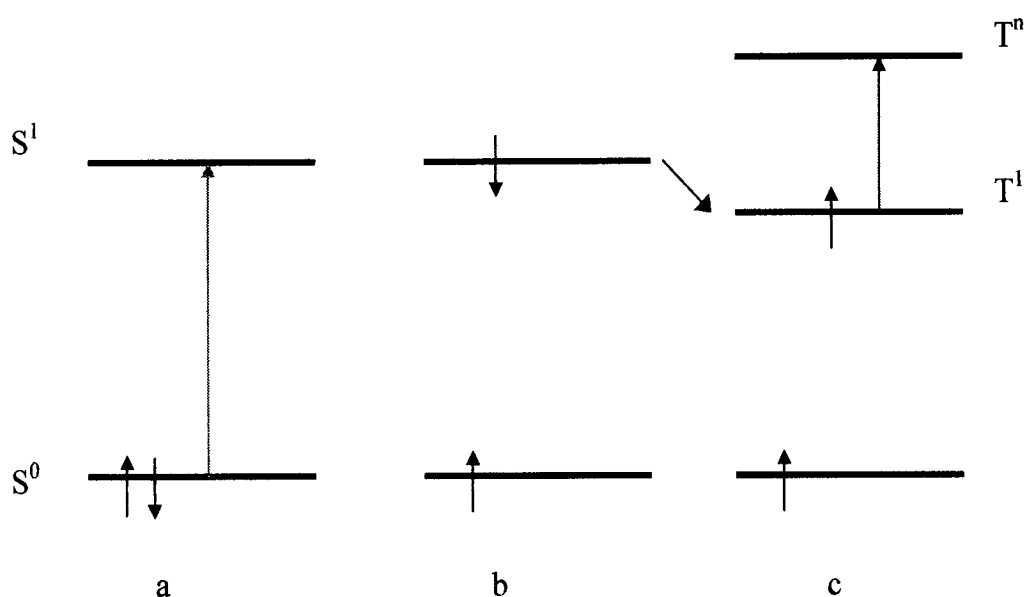
Figure 13. Creation of triplet excitons by photoexcitation; (a) photoexcitation of ground state, (b) singlet exciton formation; (c) ISC to form triplet excitons and photoinduced absorption within the triplet manifold.

The change in absorption can be related to the number of excited states generated through Equation 8[53].

$$ -\frac{(\Delta T)}{T} = \sigma \frac{N}{A} $$

Equation 8. Relationship between change in absorption and excited state population[53].

Where:

$\dfrac{(\Delta T)}{T}$	Steady state photoinduced absorption signal
σ	Energy dependent absorption cross-section of photoexcitation
N	Total number of photoexcitations
A	Area of sample exposed to probe beam

A quantitative knowledge of the photoinduced absorption bands; their energy, lifetime and dependence on temperature, pump beam photon energy, pump beam intensity and beam polarisation can be obtained through photoinduced absorption. Varying the sample type and conditions (the temperature, atmosphere, polymer chain separation have all been varied in these experiments) also yields useful information. Such a characterisation of the absorption bands reveals important information on the nature of the photoexcited states.

In addition to the photoinduced changes in the absorption, some materials will exhibit luminescence following a photoexcitation. In fact, two of the materials studied in this thesis (polypyridine (PPy, Chapter 4) and polyfluorene (PFO, Chapter 5)) are strongly luminescent. In an absorption experiment a photoluminescence signal will show up as a region of negative absorption (positive transmission change), as does photobleaching.

The basic requirements for measuring changes in the absorption of a sample of polymer are given below. In order to map out the electronic states white light transmission spectroscopy is used, shown in Figure 14.

Probe beam ⇒ ▮ ⇒ [Monochromator] ⇒ [Detector]

Sample   Monochromator   Detector
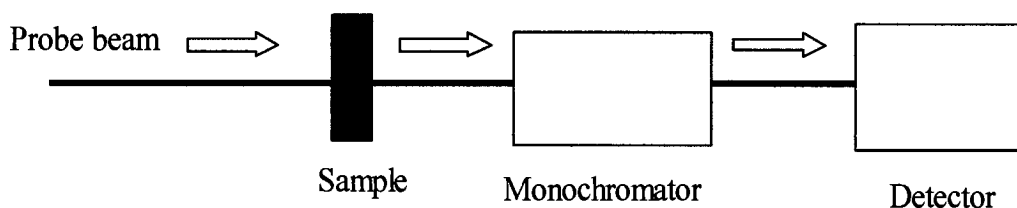
Figure 14. Transmission spectroscopy.

A white light probe beam is shone through the sample, the light transmitted through the sample is dispersed through a monochromator and the detector measures the intensity of light at that particular frequency. The detector output is a current that is proportional to the incident intensity. By scanning the monochromator over a wavelength range and logging the intensity at points along this scan, the absorption spectrum $A(\lambda)$ for the sample in the unexcited state is obtained. The probe beam must be a white light, continuum source for scanning across a frequency range. It must also have a lower intensity than the pump beam so that it does not create new electronic

levels in significant numbers. An additional monochromator could be used in front of the sample to limit the white light to the wavelength accepted by the second monochromator. The monochromators would then have to be scanned synchronously. We have not used the dual monochromator route but use broadband absorption filters to restrict the wavelength range of light incident on the sample to the range of the particular scan in progress.

With the pump beam turned on (Figure 15) $A(\lambda) + dA(\lambda, t)$ is measured, where $dA(\lambda, t)$ is the change in absorption due to excited polymer chains. It is clear that $dA(\lambda, t)$ can be positive and negative in different wavelength regions; a positive $dA(\lambda_1, t)$ corresponding to new absorption bands and a negative $dA(\lambda_1, t)$ corresponding to photobleaching or photoluminescence.
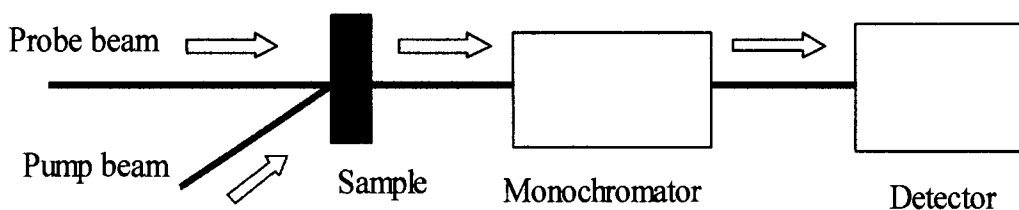
Figure 15. Photoinduced absorption spectroscopy

In order for the pump beam to create an excited state population it must be absorbed by the polymer – that is, matched to the absorption band of the sample. The pump beam must also be intense and monochromatic to create an excited state population big enough to yield a measurable $dA(\lambda, t)$ signal. These requirements mean that in general a laser must be used.

It is now necessary to consider the evolution of the photoinduced absorption signal in time. Following a single excitation pulse from the laser, an initial excited state population is created (Figure 16). The initially created excited states decay away with a certain profile and lifetime. (The initial states may decay directly to the ground state and/or evolve into different types of excited state but that is irrelevant to the current discussion.) Different experimental configurations can follow this decay with different resolutions. Optically gated systems can follow the decay with

femptosecond (10^{-12} s) resolution, whilst electronically gated systems are capable of nanosecond (10^{-9} s) resolution.
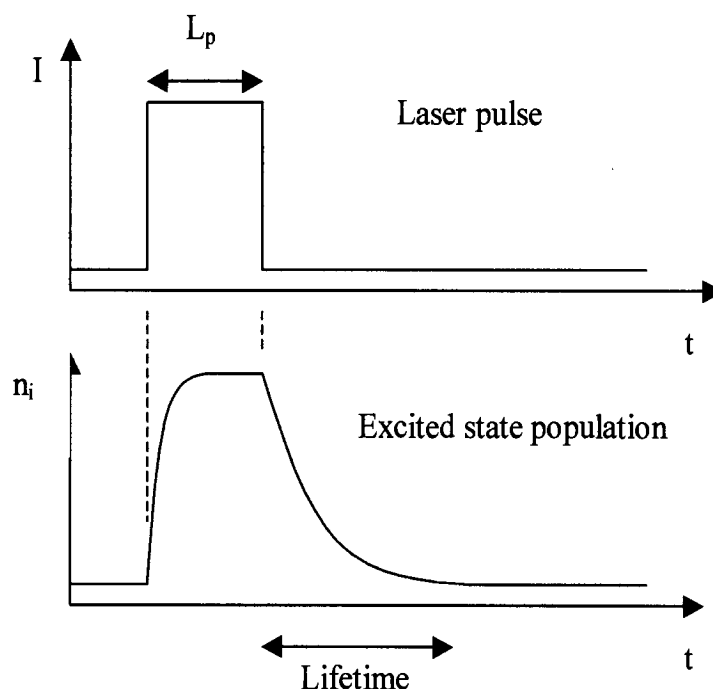
Figure 16. Initial photoexcitation event

The experiment carried out in this work is quasi steady state photoinduced absorption, shown in Figure 17. A continuous series of pulses is used instead of a single laser pulse. The laser pulses have a constant frequency (usually in the range 5 – 500 Hz). This induces a fluctuating $dA(\lambda)$ signal with the same frequency in the external detection system; the signal is recovered using a lockin amplifier. For this to work the excited state lifetime must be short enough that the induced absorption decays significantly in the laser off period, thus giving an AC signal at the laser frequency. However, if the state lifetime is too short not enough probe photons will interact with the excited state during its lifetime to give a measurable AC signal at the detector. This means that states detected by the steady state system have millisecond lifetimes, and thus that any PIA features we observe are the relatively stable remnants of the initial photoexcitation products. We can measure $A(\lambda)$ at the same time as $dA(\lambda)$; it is simply seen as a DC level in the detection system.
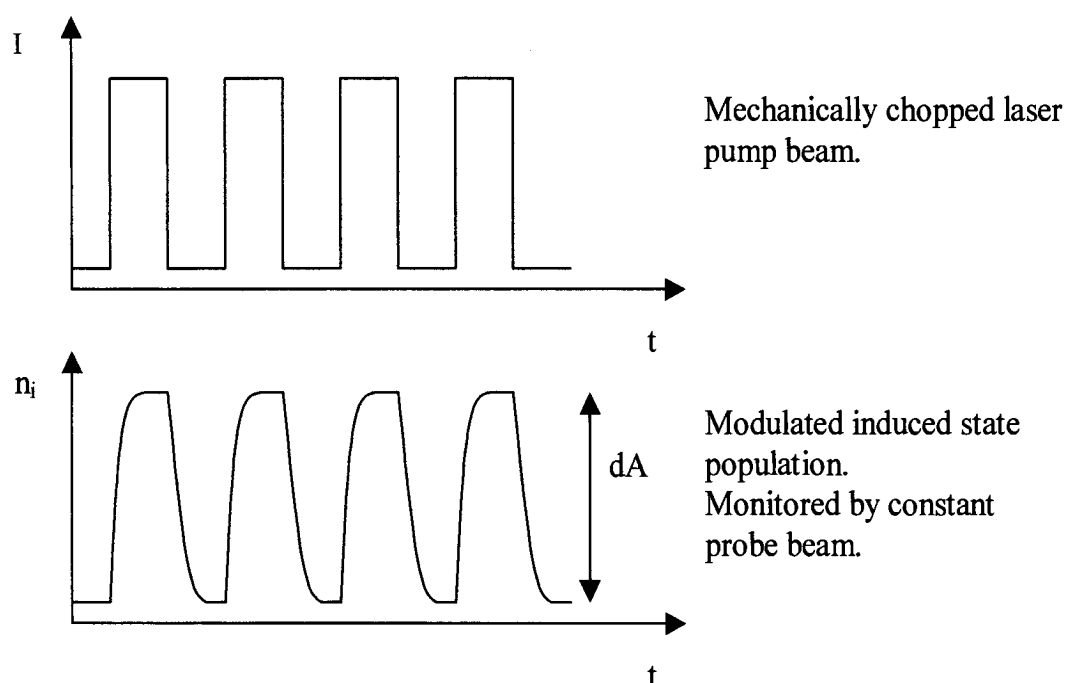
Figure 17. Quasi steady state photoinduced absorption.

Changing the pump modulation frequency ω changes the induced population $dA(\lambda)$. The relationship between ω and $dA(\lambda)$ signal strength can be used to determine the steady state lifetime of the excited state and the type of decay (monomolecular, bimolecular or dual) that is dominant.

A monomolecular decay is one where the rate of change in the excited state density dn/dt follows the form shown in Equation 9[54]. Here $G(t)$ is the creation term, which is periodic with angular frequency ω, the strobe frequency of the laser pump beam and γ is the inverse lifetime of the state ($\gamma = \tau^{-1}$). An excited state is said to undergo monomolecular decay if it can decay without interacting with another excited state of the same type.

$$\frac{dn}{dt} = G(t) - \gamma n$$

Equation 9. Monomolecular rate equation.

The solution to Equation 9 can be solved analytically[54] for the steady state case, yielding Equation 10. Here g is the efficiency of photoexcitation generation, I is the pump intensity and ϕ is the phase of the incoming radiation.

$$n(t) = gI\tau \left[\frac{1}{\sqrt{1+\omega^2\tau^2}} \cos(\omega t - \phi) + 1 \right]$$

$$\tan(\phi) = \omega\tau$$

Equation 10.

It can be shown[54] that the size of the steady state population n_s is related to the pump frequency ω, the state lifetime τ and the pump intensity I through the well known Equation 11.

$$n_s \propto \frac{I\tau}{\sqrt{1+\omega^2\tau^2}}$$

Equation 11. Steady state dependence of n_s upon chop frequency ω for a monomolecular decay.

The steady state population is proportional to the dA signal measured in the steady state PIA experiment. The equation predicts a pump intensity dependence of dA. The dependence on chop rate ω falls into two broad domains: for $\omega\tau \ll 1$ (small chop frequencies) the dT signal should be independent of ω. For $\omega\tau \gg 1$ the dT signal should show a ω^{-1} dependence. The crossover region between these two domains can be used to obtain an approximate value for τ. A more accurate value for τ is obtained by fitting Equation 11 to a dataset containing values of dA for a range of ω. It is also apparent from Equation 10 that ϕ approaches 0 for small values of the lifetime, τ, and that ϕ approaches $\pi/2$ for very large values of τ. The in phase (ϕ=0) and out of phase ($\phi = \pi/2$) photoinduced spectra can be used to detect states with different lifetimes.

A bimolecular rate equation follows the form shown in Equation 12[55]. This type of decay becomes important for polarons and bipolarons where polaron-polaron

annihilation from the collision of oppositely charged polaron states is the dominant decay mechanism. Triplet-triplet annihilation (see section 2.6) is also a bimolecular decay process.

$$\frac{dn}{dt} = G(t) - \beta n^2$$

Equation 12. Bimolecular rate equation.

It is apparent from Equation 12 that we cannot introduce a single value for the lifetime since this will continuously vary through the decay process as the population n changes. Fortunately the steady state lifetime τ_s is still a meaningful quantity. Equation 13 shows[55] the steady state photoinduced absorption signal dependence for a symmetric square wave modulation of the light intensity.

$$n_s = \frac{N\alpha \tanh \alpha}{\alpha + \tanh \alpha}$$

Equation 13. Steady state dependence of n_s upon chop frequency ω for a bimolecular decay.

Where:

$$N = \sqrt{\frac{gI}{\beta}}$$

$$\alpha = \frac{\pi}{\omega \tau_s}$$

$$\tau_s = \frac{1}{\sqrt{gI/\beta}}$$

The new parameter, g, is the efficiency of excited state photogeneration. For $\omega \tau_s \gg 1$ (small values of α), the signal tends to zero as $N\alpha$; that is, with an ω^{-1} dependency as

in the monomolecular case. As $\omega\tau_s \ll 1$ (large values of α), the signal tends to $N\alpha/(1+\alpha)$ and when α becomes very large, $n_s \approx N$, independent of chop rate. Nevertheless it is clear that in the high chop frequency limit the monomolecular and bimolecular decays are equal but they are dissimilar in the low frequency limit. Fitting a dA vs. ω dataset to the bimolecular decay function yields a value for τ_s.

Finally it is possible[55] to obtain an expression for the case when both monomolecular and bimolecular decay terms are present. This is shown as Equation 14.

$$n_s = \frac{gI\tanh\left(\dfrac{\gamma\pi}{2\omega}\right)\tanh\left(\dfrac{P\pi}{\omega}\right)}{\dfrac{\gamma}{2}\tanh\left(\dfrac{P\pi}{\omega}\right) + P\tanh\left(\dfrac{\gamma\pi}{2\omega}\right)}$$

Equation 14. Steady state dependence of n_s upon chop frequency ω for a dual decay rate equation.

Where:

$$\gamma = \tau^{-1}$$

$$P = \sqrt{\beta gI + {\gamma^2}/{4}} = (2\tau)^{-1} + (\tau_{s1})$$

In order to obtain the type (monomolecular, bimolecular and dual) and appropriate photoexcited state lifetime(s) chop rate dependency data (dT vs. ω) was fitted to Equation 11, Equation 13 and Equation 14 in this work. Each fit was performed using the built-in Levenburg-Marquardt[56] method of Origin[57] that calculates the error in the extracted parameters based upon signal noise and goodness of fit for a certain confidence level. Other fitting methods are available; there is a particularly elegant, ingenious and powerful method using a genetic algorithm known as Differential Evolution[58] but the Levenburg-Marquardt method is well suited to this particular problem. The function that fitted the data best was then deemed the dominant decay method. In practice, care has to be taken that the variation in detected dA signal is

purely due to the variation in ω without contributions from other mechanisms such as photodegradation of the sample under the laser beam.

In all cases higher chop rates ($\omega\tau \gg 1$) result in a lower steady state population and therefore a lower signal. However, the noise on the AC signal decreases with increasing chop rate so a compromise chop rate has to be found in order to obtain PIA spectra. Chop rates in the range 20-30 Hz have been used to obtain PIA spectra.

A real experiment measures the transmission of the sample, not the absorbance. These quantities are related through $A(\lambda) = -\log(T(\lambda)/T_0(\lambda))$, assuming negligible reflectivity. Since the transmission change due to the transient photoexcited states is small, we can approximate the photoinduced absorbance by $dA(\lambda) = -dT(\lambda)/T(\lambda)$. In the quasi steady state experiment, $dT(\lambda)$ is the AC signal; a transmission component due the excited states created by the modulated laser beam. $T(\lambda)$ is the DC signal, a transmission component due to the ground state absorption, constant whether the laser is on or off.

The apparatus used will modulate the measured $T(\lambda)$ and $dT(\lambda)$ since the monochromator will pass some wavelengths of light more strongly than others and the detector light intensity to voltage relation is dependent on the light wavelength. Fortunately $dT(\lambda)/T(\lambda)$ is independent of the apparatus response function and photoinduced absorption spectra are plots of $-dT/T$ as a function of hc/λ without any correction for the instrument function.

The measured dT signal is an AC signal and thus will have a magnitude and phase. The phase of the AC signal is a measure of its shift relative to the reference AC signal: in this case the chop rate of the laser.

3.3. PIA Instrumentation & developments

3.3.1. Experimental realisation

This section will detail how the principles described previously are implemented in a real experiment. Figure 18 shows the experimental apparatus.
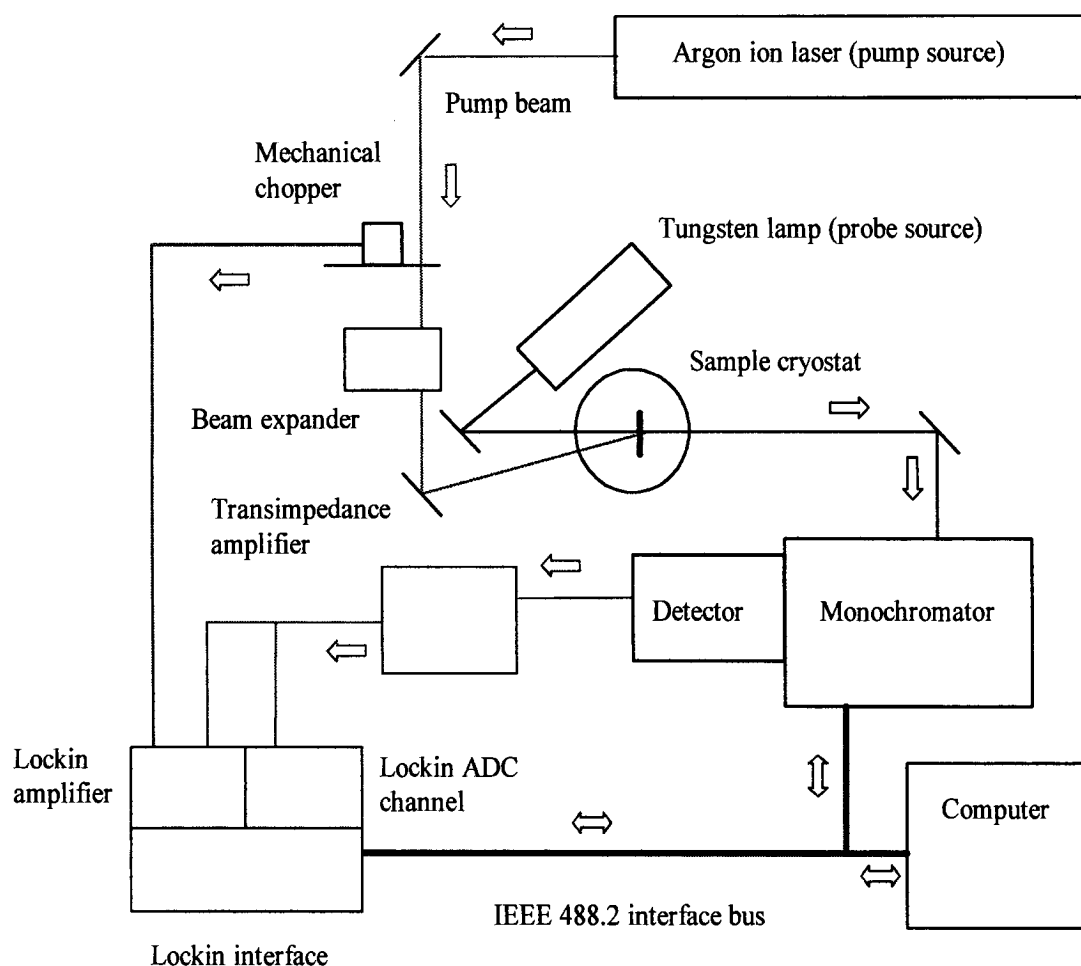

Figure 18. Quasi steady state PIA instrument.

Pump Beam

A 6W Argon ion laser is used as the pump source. This laser is able to emit light at a variety of wavelengths and so is suited to a range of different polymers. Pump beam intensity is variable by altering the current supplied to the Argon ion laser or by placing a neutral density filter into the path of the pump beam.

The pump beam is mechanically chopped to give the required strobing effect. The chopping frequency is variable between about 5 Hz and 550 Hz, with a change of chopper blade at about 160 Hz. The chopper produces an AC signal of the same frequency as the strobing rate and this is used by the lockin amplifier to recover the AC component of the detector output. A value of about 20-30 Hz is used for most of the spectra presented here; this is a reasonable compromise between signal strength and AC noise. The entire range of chop frequencies is used in a chop rate characterisation of photoinduced absorption peaks.

It is clear that the pump and probe beams must illuminate the same area of the sample. Misalignment could result in any photoinduced absorption signal from the sample being reduced in magnitude or not detected at all.

It is also important to investigate the largest possible sample area in order to prevent variations in the polymer surface from distorting the results; the large area averages out such sample variations. The pump line contains a beam expander which ensures that the pump beam fills the entire exposed area of the sample inside the cyrostat (10 mm diameter). The lenses inside the beam expander are not achromatic; the position of the converging lens with respect to the diverging lens must be adjusted to produce a parallel beam for different pump wavelengths.

Sometimes very high power densities are required at the sample surface before any significant photoinduced absorption signal is observed. In this case the beam expander is removed from the pump line and the probe beam similarly cut down.

Unfortunately the probe beam photo degrades the polymer samples, so a limited time is available to collect photoinduced absorption data over a wide wavelength range.

Probe Source

A Tungsten lamp is used as the probe source. This puts the upper limit of photon energy at around 3 eV since the lamp intensity falls off rapidly at this energy. A xenon arc lamp was tried as a UV source but it was not possible to stabilise the light output sufficiently.

In order to limit the energy absorbed by the polymer film or solution whilst an experiment is in progress, the wavelength of probe light is filtered so that only the wavelengths required for the experiment falls on the sample. A water filter is used to block out the IR whilst performing a visible range scan to minimise heating effects.

Sample cryostat

The samples used are either thin films on sapphire substrates or solutions of the polymers under study. The thin films are mounted within an Oxford Instruments liquid nitrogen bath cryostat, which will hold the sample at temperatures between 77 and 300 K.

The sample atmosphere may also be controlled within the cryostat for the thin film samples. Typically dry helium and dry air were used in these experiments. Helium is simply introduced into the cryostat sample chamber by use of a gas line and bladder; the chamber was evacuated and refilled with helium about 5 times in order to flush out all contaminants.

In order to fill the sample chamber with dry air, the same evacuation/fill cycle is used. A supply of dry air was obtained by allowing air from the room to pass through a copper coil that was suspended in liquid nitrogen.

The solution state experiments were performed in a quartz cuvette at room temperature. The cuvette arrangement incorporated a freeze-thaw cell that could be used to remove the dissolved oxygen in the solution.

Sample Preparation

The polymer thin films were produced by spin-coating solutions of the polymer in question onto a rotating sapphire substrate. Firstly the polymer is dissolved into an appropriate solvent to make a solution of about 20 mg of polymer per millilitre of solvent. For the spin coating process it helps if the solvent is volatile, but obviously the solvent must be able to dissolve the polymer. The solution is left to mix for a

couple of hours and then filtered to remove any residual undissolved polymer. Then the target substrates are cleaned in IPA and mounted on a vacuum chuck that rotates the substrate. The substrate is then covered with the polymer solution and the thin film spun until it has dried. If the solvent isn't particularly volatile then it's necessary to heat the substrate using a heat gun or lamp in order to evaporate the solvent. Some experimentation with substrate preparation, solution concentration, spin speeds and durations and applied heat is required to produce good quality, uniform thin films with the right absorption. The process yields films of about 100 nm thickness.

Scanning Monochromator and Detector

Using a diffraction grating, the monochromator selects out a single frequency of the light that has come from the sample. This light is then shone onto a solid state detector, a silicon photodiode for light in the visible region, a cooled (80 K) indium arsenide photodiode for infrared light. Both these detectors give a current that is proportional to the intensity of light incident on them if the intensity is within the linear response region of the detectors. This current is passed through a transimpedance amplifier to yield an amplified voltage proportional to the current. Gains of about 10^4 to 10^5 were used. The intensity of light passed through the monochromator can be adjusted by altering the size of the entrance and exit slits. The voltage that the detector gives out has two components when the experiment is running; an AC component that is proportional to the dT signal, and a DC component which is proportional to the T signal.

The monochromator was calibrated by routing the laser beam along the main optical path (probe beam path) of the system. Back reflections from the monochromator optics were used to ensure that the probe light entered it perpendicularly.

The monochromator is connected to the controlling computer using an IEEE 488.2 interface. All functions of the monochromator are controlled from the computer.

Transimpedance Amplifier and Lockin Amplifier

The signal from the detector is multiplied by a transimpedance amplifier that scales the AC and DC components of the signal equally. This amplification occurs electrically close to the detector in order to minimise signal degradation; in the case of the silicon photodetector the amplifier is integrated onto the photodiode chip.

The AC component occurs at a certain frequency ω, the frequency of the strobe rate of the pump beam. This frequency is input separately into the lockin from the chopper, and is known as the reference signal. The lockin looks for the largest signal that occurs at the given input frequency and it will give the magnitude of this signal, R, and the phase difference, θ, between the AC signal and the reference signal. This phase difference is important because it gives a measure of the delay between the turning on of the pump beam and appearance of the excitation that the pump beam creates. This can be used to characterise the excitations since different excitations will in general have different decay lifetimes and so different phases. There is a problem, however. Although the reference signal will have the same frequency as the strobing pump beam, it will not necessarily have the same phase; the pump beam and reference signal will be out of step. The detector contributes to this difference; the capacitance of the detector changes with the frequency of the AC component that it is picking up, and hence the phase lag that the detector introduces is dependent on the pump strobe frequency. This implies that a reference point is needed.

One of the parameters that can be input into the lockin is a reference phase; the value for the phase of the AC signal the lockin gives will be the phase difference between the AC component and this reference phase. This reference phase can be set so that an output phase of 0 degrees corresponds to a signal that is in phase with the pump strobing. In order to obtain an absolute value for the phase difference (the delay between the AC signal and the pump beam strobe), the reference phase must be calibrated for the pump strobe frequencies used. Typically this was performed on the fluorescence signal for the luminescent polymers studied.

Once the reference phase has been established, plots of the quasi CW PIA data are then made of the in phase dT/T component and out of phase dT/T component from the

data inputs T (DC signal level), R (AC signal magnitude) and θ (AC signal phase) as shown in Equation 15.

$$\frac{dT_{InPhase}}{T} = \frac{R}{T} Sin\theta$$

$$\frac{dT_{OutOfPhase}}{T} = \frac{R}{T} Cos\theta$$

Equation 15. In phase and out of phase components for dT/T data.

By plotting the referenced, orthogonal phase components of the dT/T signal against energy, it is possible to easily determine the phase relationships between features in the plot. It is also sometimes possible to recover hidden features: that is, to detect PIA features that occur over similar energy ranges but have different phases.

A further phase complication arises from the requirement to use two different detectors in order to cover a sufficiently wide spectral range. The different detectors have different RC constants and therefore the reference phase needed will be different. Typically the Si detector was used for a baseline phase calibration on the fluorescent signal from the polymer. When the data from the InAs and Si detector were collected, care was taken so that their spectral ranges overlapped. A phase correction was then introduced into the InAs data such that the in phase and out of phase components from the two detectors matched up in the overlap region.

<u>Computer</u>

The monochromator and lockin amplifier are connected to the computer using an IEEE 488.2 interface bus. A custom computer program was written from scratch in order to collect and analyse the data, example screenshots are shown in Appendix A. The main task of the program that the computer runs is to perform a scan, measuring dT and T over a certain photon energy range and compiling this data into a dT/T spectrum. Additionally the program will move the monochromator to a certain photon energy and measure dT and T. This function is important when sitting at a dT/T feature and varying some other experimental parameter.

When the monochromator is moving its diffraction grating to a new wavelength, light still passes through the monochromator; whilst the grating is moving the light output has AC components because of the rotation of the grating. When performing a scan, the application must wait after every monochromator move for the lockin signal to stabilise.

A number of readings from the lockin amplifier are taken at every data point, whether in a scan or a spot measurement for peak characterisation. These values are then averaged to obtain a more stable signal; low signals require more readings to be taken. If the signal drops to below the noise level then it is very difficult to obtain usable data, no matter how many readings are taken.

3.3.2. System Improvements

Initially the experimental setup was developed for obtaining information from PANi (Chapter 6), which yields low signal levels but fortunately is very stable under the laser beam. The materials that were subsequently measured (PPy and PFO) have much greater dT/T signal levels but lasted much less time in the system. For experiments on these materials to be completed, it was necessary to improve the data collection time so that an entire data set could be collected before the sample degraded.

In order to speed up the entire scan process it is necessary to reduce the number of readings (increase the signal level) and/or to reduce the time taken to collect each reading (decrease the communications overhead). Both these approaches have been followed.

Signal level

Increasing the signal level involves increasing the intensity of the pump/probe beams and improving the collection efficiency. A more intense pump leads to a higher excited state population and therefore a higher dT/T signal. However, the higher

pump also reduces the lifetime of the sample, and so at some point the increase in speed from the higher signal is offset by the decrease in sample lifetime. Such an optimisation generally results in a different pump power for each polymer.

The main improvements to the signal level have come about through an adjustment of the collection optics stage. This has been achieved by moving the collection mirror closer to the sample and the addition of some new mirrors and lenses to bring the collected light beam onto the monochromator. The PIA and photobleaching signals are contained within the probe light beam and this is focussed onto the sample and collected with two matched focussing mirrors. However the photoluminescence signal is emitted over all angles and not just in a narrow cone. Moving the collection mirror closer has improved the collection efficiency of the photoluminescence signal considerably. This is clearly shown in Figure 19, which plots PIA spectra for identical samples with the two different collection optics configurations.
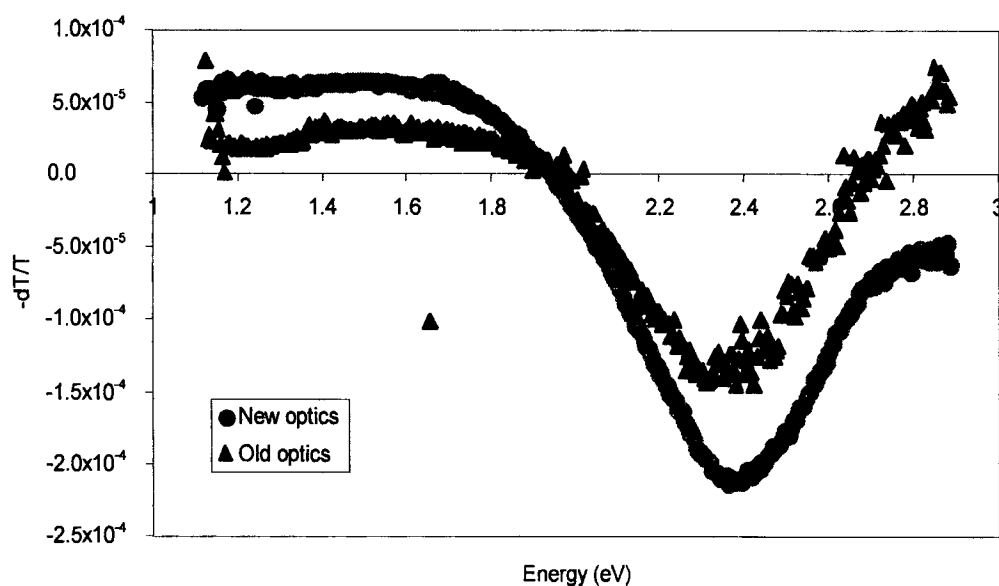
Figure 19. PIA spectra for a PPy sample collected with the old and new optics configurations.

Collection speed

The collection overhead has been reduced considerably by improvements that have been made to the computer interface. The interface is implemented using a specialised card installed in a computer. The card is controlled from the computer by calling functions in a software interface supplied with the card. The card then communicates with the instruments using the IEEE 488.2 protocol, transferring text

data. By improving the speed of the computer application, updating the computer hardware, and using new drivers for the interface hardware, it was possible to significantly reduce the communications and processing overhead.

3.4. Pulse radiolysis

This thesis makes extensive use of experimental data obtained using the technique of pulse radiolysis, performed at the Paterson Institute for Cancer Research Free Radical Research Facility (Manchester UK). Except in the case of PPy these data were not collected as part of the thesis. However the technique requires careful explanation given the importance of the pulse radiolysis data to the interpretation of the quasi steady state photoinduced absorption spectra.

Many different excited states can be photogenerated in a conjugated polymer and unambiguous assignment of a photoinduced feature to a particular excited state is not always possible through photoinduced absorption data alone. The technique of pulsed radiolysis creates triplet or charged states directly on a target polymer in solution. Transient absorptions associated with the state can then be identified, giving the absorption fingerprint of the state. If the fingerprints are present in the photoinduced absorption spectra (allowing for a solvatochromic shift in some cases) then we know they are created as a result of photoexcitation. The technique of pulsed radiolysis has only been applied to conjugated polymers over the past few years in the pioneering work of Monkman and Burrows et al [44], and has proved to be of great value in unambiguously determining the nature of the excited states in various materials. Unfortunately the technique requires an electron beam in the 1-10 MeV range; the amount of hardware required to generate this means that the experiment can only be performed at limited number of locations.

3.4.1. PR Basics

There are some similarities between the techniques of pulse radiolysis and photoinduced absorption: both techniques use transmission spectroscopy to detect the

changes in a sample as a result of some external excitation. In the case of pulse radiolysis experiments of the type referenced here, the sample is irradiated for a short time by an electron beam from a 10 MeV LINAC. The experimental setup used for these experiments is shown in Figure 20.
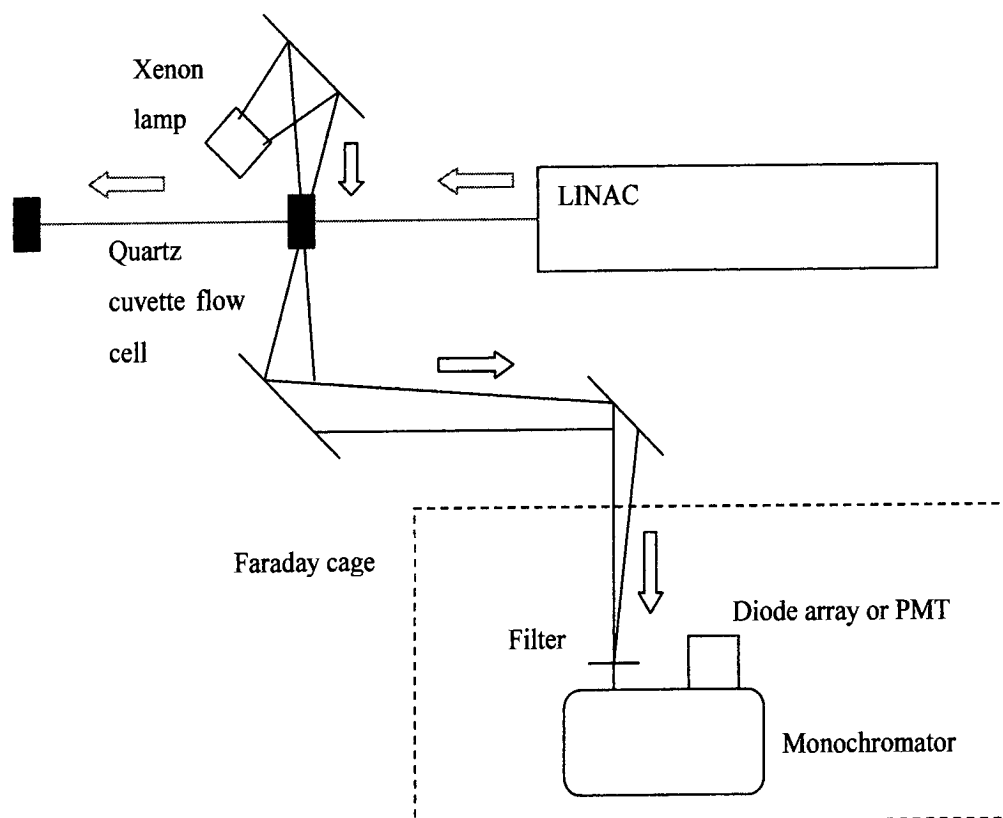
Figure 20. Pulse radiolysis spectrometer, taken from the literature [57]

LINAC

The LINAC generates a beam of electrons that are directed at the flow cell target. In these experiments the beam is at 10 MeV. It is possible to control the beam current and hence the dose delivered to the sample. This is usually done by adjusting the pulse duration in the range 10 ns to milliseconds.

Xenon lamp

The Xenon lamp is a stabilised steady source. The light is focussed onto the sample and then through it into a collection optics system which delivers the light to the monochromator.

Cuvette flow cell

The quartz cuvette contains the solution of solvent, conjugated polymer of interest, and possible acceptor material (see section 3.4.2). Since O_2 quenches triplet states, the solutions have argon gas bubbled through them for 30 minutes before exposure to the beam. A reservoir of solution is connected to the cuvette so that the solution can be automatically renewed after every shot from the LINAC. This avoids any possible problems with decomposition of the solution.

The electron beam ionises the solution in the reaction:

$$X + e^* \rightarrow X^+ + e^- + e^*$$

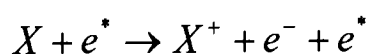Here, X represents all different components of the solution (solvent and solute(s)). The high energy incoming electrons e^* are absorbed by these components nonselectively; in dilute solutions this means that the interaction between the electron beam and the solvent is by far the most important process, simply because there are many more solvent molecules to interact with. There are two groups of solvent of interest where the evolution of the excited state proceeds differently. In some solvents, such as benzene, the X^+ and e^- components mainly recombine to form new singlet and triplet excited states:

$$X^+ + e^- \rightarrow {}^1X^* + {}^3X^*$$
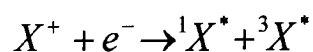
In other solvents, the charged separated species may remain separate to give the positively charged radical cation X^+ together with a solvated electron (e_{solv}^-), or the e^- may generate a radical anion:

$$e^- + X \rightarrow X^-$$
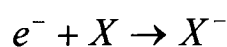
These charges or excitation energies are then transferred via collision to the target solute (conjugated polymer) of interest, as will be discussed in more detail later. The

fact that the initially created species (triplet or charged) is purely dependent on the choice of solvent means that pulse radiolysis can selectively introduce charged or triplet states onto the target conjugated polymer solute, which is a big advantage. One must simply find a solvent of each type that the target conjugated polymer will dissolve in.

Monochromator and detection system

Light from the Xenon lamp is focussed through a grating monochromator and onto a gated photodiode array or fast PMT, Si or Ge diode.

The diode array is used to obtain spectral data on the transient absorptions. The gate on the diode array is typically set to between 1- 350 µs after the electron beam trigger. By adjusting the diode array gate time and capturing multiple sets of spectral data from a particular sample, it is possible to track the evolution (grow in and decay) of the various transient absorptions. The use of the flow cell allows for multiple experiments to be performed before a new solution is needed. The experiment uses a single shot, gated collection method, not a quasi steady state method as with the photoinduced absorption experiment.

The fast PMT is used to obtain accurate signal decay data of a signal at a single wavelength.

3.4.2. Triplets

Benzene and triplet energy transfer

Upon exposure to the electron beam, liquid aromatic solvents such as benzene and toluene yield high concentrations of singlet and triplet excited states. With benzene, the relative triplet and singlet yields are 4.2 and 1.6 respectively[60,61], with ions and electrons being created in smaller yields[61,62]. These excited states can be transferred to acceptor polymers either through the Forster (see section 2.5.1) or Dexter (see section 2.5.2) mechanisms discussed previously. Collision between the excited donor

and the polymer is required for all energy transfer processes to occur. During the collision the Forster or Dexter mechanisms transfer the energy and electron transfer mediates the charge states. With triplet energy transfer the Dexter, or electron exchange, mechanism is dominant.

Benzene triplet lifetime and acceptors

The benzene triplet lifetime is unfortunately short, of the order of nanoseconds[62], which precludes generating significant triplet populations in the target conjugated polymer solute. A method for getting around this restriction was developed[63,64] where an additional solute, a triplet sensitizer, A, is added to the benzene solvent and the sample conjugated polymer solute of interest, S. The solute A has a long-lived triplet state: triplet energy transfer occurs from benzene->A->S provided that the concentration of benzene is much greater than that of A, and that of A much greater than that of S. Additionally there must be a down-hill energy ladder from benzene to A to S. Furthermore, if the sensitizer A has a high internal excited singlet to triplet ISC rate, then much of the initially generated benzene singlet energy can be mopped up and stored in the long lived $^3A^*$ state. In this scheme the transient absorption spectra that are then measured of S are of pure $^3S^*$, with no signal pollution from singlet S^* or even charged $S^{+,-}$ states:

$$Bz + e^* \rightarrow {}^1Bz^* + {}^3Bz^* + e^*$$
$${}^1Bz^* \rightarrow {}^3Bz^*$$
$${}^1Bz^* + A \rightarrow Bz + {}^1A^*$$
$${}^3Bz^* + A \rightarrow Bz + {}^3A^*$$
$${}^1A^* \rightarrow {}^3A^*$$
$${}^3A^* + S \rightarrow A + {}^3S^*$$
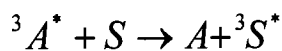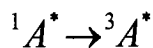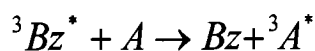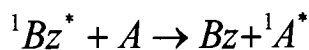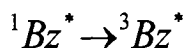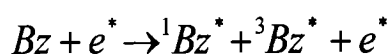
Acceptor energy levels: determination of S_0-T_1 level in conjugated polymers

For the sensitizers, A, to be able to transfer triplet energy to the polymer under investigation S, the triplet energy of A must be greater than that of S. By performing repeat experiments using sensitizers with different known triplet energies it is

54

therefore often possible to determine the cut off point for triplet energy transfer and thus obtain a range of energies within which the S_0-T_1 gap of the polymer, S, must lie. Obviously the accuracy that each polymer can be measured to depends on the energy gap between the adjacent triplet donors that do and do not cause S to show transient absorptions. The range of available donors is tabulated elsewhere[44], and stretches from benzophenone (2.97 eV) down to rubrene (1.14 eV). This process is illustrated in Figure 21. Initial exposure to the electron beam creates benzene singlet and triplet states. Triplet energy transfer occurs from benzene to the triplet donor that is in solution. Figure 21 shows T^1 levels from multiple donors but only one of these donors is present in any single experiment. Only those donors whose triplet energy level is greater than the T^1 level of the polymer can transfer triplet energy to it. The figure does not show the ISC processes within benzene and the donors.

S^1 T^2

T^1 PIA

T^1 S^1

ET   ET

ET T^1

S^0

Benzene → Triplet donors → Polymer
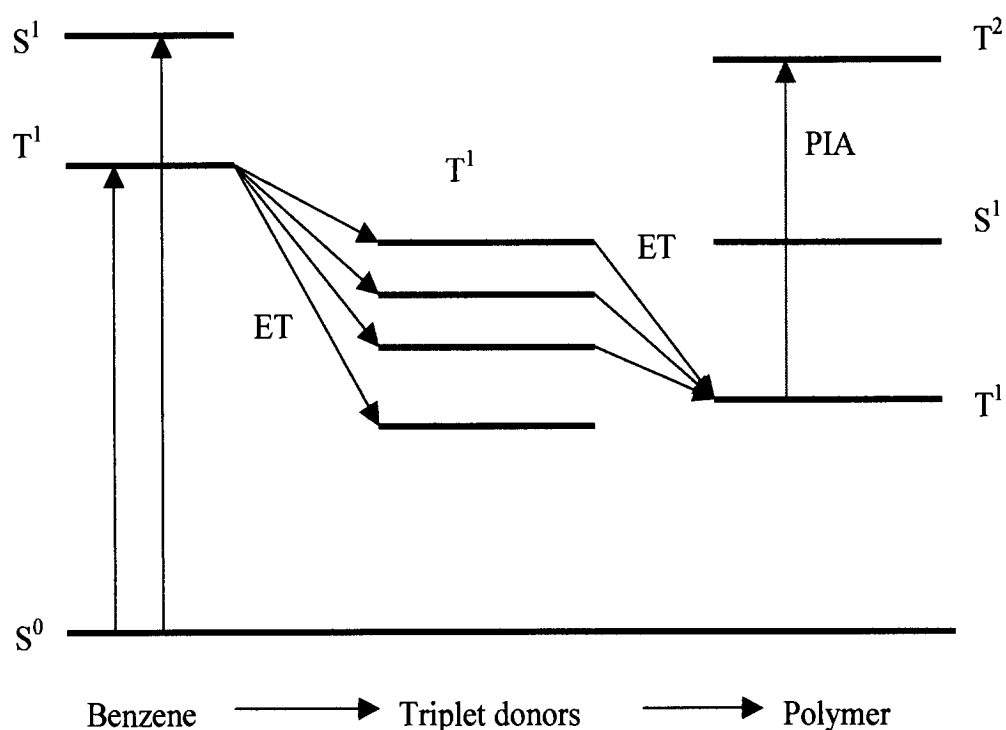
Figure 21. Down hill triplet energy transfer process in pulse radiolysis[44]

A further low energy band in the S_0-T_1 energy gap is possible by allowing molecular oxygen into the solution. As oxygen has a triplet ground state, it quenches triplet states through the energy transfer reaction[44]:

$$^3O_2 + {}^3S^* \rightarrow O_2^* + S$$
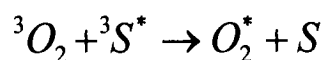
The triplet energy level of molecular oxygen is[44] 0.94 eV: if the triplet transient absorption disappears when oxygen is allowed into the solution, then the S_0-T_1 energy gap must be greater than 0.94 eV. The introduction is also a useful confirmation of the triplet signal via their oxygen quenching.

3.4.3. Charged States

Other solvents form positive radical ions or solvated electrons or negative radical ions when exposed to the electron beam. These species can then generate either positive or negative polymer states S^+ or S^-. Using pulse radiolysis it is therefore possible to differentiate between positive and negative polarons. For example, with chloroform a radical cation is formed upon exposure to the electron beam ($e^\bullet$):

$$CHCl_3 + e^\bullet \rightarrow CHCl_3^+ + e^- + e^\bullet$$

The solvent can then interact with the target polymer as follows:

$$CHCl_3^+ + S \rightarrow CHCl_3 + S^+$$
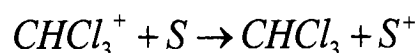
3.4.4. Triplet-triplet absorption spectra in solution

In order to understand the transient absorption data from a pulse radiolysis experiment it's helpful to examine a case from the literature[42,65] in which triplet energy is transferred to MEH-PPV (Figure 22) using the pulse radiolysis technique, and the results are compared to those from photoinduced absorption.
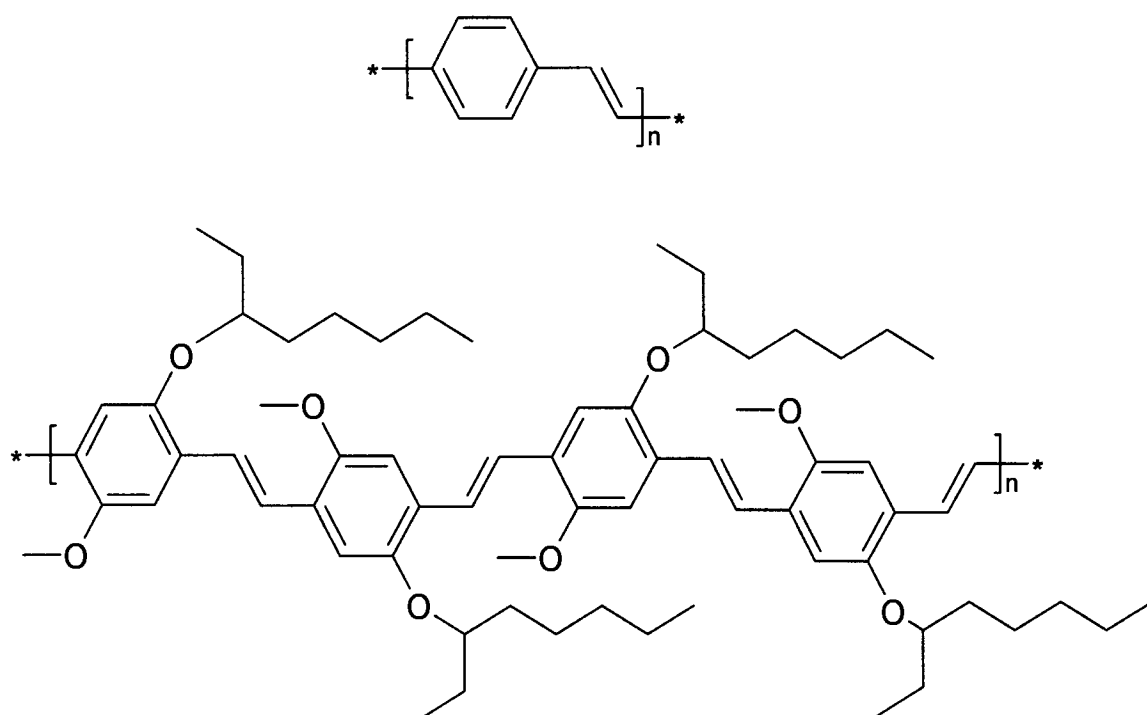
Figure 22. PPV (top) and MEH-PPV (bottom)

Figure 23 shows a temporally resolved transient absorption spectrum of the type obtained through pulse radiolysis experiments. In this case, upon radiolysis of an Argon saturated solution of the biphenyl triplet sensitizer in benzene a transient absorption is observed at 3.4 eV (360 nm). This is an induced absorption within the triplet manifold[44,45]. The tail of the bleaching for the biphenyl transition is also observed at 4.1 eV (300 nm), at the limit of the experimental range. With MEH-PPV added to the solution, the biphenyl signal remains but its induced feature decays with time and there is an associated induced absorption at 1.5 eV (830 nm) and bleaching at 2.4 eV (510 nm). The rate of grow in of the induced absorption is identical to the decay of the biphenyl signal, indicating the transfer of triplets from biphenyl to MEH-PPV. The rates of formation of the new induced absorption and new bleaching are also identical, indicating that electrons are excited out of the MEH-PPV ground state to form a new occupied triplet state, absorption from which is observed at 1.5 eV.
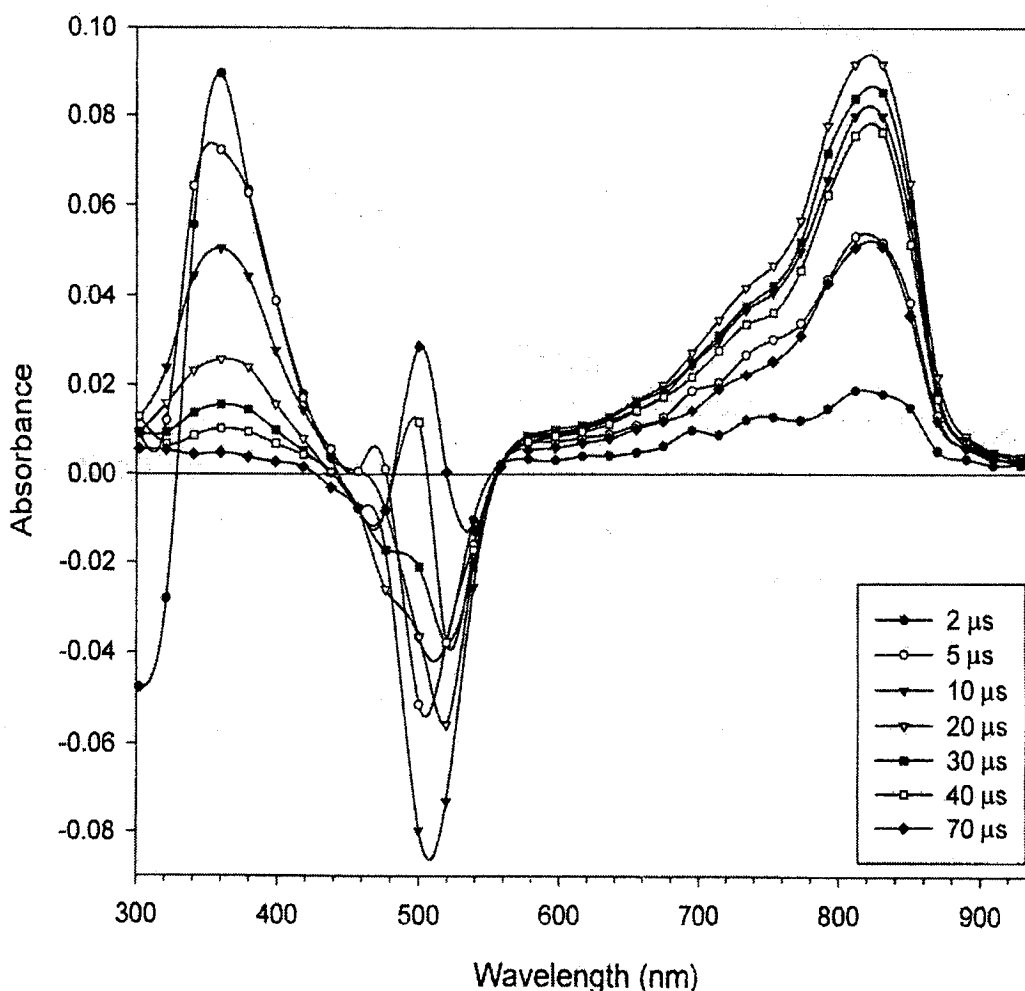
Figure 23. Transient absorption spectrum of MEH-PPV following triplet energy transfer[44].

The new induced absorption from the triplet states introduced by pulse radiolysis is very similar to that observed through quasi steady state photoinduced absorption experiments on thin films of MEH-PPV[66]. In fact there is a small 100 meV energy shift between the room temperature solution state PR and low temperature solid state PIA experiments. This low figure indicates a neutral triplet, as there is little solvatochromic shift between the excited state and the polar solvent. Additionally the state must be localised such that there is little alteration in the energy of the state from inter-chain interactions that are present in the thin film.

Comparisons of this type between PIA and PR have been used in this work.

Chapter 4. Experimental Study of Polypyridine

4.1. Introduction

Poly(p-pyridine) (PPy) was first synthesised and characterised by Yamato *et al*[67], who showed that (PPy) is luminescent and stable with respect to oxidation. A group[68,69] at Ohio State University confirmed this work and studied the photophysical properties in more detail. More recently, changes to the synthesis route for PPy[70,71] have yielded further progress, with photoluminescence quantum yield values of 37% being reported compared to the initial reports of ~5%. Pyridine based polymers have shown to be promising candidates for PLEDs[38,69,72,,73].

Chemical structure

The basic motivation behind studying materials such as PPy is that in order to achieve the stability required for industrial applications of these luminescent polymers, the materials must be stable against failure mechanisms such as oxidation. It is easy to remove electrons from electron-rich π orbitals in these conjugated materials. One way to increase oxidative stability is to remove electron density from the repeat units along the polymer backbone whilst retaining π conjugation and enough electron density to allow the interesting physics. In PPy this is achieved by the introduction of nitrogen atoms in to the π system of the phenyl ring, as shown in Figure 24.
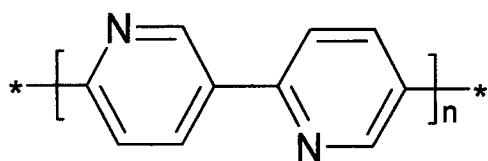
Figure 24. Chemical structure of PPy

Photophysics of PPyV

It has been shown[69] that the primary photoexcitations in pyridine based polymers are singlet excitons. The nitrogen heteroatom enhances the intersystem crossing to the triplet manifold via spin-orbit coupling[74]. In the pyridine based polymer PPyV (Figure 25), quasi steady state photoinduced absorption bands were attributed to triplet

excitons, based upon the observation of a 1.9 eV PIA band in a solution of PpyV[69], and picosecond time resolved experiments that showed the grow in of a long-lived PIA band as an initially photogenerated singlet exciton band decayed. Photoinduced absorption spectra on thin films of PPyV showed photoinduced absorption features at 0.9 eV and 1.9 eV. The 1.9 eV feature is assigned to the triplet exciton transition observed in the PPyV solution[69], however the 0.9 eV feature is not clearly assigned and no lifetime information is available from the millisecond PIA experiments for these long-lived states. These assignments of the excited states in PPyV are not completely conclusive.
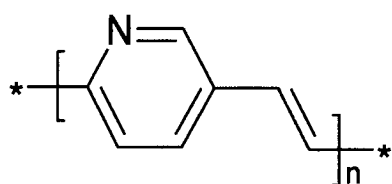
Figure 25. Chemical structure of PPyV

In order to determine the exact nature of the photoexcited states in PPy, photoinduced absorption experiments have been performed on thin films of PPy under various conditions. Pulse radiolysis experiments are utilised in order to obtain an unambiguous assignment of the excited state.

4.2. Results

Ground state absorption and photoluminescence
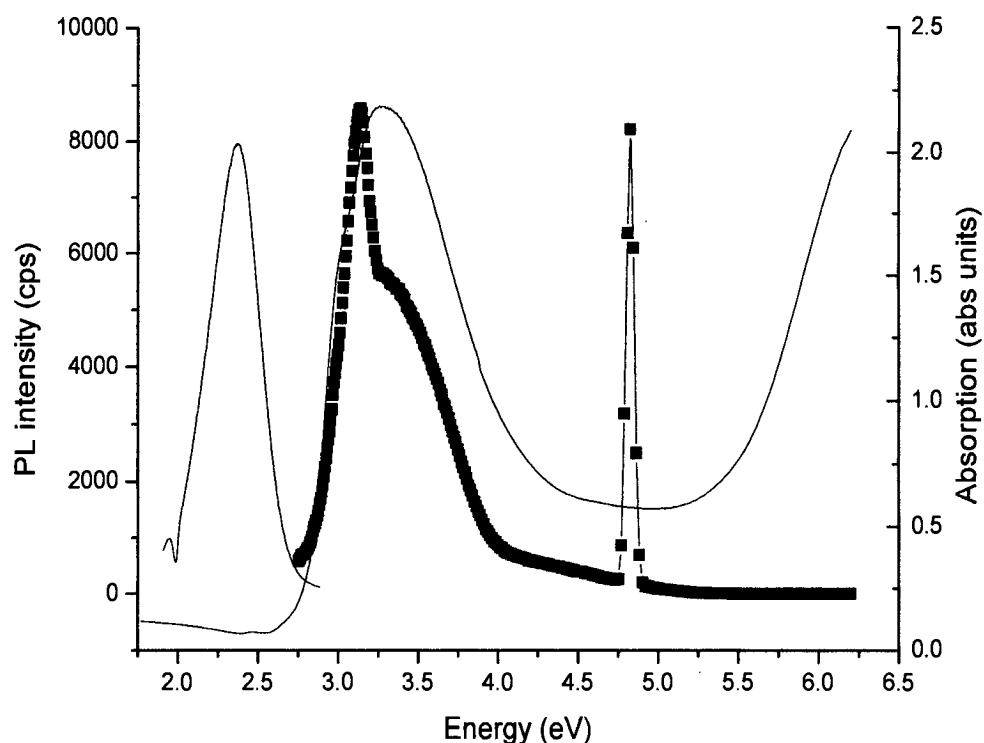
Figure 26. Photoluminescence (smooth, left), excitation (dotted) and absorption (smooth, right) spectra for PPy at 300K.

Figure 26 shows a composite plot of photoluminescence, excitation and absorption data. The PL data were taken for an excitation wavelength of 350 nm (3.54 eV). The excitation data were taken by monitoring the photoluminescent signal at 515 nm (2.4 eV). The spike in the excitation plot at 4.8 eV (258 nm) is caused by the second order diffraction of 258 nm at 516 nm; some pump light is being reflected into the detection system.

Photoinduced absorption data at 87 K

Figure 27 shows a photoinduced absorption spectrum of a thin film of PPy on a sapphire substrate in a Helium atmosphere at 87K. A pump power of 40 mW was used, yielding approximately 0.5 mW/mm^2 at the sample from the UV lines of an

argon ion laser (pump at 3.5 eV, the peak of the PPy absorption band, see Figure 26) with a chop rate of 22 Hz. The lockin amplifier was autophased on the photoluminescence peak before the experiment was performed.
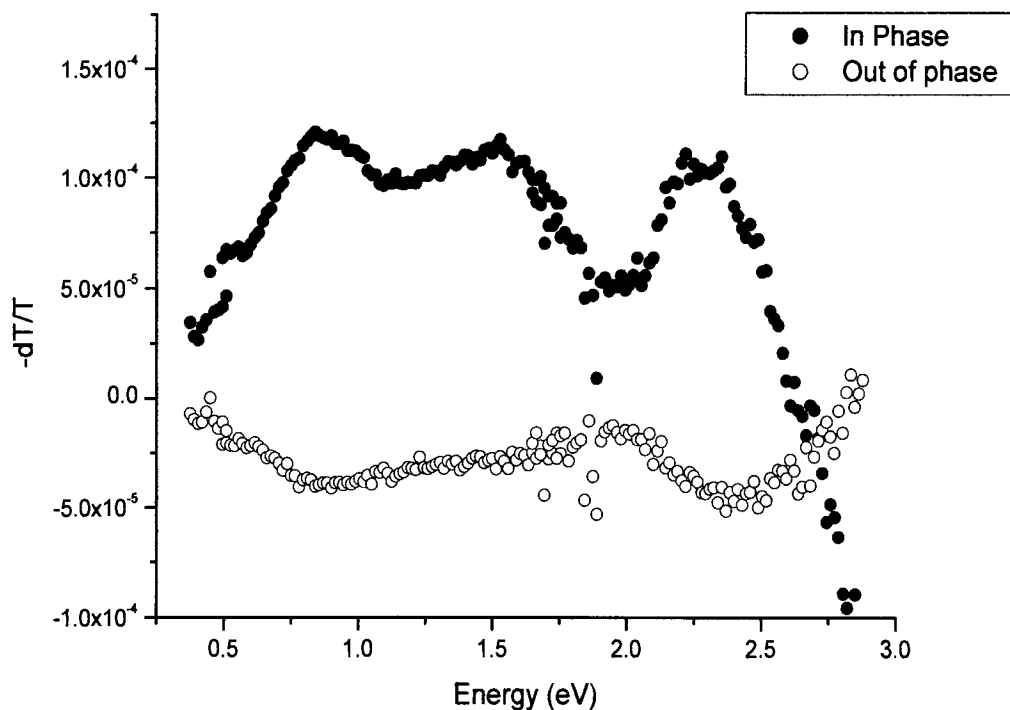
Figure 27. Quasi steady state photoinduced absorption spectrum of PPy in He at 87K.

Four features are clearly visible in the plot. There are photoinduced absorptions at 0.8 eV, 1.5 eV and 2.3 eV together with a photobleaching effect at ca 3 eV. There is a slight phase shift between the broad 0.8 eV and 1.5 eV peaks but this could be an experimental effect due to incorrect phase matching at the infra-red / visible detector change at 1.1 eV. The peak at 2.3 eV is phase shifted further still but this is due to the onset of a photoluminescence band underneath the strong photoinduced absorption signal (see Figure 28 below). The noise seen in the dT/T signal at around 1.8 eV arises because the DC (T) level measured at the detector is near the noise floor; hence a steady dT signal is divided by a very small, fluctuating number. The low dc transmission is an instrumentation effect caused by the onset of the absorption band of an order-sorting filter.
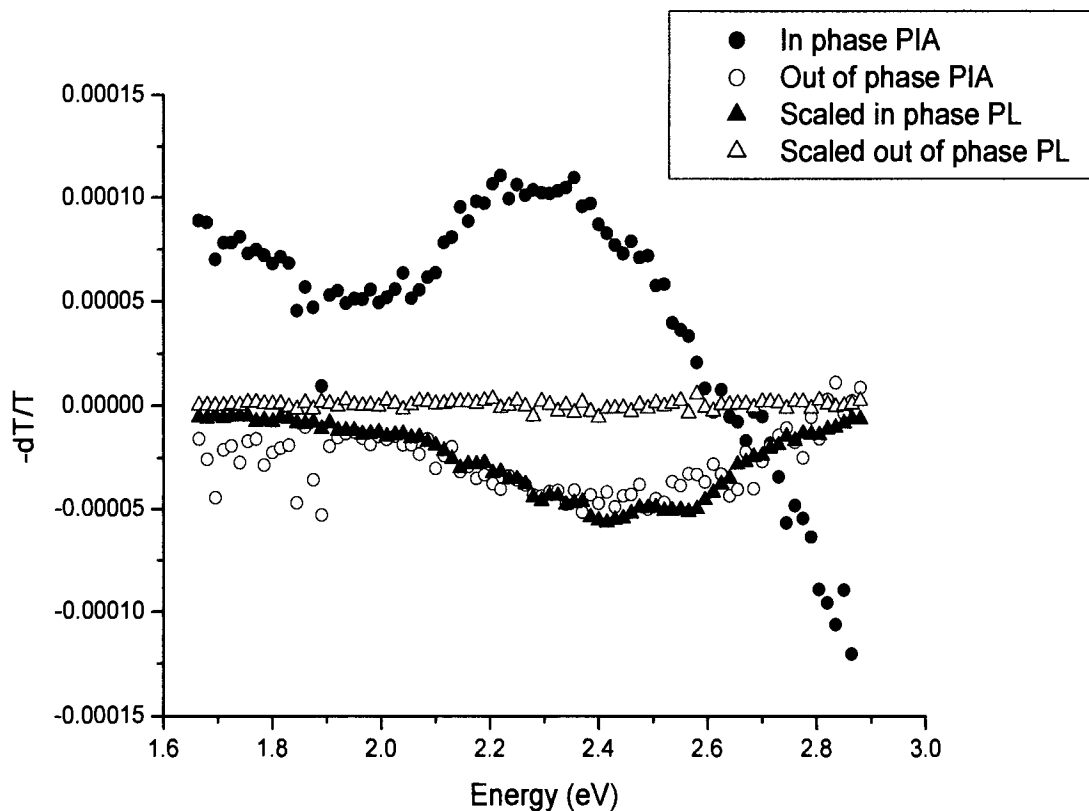
Figure 28. Quasi steady state photoinduced absorption spectrum of PPy in He at 80K compared with a photoluminescence spectrum obtained using the same apparatus.

Figure 28 shows a section of the photoinduced absorption spectrum plotted together with photoluminescence data. The photoluminescence data was obtained in the photoinduced absorption apparatus simply by blocking off the probe beam. An AC signal is still detected because photoluminescence is obviously an emissive process. It is this raw, unscaled AC (dT) signal only that is plotted as the PL spectrum in Figure 28. It can also be seen that the pure dT PL data is smoother than the dT/T PIA signal and reveals a vibronic structure to the emission. This implies that radiative recombination takes place on well-ordered chains with approximately the same band gap as otherwise the vibronic features would be smeared out by the distribution of energies at the emission centres. This vibronic structure is not seen in the room temperature PL (see Figure 26) data because the higher levels of thermal excitation are sufficient to smear out the vibronic bands.

These results clearly show that with careful use of a reference phase hidden features can be recovered from the dT/T data by resolving the AC signal into two orthogonal components (in phase and out of phase). We have been able to detect the residual PL signal that exists underneath the strong photoinduced absorption feature at 2.3 eV. Unfortunately, the unavoidable presence of the PL signal prevents any information being gathered on the phase shift of the 2.29 eV feature (and therefore its delay with respect to the pump laser). The phase shift between the 1.5 eV and 0.8 eV features and the PL only signal implies that there is an appreciable delay between the emission of the PL and the detection of the PIA signal. This indicates a difference in the lifetime of the PL and PIA features, as expected.

When performing photoluminescence experiments at low temperatures it is readily apparent to the eye that the colour of the emission is different to that at room temperature. This difference prompted the room temperature photoinduced absorption experiments that are detailed in a later section.

Chop rate characterisation of PIA features

Chop rate dependencies were then measured for each of the three photoinduced absorption peaks in order to obtain more lifetime information. In practice, the chop rate data were difficult to obtain because laser degradation of the sample lowers the measured dT/T signal continuously during the chop rate experiment. The laser power was carefully adjusted to maximise sample lifetime whilst still being intense enough to yield measurable signals at the higher chop rates. The experiments were all performed on fresh PPy films in order to maximise the available signal and lifetime. Following these precautions a pump power of 30 mW over the sample (0.38 mW/mm^2 power density) was used. The chop rate data are plotted in Figure 29 to Figure 32.
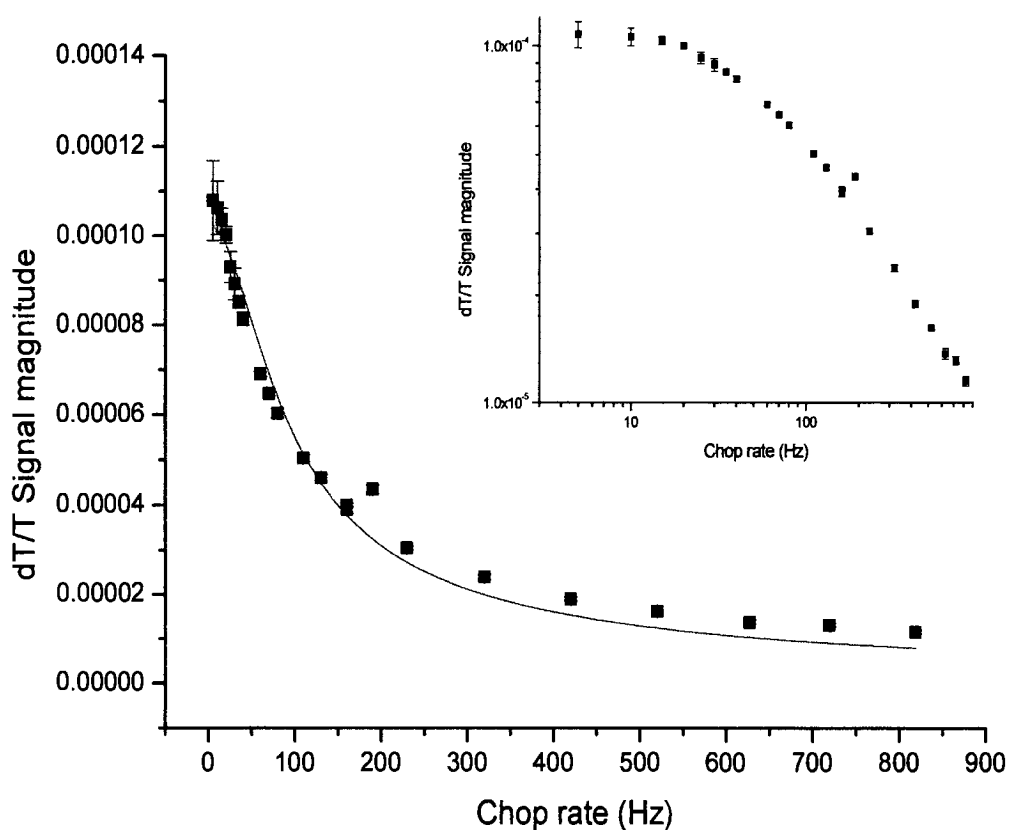
Figure 29. Chop rate dependence of 2.29 eV peak in He at 87K.

The log-log plot inset of Figure 29 shows the well-known form described in Equation 11 for a monomolecular decay profile. There is a low-ω region in which the signal level is independent of chop rate, ω ($\omega\tau \ll 1$) and a high-ω region of strong frequency dependence ($\omega\tau \gg 1$). In practice the data were indeed best fitted using a monomolecular decay function (Equation 11) and the main plot of Figure 29 shows the chop rate data together with a solid curve representing the best fit to the monomolecular function. The data were fitted using the Levenberg-Marquardt method. The fit returns a value for the feature steady state lifetime, τ, and in this case $\tau = (15.81 \pm 0.86)$ milliseconds.

The relatively large monomolecular lifetime of the 2.29 eV feature suggests that it is due to a transition within the manifold of an optically generated triplet exciton state. This is because the other long-lived states (polarons/bipolarons) decay through mutual annihilation – that is bimolecularly. Triplets can mutually annihilate to decay

bimolecularly also but it is evident that this process is not dominant in this system. In order to support the conclusion the chop rate experiment was repeated with dry air (and therefore oxygen) in the sample chamber. The presence of oxygen quenches triplet states since the ground state of oxygen is a triplet, as shown in Equation 16. A small increase in sample temperature was necessary in order to maintain the oxygen in a gaseous state. These data are plotted in Figure 30.

$$^{3}O_{2} + {}^{3}S^{*} \rightarrow O_{2}^{*} + S$$
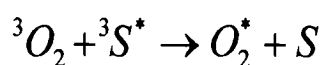
Equation 16
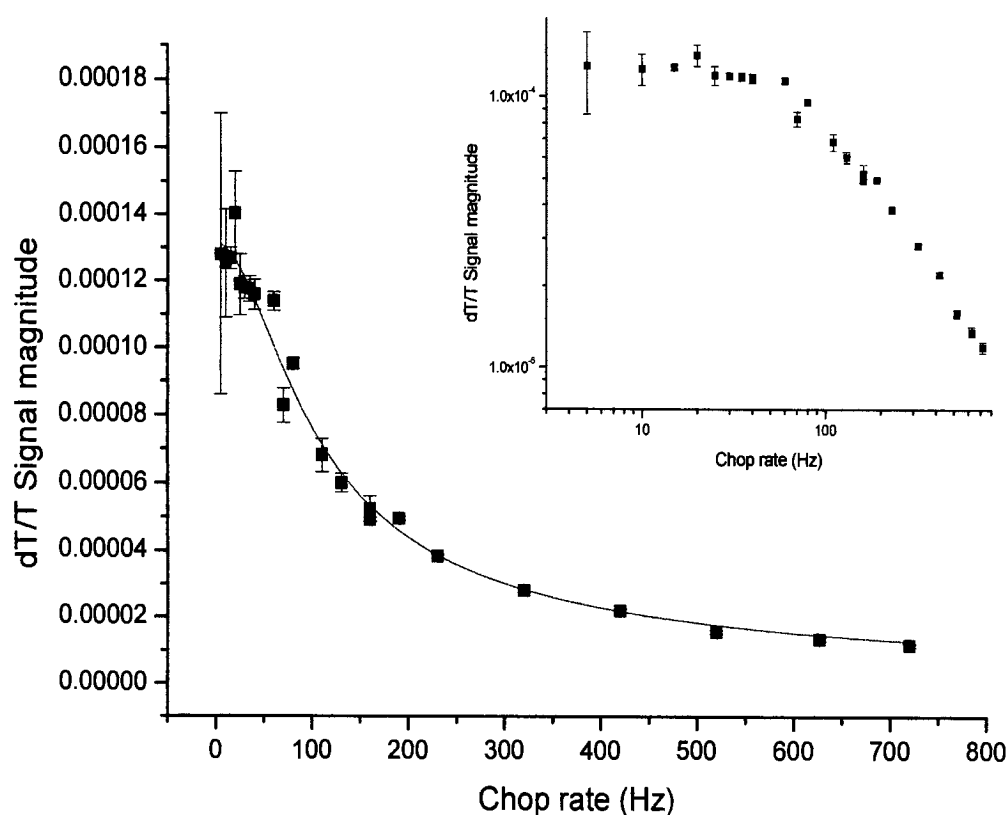
Figure 30. Chop rate dependence of 2.29 eV peak in air at 92K.

As before the log-log plot inset of Figure 30 shows a region where the signal strength is independent of chop rate. Comparison with Figure 29 shows that the flat region persists over a longer range of chop rates. This indicates that the ac signal from the photoinduced state is better able to keep up with the increasing laser pulse frequency and therefore that the state has a shorter lifetime. This is confirmed by a fit to the

monomolecular decay function that reveals a slightly reduced feature steady state lifetime τ of (14.11 ± 0.76) milliseconds. In addition, the Chi^2 fit is better with Oxygen added, indicating that the monomolecular decay channel has become more dominant, as would be expected for triplet quenching to form singlet oxygen. Data presented later (Figure 34) indicates that the lifetime of this feature should not be altered by the minor increase in temperature. The reduction of the 2.29 eV feature lifetime in the presence of oxygen provides strong additional evidence for this absorption being the result of a triplet state through the addition of an extra decay path for the triplet state via the oxygen.
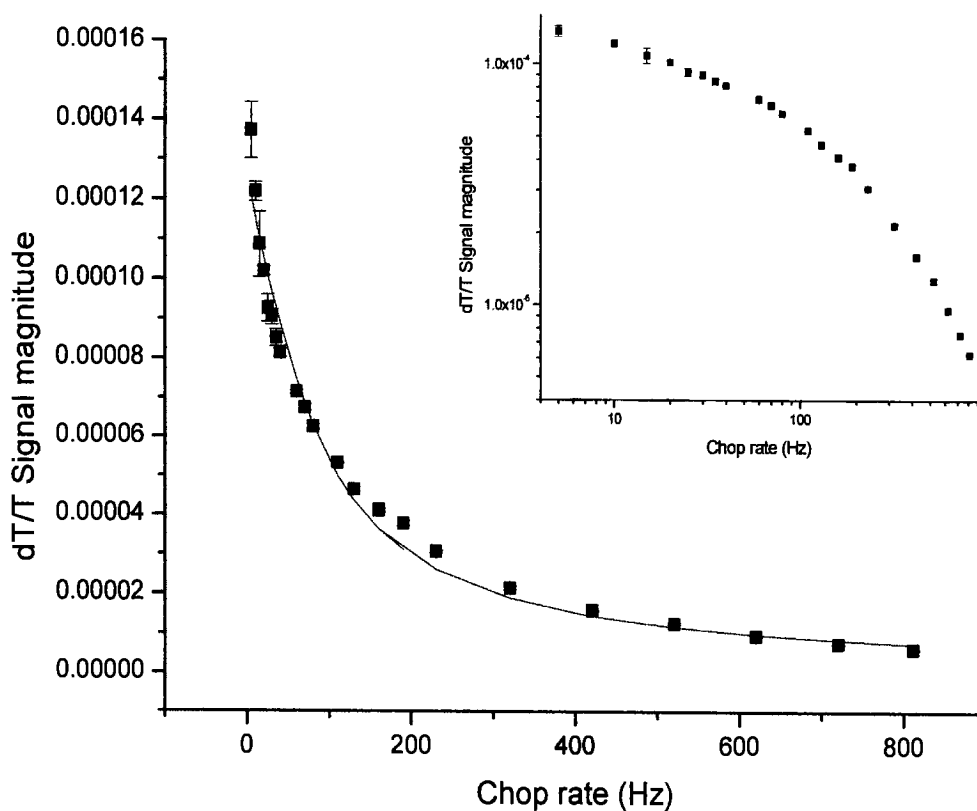
Figure 31. Chop rate dependence of 1.50 eV peak in He at 87K.

Figure 31 shows the chop rate dependence for the 1.5 eV feature. As can be seen by the log-log plot insert this feature does not follow a monomolecular decay profile as the as the signal drops continuously. The data are best fitted using a bimolecular decay

profile (Equation 13), and the solid curve shows an optimised fit to this function, giving a steady state lifetime of (32.4 ± 2.3) milliseconds.
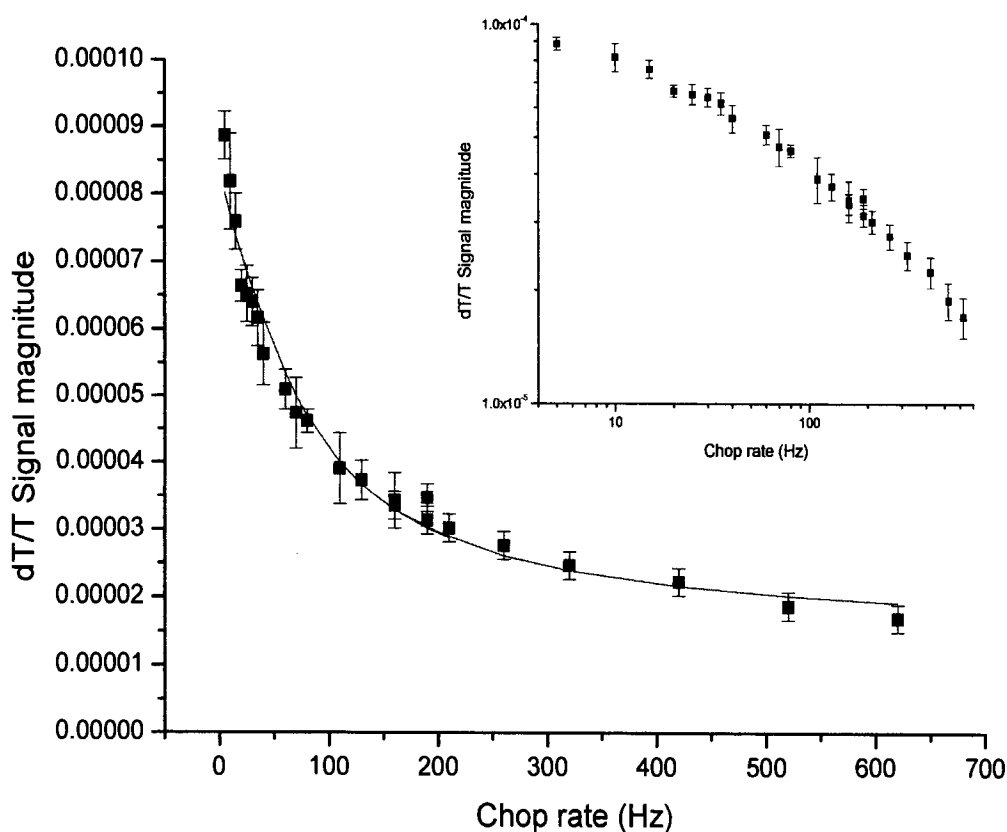
Figure 32. Chop rate dependence of 0.8 eV peak in He at 87 K.

The chop rate dependence shown in Figure 32 for the 0.8 eV feature shows a similar bimolecular nature to that seen in Figure 31. In order to obtain a reasonable fit in this case it was necessary to add a small constant (a dT/T shift of 1.0×10^{-5} or approximately 6 μV in AC signal terms) onto the bimolecular decay function. Experimentally the signal shift arises from a thermally induced modulation of the light transmitted through the sample and/or an AC noise offset from the infra red detector. The fitting process gives a value of (35.0 ± 5.0) milliseconds for the steady state lifetime, which is identical within the errors to the value obtained for the bimolecularly decaying feature at 1.5 eV. Given the similarity between the chop rate dependency and PIA spectrum phases of the 0.8 eV and 1.5 eV features it seems likely that both transient absorptions arise from the same excited state. This, together with the bimolecular decay profile

indicates that the excited state is a polaron (see section 2.4.2). This means that the decay of the state proceeds as n^2 (n population of molecules in this excited state) and hence that this excited state is destroyed when two such states recombine. The 1.5 eV feature is therefore characteristic of a charged species, as photoexcited charge pairs require an opposing charge to be destroyed. Such charged states can have the millisecond lifetime observed here if charge pairs photocreated on one chain become separated through interchain diffusion. It should be noted that running a photoinduced absorption experiment on a solution of the material under investigation is often a good way of determining whether a particular photoinduced feature is due to an inter-chain excitation; the feature should disappear in a dilute solution. Such a solution experiment has not been performed for PPy. Triplet-triplet annihilation (see section 2.6.4) is another bimolecular decay process but it is apparent from the data presented earlier that the triplet PIA is at 2.29 eV and has a different lifetime.

Information obtained from the photoinduced absorption experiments performed at 87K is summarised in Table 1.

Energy	Type	Lifetime at 87K	Proposed origin
2.29 eV	Monomolecular	(15.81 ± 0.86) ms	Triplet exciton; transition within triplet manifold
1.5 eV	Bimolecular	(32.4 ± 2.3) ms	Polaron; transition to/from sub-gap levels and CB/VB
0.8 eV	Bimolecular	(35.0 ± 5.0) ms	Polaron; transition to/from sub-gap levels and CB/VB

Table 1. Summary of photoinduced absorption results at 87K

Photoinduced absorption data at 300K

Figure 33 shows a photoinduced absorption spectrum of a PPy thin film in air at 300K. A pump power of 40 mW was used, yielding approximately 0.5 mw/mm^2 at the sample with a chop rate of 22 Hz. The increased sample temperature means that it is very difficult to obtain real IR data from the sample so the range of the scan is reduced over that of Figure 27. The figure shows two main features, a photoinduced absorption at about 1.5 eV and a photoluminescence signal at 2.4 eV. The photoluminescence signal

has a slightly different phase to the photoinduced absorption feature. The 1.5 eV peak is assigned to the charged state discussed previously.
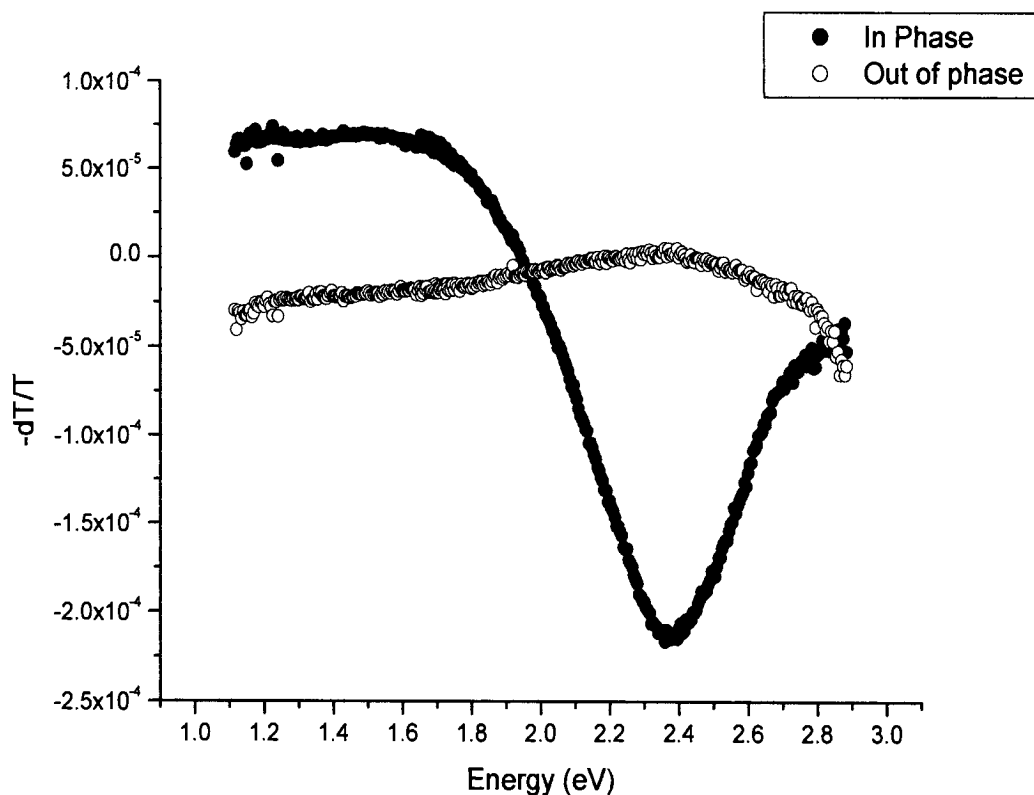
Figure 33. Quasi steady state photoinduced absorption spectrum of PPy in air at 300K.

By comparison with Figure 27 we see that the triplet feature at 2.29 eV has disappeared to reveal the photoluminescent feature, and conclude that one or both of the following two processes are responsible. The photoluminescence signal could be stronger at the higher temperature so that it is obscuring the PIA signal. The lifetime of the triplet state we have assigned to the 2.29 eV feature could also be much reduced at 300K. In an attempt to resolve this ambiguity another experiment has been performed, as shown in Figure 34.

Temperature dependence of 2.29 eV feature

Figure 34 is a plot of the magnitude and phase of the 2.29 eV dT/T peak as a function of temperature. As the temperature increases, the magnitude and phase of the photoinduced absorption changes. Photoinduced absorption is a kind of two-photon experiment; a pump beam photon must create the excited state and a probe beam photon must interact with it during the lifetime of the state. A reduction in the signal strength with increasing temperature shows that the numbers of such pump photon → excited state → probe photon interactions decreases with temperature and therefore that the triplet state lifetime (or window of probe photon opportunity) decreases with increasing temperature. The change in phase shows there is another AC component that is contributing to the resultant signal detected by the lockin amplifier. This signal is the buried PL signal; as the magnitude of the PIA signal decreases the resultant AC signal sweeps around to the magnitude and phase of the PL signal. The lockin amplifier was autophased previously at 2.29 eV with the probe light off: zero phase therefore corresponds to the PL signal only.
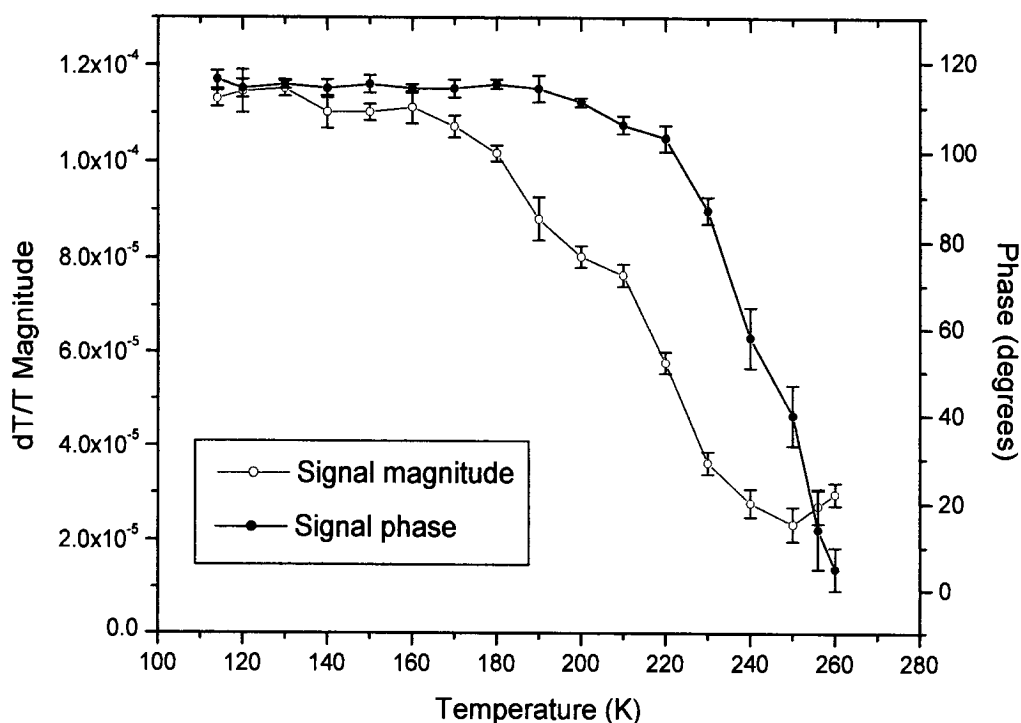
Figure 34. Temperature dependence of the 2.29 eV PIA peak in dry air.

At around 250K the magnitude and phase level off. At this point, we can say that the Quasi-cw photoinduced absorption experiment is unable to get enough probe photons through the excited state population to allow a meaningful PIA signal to be obtained. We are therefore measuring the PL signal only. The PL feature emits its own signal photons (by definition) and so the PL signal strength detected by the instrumentation is not affected by changes in lifetime. It is possible that the photoluminescent yield (and therefore AC signal at zero phase) also changes with increasing temperature but this would require a separate no-probe experiment which has not been performed. Instead PL spectra were measured at 300 K and 80K, and this data is presented below.

Furthermore, this temperature dependence confirms that the different lifetimes obtained from the chop rate dependence of a sample in He at 87K (Figure 29) and in air at 92K (Figure 30) is purely due to the presence of O_2.

Photoluminescence data

Photoluminescence data can be obtained in the photoinduced absorption apparatus by switching the probe beam off. Figure 35 shows PL data obtained in this way for a PPy thin film in a helium atmosphere at 300K and 80K. The spectra have not been corrected for the instrument response function, although this will of course be the same for both spectra.
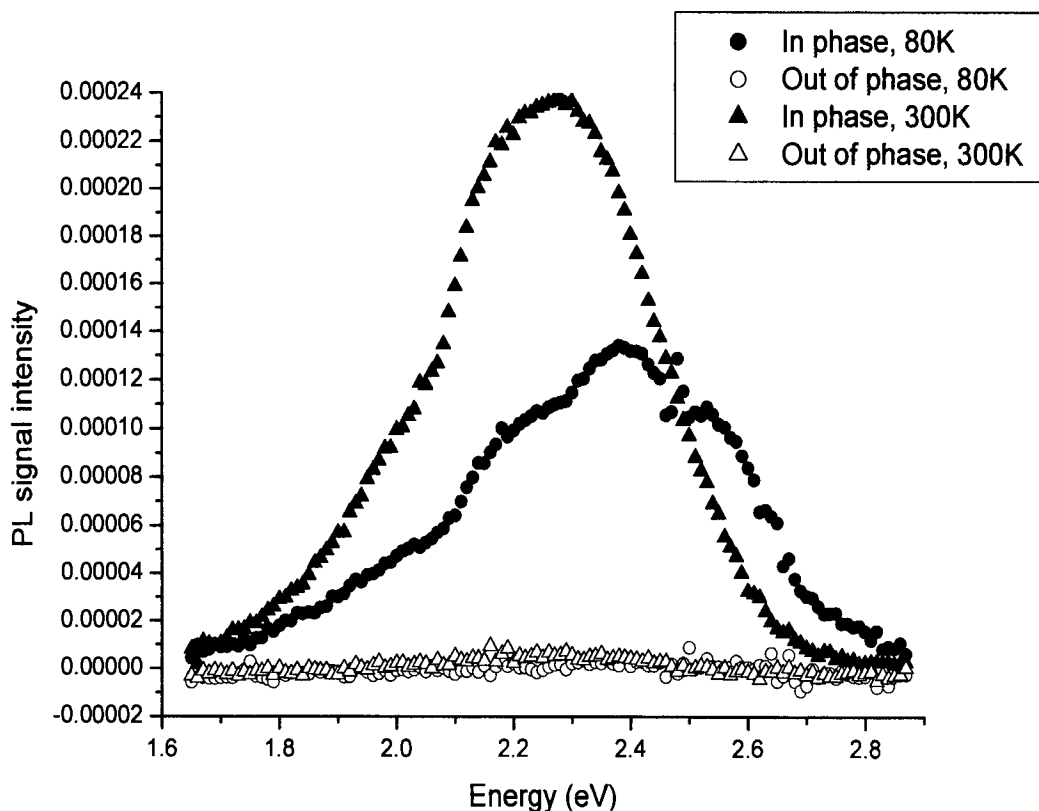
Figure 35. PPy photoluminescence spectra.

Figure 35 shows a clear difference between the spectra at 80K and 300K, one that is contrary to normal experience. Typically, the PL redshifts as the temperature decreases in response to increased monomer alignment and therefore increased delocalisation at low temperatures. However in this case the PL blueshifts as the temperature decreases: a green component of the PL spectrum at 2.3 eV becomes weaker whereas a blue component at 2.5-2.6 eV becomes stronger.

Pulsed radiolysis data

Whilst the photoinduced absorption data is convincing, its interpretation can be open to some dispute. Pulsed radiolysis experiments (see section 3.4) provide a way of directly generating specific excited states in a target polymer. If the absorption bands so created match up with absorption bands observed by a photoexcitation of the sample, then we know that the particular excited state is generated in the polymer as a result of photoexcitation. This technique has been used for PPy by Monkman *et al*[65,75].

These experiments rely on dissolving PPy in various solvents to inject different types of excited state. Unfortunately normal PPy is only soluble in formic acid, which limited the investigation to injecting negative charged states only. Fortunately a synthesis route for regio-regular PPy (rPPy) was developed and this material is marginally soluble in benzene, allowing triplet injection experiments to be performed. The addition of triplet energy donors into the benzene solvent allows the injection energy of triplets into rPPy to be tuned. By adjusting the energy donors it is possible to determine the absolute (S_0 – T_1) energy of the triplet state, which cannot be determined using photoinduced absorption methods.

Figure 36 shows the induced absorption obtained when using a biphenyl energy donor in a benzene solution which had argon gas bubbled through it for 30 minutes to degas the solution. A triplet-triplet absorption is seen at 590 nm (2.1 eV). This absorption is quenched by the addition of O_2 into the solution, confirming that it is a triplet species. The group were able to determine that the S_0-T_1 energy is 2.4-2.5 eV in rPPy.
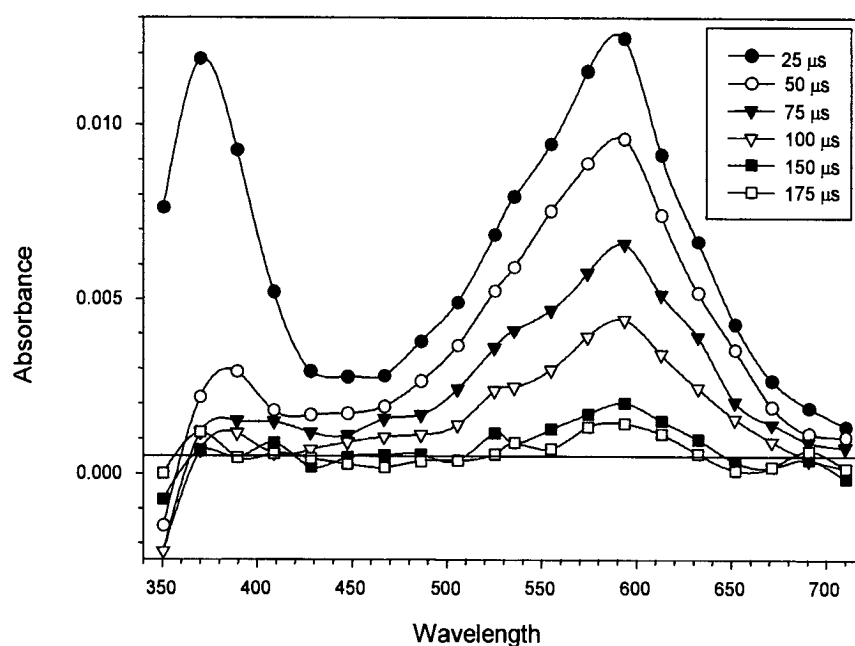
Figure 36. Triplet-triplet absorption spectrum of rPPy in benzene solution containing biphenyl triplet energy donors[65].
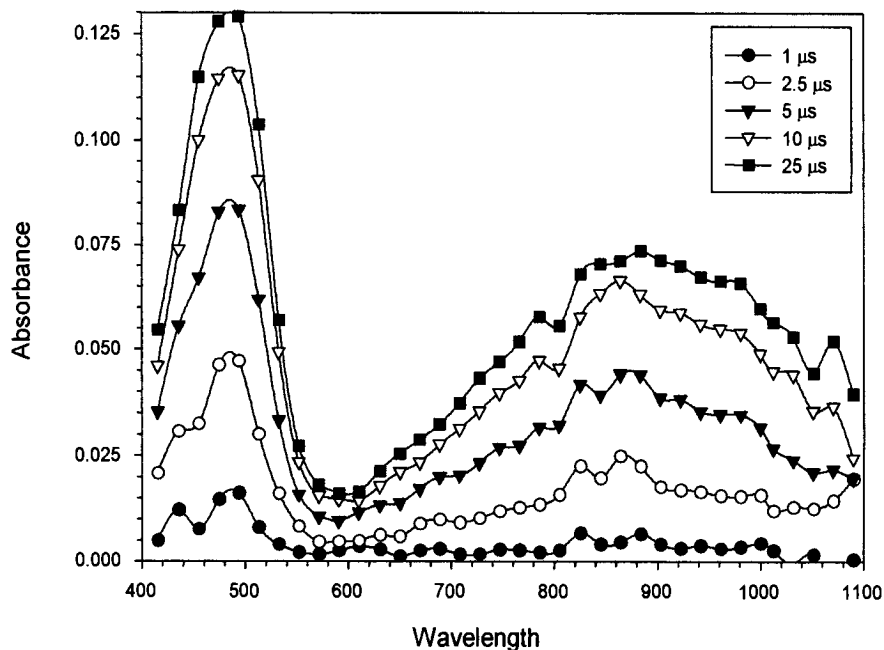
Figure 37. Negative polaron absorption from rPPy in formic acid[75].

Figure 37 shows the transient absorption generated by radiolysis of rPPy dissolved in formic acid. This process generates negative polaron species on the target material. Two transient absorptions are seen in Figure 37, at 480 nm and 890 nm. The 480 nm absorption is due to the formate cation whereas the 890 nm (1.4 eV) absorption is due to the negative polaron: a second polaron peak was supposed to be present but outside the detection range of the Si photodiodes used in the experiment.

4.3. Discussion

Feature origin	PIA energy	PR energy
Triplet-triplet absorption	*2.29 eV*	*2.1 eV*
Polaron	*1.5 eV*	*1.4 eV*
Polaron	*0.8 eV*	*Out of range*

Table 2. Excited state species and associated transient absorption energy as determined from photoinduced absorption and pulsed radiolysis experiments.

There is an excellent correspondence between the results obtained through thin film photoinduced absorption and solution state pulsed radiolysis. Taken together these results yield the first unambiguous assignment of the photoinduced states in PPy.

Triplet State

A triplet state is observed at 2.1 eV from the pulsed radiolysis experiment, confirming the initial assignment of the 2.29 eV photoinduced absorption to a transition within the manifold of a triplet exciton state. The difference in energy between these two features can be assigned to a solvatochromic shift in the solution used in pulsed radiolysis. The triplet absorption is most likely due to a T_1-T_2 transition. Transitions to higher electronic levels within the triplet manifold (e.g. T_1-T_3) are possible but these absorptions will be difficult to measure, masked as they are by the fundamental absorption band of the polymer (onset at ~ 3.0 eV). It might be possible to detect these states using photoinduced absorption but our current white light source (a tungsten filament lamp) does not output enough light in the blue/UV to obtain reasonable signals through the absorption band. A carefully stabilised Xenon arc lamp is required in order to obtain the UV output demanded by such an investigation. A Xenon lamp has been tried but the light output fluctuated slightly and this was detected as a massive AC signal at the lockin amplifier over the range of frequencies normally used. This noise level was about a factor of 20 greater than the biggest photoinduced absorption signal seen in PPy.

From the chop rate experiments, we know that the steady state lifetime of this triplet state is (15.81 ± 0.86) milliseconds in helium at 87K and that this value falls to (14.11 ± 0.76) milliseconds in the presence of O_2 at 92K. The additional decay path through an interaction with atmospheric triplet oxygen to form singlet oxygen has shortened the state lifetime in this case. The heavy nitrogen atom in PPy acts to enhance the spin-orbit coupling and leads to generation of these large triplet exciton populations. The enhanced spin-orbit coupling also allows the triplets predominantly to decay directly to the ground state, giving the observed monomolecular decay profile. (Other dominant decay routes, such as TTA are bimolecular).

In air at 300 K we are unable to detect a triplet absorption in quasi CW PIA (seeing only the PL signal). A time resolved PIA experiment under these conditions obtains a triplet lifetime of 5ns. This lifetime is too short for a detectable number of probe photons to interact with the triplet excited state in the quasi CW PIA experiment so these results too are consistent. This lifetime shortening effect is demonstrated quite clearly in Figure 34, which shows how the triplet signal observed in a quasi steady-state experiment decays with temperature.

In order to explain the difference in triplet lifetime we need also to consider the photoluminescence data. This clearly shows an increased blue component and reduced green component at low temperature where the triplet lifetime is greater. The PL is dominated by the green component at room temperature when the triplet lifetime is short. Given that pulsed radiolysis gives the S_0-T_1 energy to be 2.4 eV in solution (in the vicinity of the solid state green emission) it seems clear that the green component is due to a radiative triplet decay (phosphorescence). This radiative decay channel has a short lifetime which leads to the short (5ns) lifetime obtained for the triplet state in the time resolved PIA experiment. Conversely, when the temperature is low, the triplet radiative channel closes off leading to a weaker green emission and a longer triplet decay lifetime (16 ms) dominated by slower non-radiative decay channels. If the radiative triplet decay is mediated by an interaction with triplet oxygen to form a singlet complex, then the rate of radiative decay could well be dependent on temperature. With less thermal energy around fewer such complexes would be formed and so the radiative lifetime would increase. Formation of oxygen complexes can occur in the absence of an oxygen atmosphere because the thin film will contain

oxygen. Steps can be taken to remove the oxygen from the film but this has not yet been done.

Additionally the low temperature PL spectrum shows an enhanced blue emission: this PL component is from the singlet exciton ($\Delta E(S_1\text{-}S_0) > \Delta E(T_1\text{-}S_0)$). The fact that this blue component becomes stronger at low temperature suggests that the conversion rate from singlet excitons to triplet excitons is also activated or influenced by temperature. The enhanced ISC rate at high temperatures could be due to a higher monomer torsion angle leading to increased spin-orbit coupling to nitrogen at expense of delocalisation.

The presence of a strong triplet emission component is a useful feature when making real LED devices. It is generally held that electron spin statistics determine that positive and negative polarons give rise significant proportions of triplet excitons (see section 2.4.2) when they recombine in the junction area of an electroluminescent device. A polymer that shows efficient (and fast!) phosphorescence could result in devices with a much greater external efficiency than polymers that are solely singlet emitters.

Charged state

In addition to the triplet state a charged state is also detected following the initial photoexcitation. The signature of this state is seen at 1.5 eV and 0.8 eV in the solid state, and at 1.4 eV from pulsed radiolysis. Unfortunately the range of the pulsed radiolysis experiment is limited and it cannot investigate below about 1.1 eV. From the correspondence between the 1.5 and 0.8 eV chop rate dependencies it seems clear that these arise from the same excited state, even though we cannot confirm this through pulsed radiolysis. Indeed, twin peaks should be detected below the absorption edge in the case of polarons and bipolarons. Strictly speaking polaron states should have a third absorption feature but this has a very low oscillator strength and could be present but not detected.

The 1.5 eV and 0.8 eV features are broad and this is explained by the wide density of states that arises from a distribution of chain lengths and defects within the material.

4.4. Summary

A combination of steady state photoinduced absorption and pulsed radiolysis has allowed us to unambiguously determine the nature of the long-lived photoexcited states in PPy for the first time. The use of pulse radiolysis in such investigations is unlikely to become widespread, as not many research groups have access to 10 MeV linear electron accelerators.

Two distinct long-lived species are detected in solid-state samples of PPy at low temperature: a charged (polaron or bipolaron) state with PIA bands at 1.5 eV and 0.8 eV and a triplet state with a PIA band at 2.29 eV. At room temperature, only the charged state signature is detected. It has been demonstrated that phosphorescence from the triplet state dominates the emission from the sample at room temperature and that this reduces the lifetime of the triplet state well below the detection threshold of the quasi steady state PIA experiment. This has important real world consequences as the use of phosphorescent materials could enhance the efficiency of polymeric LEDs.

To further analyse this system, it would be useful to try to measure a complete PIA spectrum at room temperature to verify the assumption that the polaron/bipolaron state does not change. The present room temperature PIA spectrum is restricted to the visible range. Measuring the dependence of the PIA peak signals on pump beam intensity would also be helpful, as this reveals information on the kinematics of the system. Complete photoluminescence spectra at a range of temperatures would help demonstrate the evolution of the phosphorescence component of the emission.

In terms of sample changes, running experiments on oxygen free thin films of PPy will test the proposition that oxygen complexes are the mechanism by which the phosphorescence gains its temperature dependence. PPy is very hard to process (it is only soluble in Formic acid) so alkyl substituted PPy would be used in any commercial exploitation of the system due to the solubility of the latter in common organic solvents. It would be useful to know the extent to which the alkyl side chains have on the photophysics of the material.

Finally, perhaps the most interesting field of further study is in time resolved studies of the absorption bands of the various excited states and of the various emission processes.

81

Chapter 5. Experimental Study of Polyfluorene

5.1. Introduction

Polyfluorene (PFO) is a stable, strongly luminescent polymer with blue emission and a solid state photoluminescence quantum yield of about 45%. Organic LEDs using PFO have been developed and continuous mode brightnesses of 25,000 cd/m^2 have been demonstrated[76]. Additionally, PFO exhibits liquid crystalline phases[77] and this property can be exploited to produce highly oriented PFO layers[78]. The one-dimensional nature of conjugated polymers means that an oriented sample will emit polarised light. The emission of polarised light is useful when making backlights for liquid crystal displays; currently light from an unpolarised LCD backlight must pass through a polariser before the liquid crystal layer. This process wastes half the light from the source; a backlight that emits polarised light innately would have greater power efficiency. Such polarised emission has been demonstrated from electroluminescent devices using PFO-derivatives following chain alignment using the liquid crystalline phase[78,79]. Alternative methods of producing oriented conjugated polymer samples are available (e.g. stretch-alignment) but these typically require more intensive processing and therefore are less amenable to commercial exploitation, especially for 100 nm films.

The photoinduced absorption experiment consists of a pump beam and a probe beam and the polarisation of these beams with respect to the direction of polymer chain alignment is an important parameter when investigating oriented samples. Changing the polarisation of the beams so that they are parallel and perpendicular to the chain alignment can yield important information on the orientation of the excited state dipoles. Signal dependence with the pump beam orientation yields information about the generation and therefore nature of the excited state. Signal variation with the probe beam yields information about the orientation of the excited state dipole.

Results from oriented samples of polyacetylene[80] (PA) and poly-para-phenylenevinylene[81] (PPV) reported in the literature show that the photoinduced signal strength is stronger with the pump beam polarised parallel to the chain direction than when it is perpendicular to the chain direction. After correcting for the different pump absorption in the two orientations, the response (or steady state population) with the

pump beam perpendicularly aligned can be greater than that with parallel alignment of the pump beam. In these cases, the effect is attributed to the intrinsic generation processes responsible for the photoexcitation of polarons. Photoexcitation produces singlet excitons and these excitons must dissociate in order to produce separate positive and negative charges; the polymer chain distorts around each charge self trapping it in a geometric distortion known as a polaron (see chapter 2). When pumping perpendicularly to the chain the singlet excitons are produced such that the electron and hole are on different chains. This increases the charge separation which results in a lower exciton binding energy and therefore it is easier for the electron-hole pair to separate and form a polaron pair. The polarons are created on separate chains by this process and this reduces the polaron recombination rate. The enhanced polaron generation efficiency (lower exciton binding energy) and the longer lifetime (reduced recombination rate) result in a greater steady state population. The generation of triplet excitons – the other long-lived state that has a new set of absorption bands and thus shows up in photoinduced absorption spectra – involves intersystem crossing from the singlet state. This process is not dependent on the exciton binding energy and hence does not show any generation efficiency enhancement when photoexciting the sample parallel or perpendicular to the chain.

Implicit in this analysis is the requirement for an interchain absorption coefficient that allows photoexcitation perpendicular to the chain axis to generate singlet excitons across (adjacent) polymer chains. This absorption comes from the overlap of the delocalised π electronic orbitals between adjacent polymer chains, in an effect known as π-stacking. An experimental measurement of the perpendicular absorption coefficient also contains contributions from the intrachain perpendicular absorption (due to the zig-zag nature of the polymer backbone) and the perpendicular absorption due to chain misalignment[83].

Following these principles, a theoretical model was developed by Comoretto *et al*[53] which relates the parallel and perpendicular steady state populations to the parallel and perpendicular pump absorption coefficients with an intrinsic anisotropy factor, I. The model starts with the relationship between the observed PIA signal and the steady state population of the excited state in question which is given in Equation 17[82].

$$-\frac{(\Delta T)_{II,\perp}}{T} = \sigma \frac{N_{II,\perp}}{A}$$

Equation 17

Where:

-ΔT/T   Steady state PIA signal.

N   Total number of photoexcitations.

A   Area of sample exposed to probe beam.

σ   Energy dependent absorption cross-section of photoexcitation.

Using a pump beam polarised parallel or perpendicular to the direction of chain orientation, we can then determine that $N_\perp / N_{II} = \Delta T_\perp / \Delta T_{II}$. Comoretto then relates this experimentally determined population anisotropy to an intrinsic anisotropy that reflects the different generation efficiencies for the parallel and perpendicular pump cases. This derivation starts with the rate equations for the pump-parallel and pump-perpendicular populations[83], shown in Equation 18 and Equation 19.

$$\frac{dn_{II}(x)}{dt} = g_{II}\alpha_{II}(1-R_{II})Ie^{-\alpha_{II}x} - \frac{n_{II}(x)}{\tau} - \beta n_{II}^2$$

Equation 18

$$\frac{dn_\perp(x)}{dt} = \left(g_{II}\left(\alpha_{II}\sin^2(\delta)+\alpha_\perp^{1D}\right)+g_\perp\alpha_\perp^{3D}\right)(1-R_\perp)Ie^{-\alpha_\perp x} - \frac{n_\perp(x)}{\tau} - \beta n_\perp^2(x)$$

Equation 19

Where:

$g_{II,\perp}$ Generation efficiency of long-lived photoexcitation with parallel and perpendicular pump polarisation.

I   Laser intensity.

α_{II} Absorption coefficient along the chain axis

85

$\alpha_{\text{II}} \sin^2(\delta)$ Perpendicular absorption coefficient due to chain misalignment[68].

$\alpha_{\perp}^{1D}$ Perpendicular intrachain absorption coefficient.

$\alpha_{\perp}^{3D}$ Perpendicular interchain absorption coefficient.

$\alpha_{\perp}$ Perpendicular absorption coefficient ($\alpha_{\perp} = \alpha_{\text{II}} \sin^2(\delta) + \alpha_{\perp}^{1D} + \alpha_{\perp}^{3D}$)

$R_{\text{II},\perp}$ Reflectivity of the polymer film.

τ Monomolecular decay lifetime.

β Bimolecular recombination constant.

The intrachain absorption coefficient $\alpha_{\perp}^{1D}$ describes absorption perpendicular to the chain axis that would be obtained from one chain in isolation. The interchain perpendicular absorption parameter $\alpha_{\perp}^{3D}$ is the perpendicular absorption that arises between adjacent polymer chains through the π-stacking mechanism described above.

Steady state photoinduced absorption measures the steady state population, which occurs when dn/dt = 0 in the rate equations given above. Equation 18 and Equation 19 can be integrated to give the total number (N_{II} and $N_{\perp}$) of photoexcitations in the steady state for the two limiting cases of dominant monomolecular and bimolecular recombination regimes. Under the monomolecular regime, $n(x) < 1/(\beta\tau)$, the steady state population ratio is then given by Equation 20. In the bimolecular recombination regime, $n(x) > 1/(\beta\tau)$, the population ratio is given by Equation 21.

$$\frac{N_{\perp}}{N_{\text{II}}} = \left(1 - \frac{\alpha_{\perp}^{3D}}{\alpha_{\perp}} + \frac{g_{\perp}\alpha_{\perp}^{3D}}{g_{\text{II}}\alpha_{\perp}}\right) \frac{(1 - R_{\perp})(1 - e^{-\alpha_{\perp}d/2})}{(1 - R_{\text{II}})(1 - e^{-\alpha_{\text{II}}d/2})}$$

Equation 20. Population ratio for low photoexcitation density.

$$\frac{N_{\perp}}{N_{\text{II}}} = \sqrt{\frac{\alpha_{\text{II}}(1 - R_{\perp})}{\alpha_{\perp}(1 - R_{\text{II}})}} \sqrt{1 - \frac{\alpha_{\perp}^{3D}}{\alpha_{\perp}} + \frac{g_{\perp}\alpha_{\perp}^{3D}}{g_{\text{II}}\alpha_{\perp}}} \frac{(1 - e^{-\alpha_{\perp}d/2})}{(1 - e^{-\alpha_{\text{II}}d/2})}$$

Equation 21. Population ratio for high photoexcitation density.

86

The intrinsic anisotropy was then defined according to Equation 22. In general, the perpendicular interchain absorption coefficient is less than the total perpendicular absorption coefficient $(\alpha_\perp^{3D}/\alpha_\perp < 1)$ and so I > 1 implies $g_\perp/g_{II} > 1$; that is, an enhancement of the generation efficiency for interchain excited states as would be expected for polarons. I <= 1 implies no interchain enhancement and thus implies a triplet state. Extracting a value for I from the photoinduced absorption data can therefore help to determine the interchain or intrachain nature of the photoexcited state.

$$I = 1 - \frac{\alpha_\perp^{3D}}{\alpha_\perp} + \frac{g_\perp \alpha_\perp^{3D}}{g_{II} \alpha_\perp}$$

Equation 22.

From Equation 21 and Equation 22, we then obtain Equation 23 for the dependence of the intrinsic anisotropy I in terms of experimentally accessible parameters.

$$I = \left(\frac{(-\Delta T_\perp)}{(-\Delta T_{II})} \left(\frac{\alpha_{II}(1-R_\perp)}{\alpha_\perp(1-R_{II})} \right)^{-1/2} \frac{\left(1-e^{-\alpha_{II}d/2}\right)}{(1-e^{-\alpha_\perp d/2})} \right)^2$$

Equation 23.

Where the ΔT here are dT/T. Typically, the polymer will not be absorbing at the photoinduced absorption feature wavelength and thus the transmission of light through the sample will not change with polymer-probe orientation. The explicit reliance on the transmission, T, is still required because the efficiency of collection of light could change with different orientations of the sample and polariser. A measurement of the reflectivity under parallel and perpendicular excitation is also needed. The absorption coefficients α can be obtained by measuring the parallel and perpendicular absorption of the sample at the excitation wavelength and measuring or assuming a value for the sample thickness.

Chemical structure

PFO is a variant of poly-para-phenylene (PPP). The structures for both polymers are given in Figure 38. PPP synthesis is difficult, yielding low amounts of a low molecular weight material due to the low solubility of the precursor in solution[84]. The addition of alkyl chains to the precursor to improve the solubility leads to the formation of dialkyl-PPP with a higher molecular weight. Unfortunately, the saturated dialkyl chains that improve the solubility also introduce a significant angular twist between adjacent aromatic units, reducing their interaction and the overall delocalisation of the π-bond states[84].

Poly-para-phenylene (PPP)

Dialkyl-PPP

Polyfluorene (PFO)
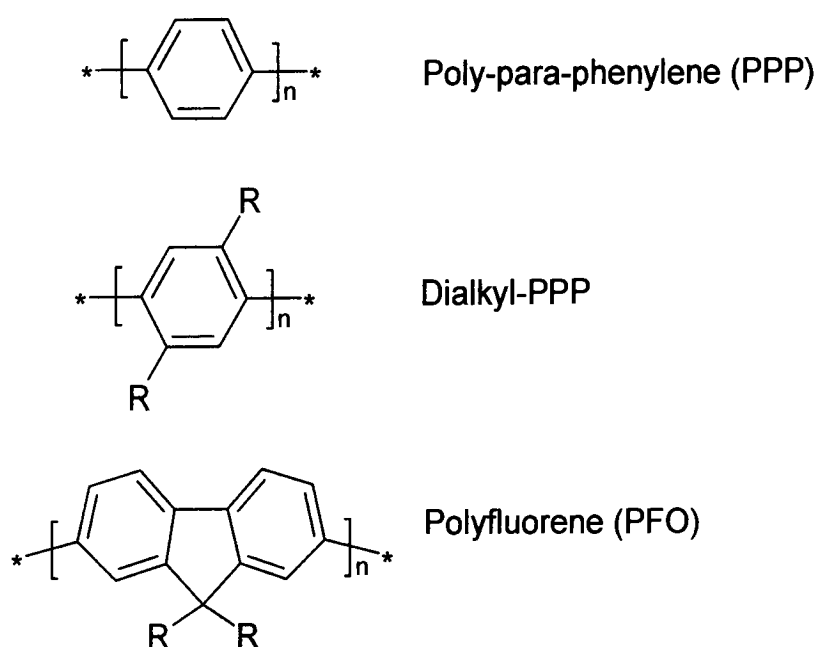
Figure 38. Chemical structures of PPP (top), dialkyl-PPP (middle) and PFO (bottom).

In PFO, pairs of aromatic units are locked together by the addition of a saturated (sp^3) bridging carbon atom, from which a pair of alkyl side chains also branch off. This locks together the two rings in a planar configuration, increasing the average conjugation length, increasing the π-bond delocalisation and hence redshifting the absorption band of the material. Adjacent pairs of monomer units are, of course, free to rotate. The absorption band of PPP is a maximum at 280 nm[84], whereas for PFO it is a maximum at about 380 nm (Figure 39). This conveniently allows PFO to be optically excited using the UV lines of an argon ion laser. The saturated side chains

make PFO more soluble than PPP through their interaction with organic solvents. Additionally the side chains increase the inter-chain separation in the solid state, reducing the inter-chain interaction and further increasing the solubility of the material. A reduced inter-chain interaction could also effect the photophysics of the excited state by suppressing the generation of inter-chain species such as polarons. Finally the side chains enforce an angular twist between adjacent monomers along the polymer chain.

5.2. Results

Ground state absorption and photoluminescence

Figure 39 shows the ground state absorption for an aligned sample of PFO at 300K. The data were obtained using a Perkin-Elmer λ-19 absorption spectrometer fitted with a pair of polarisers. A clear anisotropy is seen; at the peak of the spectrum (about 380 nm) the absorption for the parallel alignment is about 25 times that for the perpendicular alignment. The high anisotropy indicates that the polymer chains are highly aligned for this sample. At the pump wavelength the anisotropy factor is approximately 7.
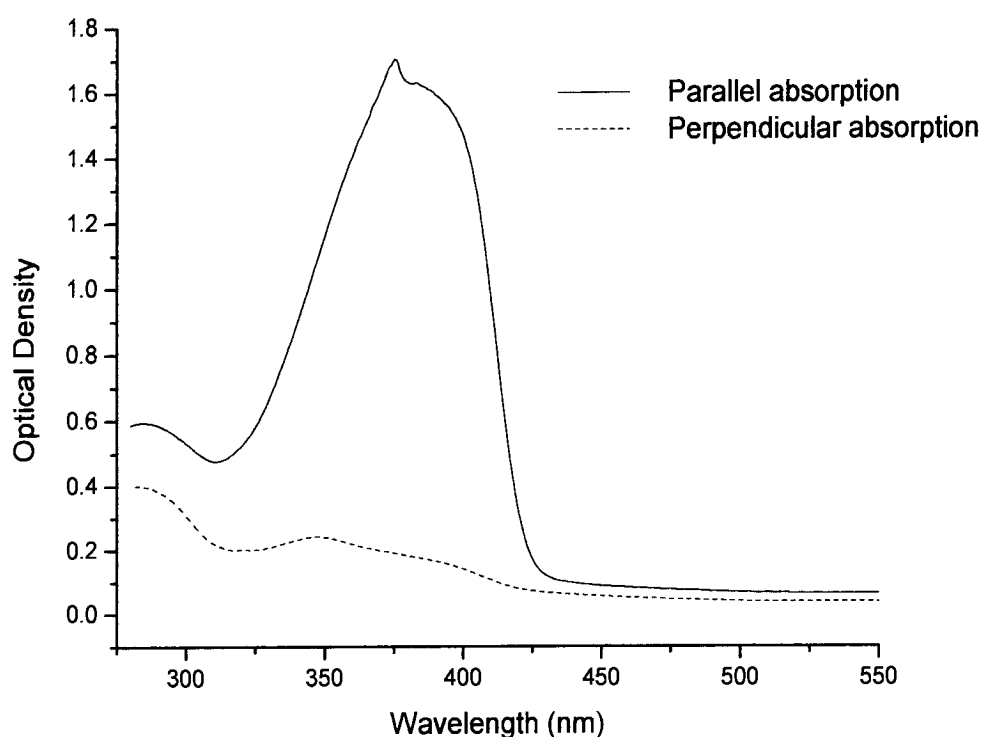
Figure 39. Ground state absorption spectra of PFO at 300K for parallel and perpendicular alignment

Two peaks can clearly be seen in the perpendicular absorption spectrum, at 350 nm and 400 nm. These features can also be seen in the parallel absorption. The notch at the top of the parallel absorption spectrum is an experimental effect caused by a filter change but there is a shoulder in the parallel absorption at 350 nm. The 350 nm

feature shows relative enhancement over the 400 nm absorption in the perpendicular absorption spectrum; it is possible that this is due to an interchain absorption process, as has been suggested for PPy. Using the argon ion laser as a pump source we can excite into the feature at around 350nm but cannot access the 400 nm absorption.

Unpolarised photoinduced absorption data at 90K

Figure 40 shows a photoinduced absorption spectrum of a thin film of unaligned PFO on a glass substrate in a Helium atmosphere at 80K. A pump power of 20 mW was used, yielding approximately 0.25 mW/mm^2 at the sample from the UV lines of an argon ion laser (pump at 3.5 eV, the peak of the absorption band). The laser chop rate was 22 Hz. The digital lockin amplifier was autophased on one of the photoluminescence vibronic side bands before the experiment was performed.

Figure 40. Quasi steady state photoinduced absorption spectrum of u-PFO in He at 90K

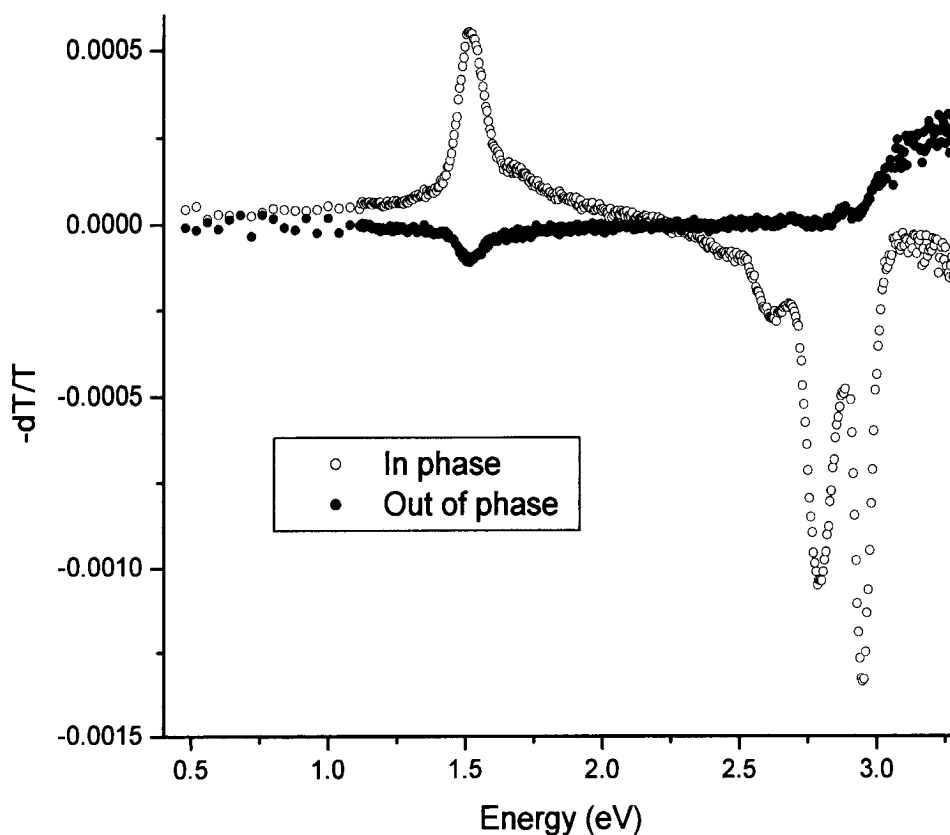Six features are visible on the plot. There is a clear photoinduced absorption peak at 1.52 eV with either an asymmetric high energy tail or a shoulder at approximately 1.7 eV. Three photoluminescence vibronics features are seen at 2.61 eV, 2.79 eV and 2.96 eV, in agreement with photoluminescence spectra for PFO reported in the literature[85]. The broad feature seen at 2.4 eV is the tail of the photoluminescence. Finally, there is an apparent photobleaching signal at 3.2 eV. Photoexcitation leads to a reduced ground state electronic population and hence a reduced oscillator strength for the ground state absorption; this is seen as an increase in transmission through the sample. The photobleaching signal at 3.2 eV (or about 340 nm) is within the ground state absorption (see Figure 39). That the photobleaching signal has a different phase to the PL signal implies that the overall electronic population of the ground state recovers at a different rate to the PL emission. This is expected when not all of the initially photocreated singlet excitons radiatively recombine to give photoluminescence. From the photoinduced absorption peak at 1.52 eV we know that some of these singlet excitons convert into long lived states, slowing down the repopulation of the ground state.

Of all these features the clear photoinduced absorption at 1.52 eV (815 nm) is the most significant for our purposes and has been characterised further. It shows a clear phase shift over that of the photoluminescence features. Figure 41 shows this feature in more detail. The data have been smoothed for clarity using a 15 point Savitzky-Golay algorithm; there are 228 data points in the reduced range plot (and 450 in Figure 40). Figure 41 also shows no phase shift between the 1.52 eV and the 1.7-1.8 eV peaks, which implies that they have the same origin. The presence of a lone PIA feature suggests that it is a transition within the manifold of a triplet exciton, since a charged state would typically have more than one PIA feature and associated infrared active vibrational (IRAV) modes. It is possible however that other PIA features are hidden underneath the strong luminescence signal and the IRAV modes – if they exist - may be at lower energy than the experimental range.
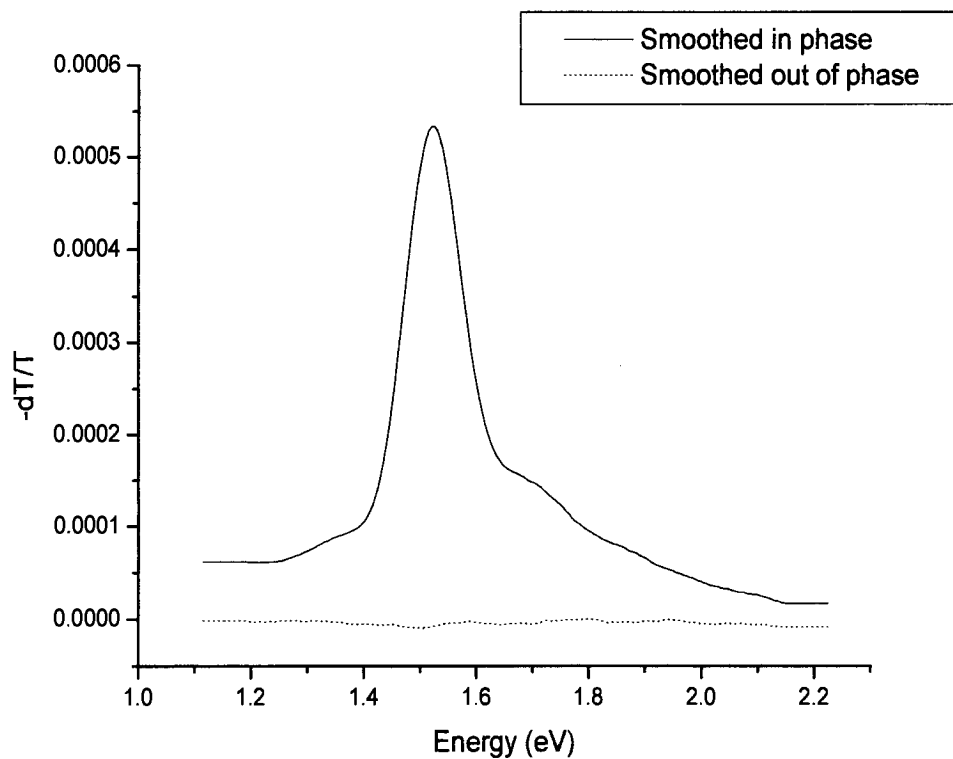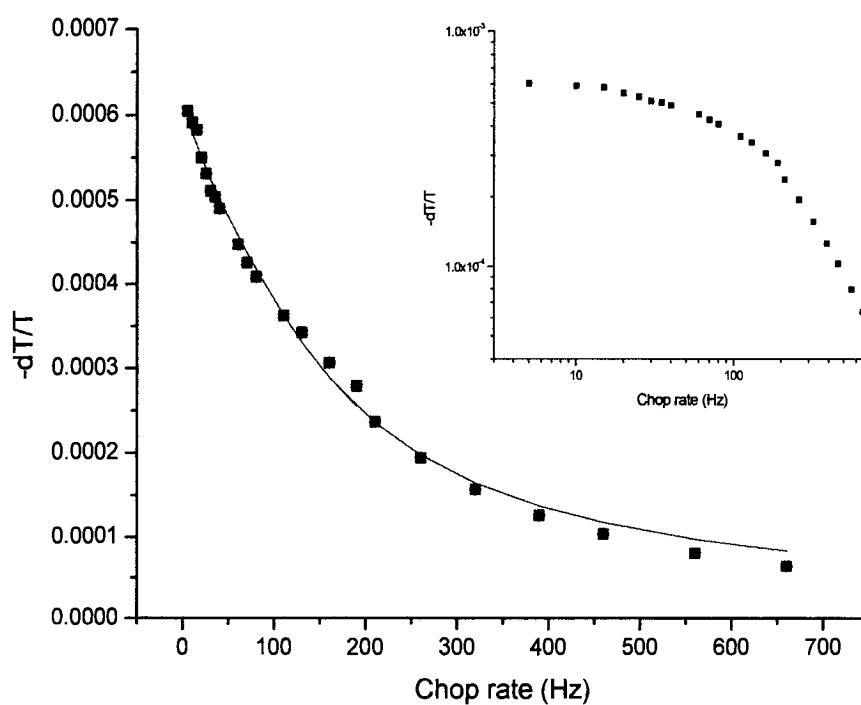
Figure 41. A section of Figure 40.

Figure 42. Chop rate dependency of 1.52 eV PIA feature for unaligned sample.

Figure 42 shows the chop rate dependency of the 1.52 eV feature for the unoriented, unpolarised sample. Apart from the variation in chop rate, all other experimental parameters were the same as used to obtain the unoriented PIA spectra. The data are plotted as points, together with a solid line that represents the best fit to the data. Fits were obtained using the Levenburg-Marquardt functionality of Origin. It can be seen from the log-log insert that the signal drops continuously, implying a bimolecular decay function, and indeed the data are best fit to a bimolecular decay, giving a steady state lifetime of $\tau_{steadystate}$ = (17.4 ± 0.5) milliseconds.

Photoinduced absorption experiments were performed on oriented samples of PFO in order to obtain a more positive identification of the excited state.

Polarised photoinduced absorption spectra at 90K

The photoinduced absorption spectrum taken on the unaligned sample (Figure 40) acts as a high signal baseline for the polarisation-dependent experiments presented in this section. As was discussed in section 5.1, experiments with chain aligned samples and polarised pump and probe light yield important additional information on the nature of the excited state.

The pump beam is vertically polarised in order to minimise reflection losses inside the laser cavity. In order to obtain excitation parallel and perpendicular to the polymer chains it is necessary to orient the sample correctly in the cryostat and rotate it through 90 degrees to obtain the perpendicular orientation. It would have been better to use a $\lambda/2$ waveplate to vary the polarisation of the pump beam. The PL signal will vary sinusoidally with the angle of the $\lambda/2$ waveplate; in this way it is possible to accurately determine the waveplate angles for parallel and perpendicular beams. Unfortunately a waveplate was not available for the pump wavelengths used.

The probe beam is not polarised so it is necessary to add a polariser to the optics system before the probe beam enters the detector. In practice, this means locating the polariser against the entrance slit to the monochromator. Any difference in the efficiency of the monochromator diffraction grating for the two probe polarisations will of course alter the dT and T signals by the same fraction, leaving the dT/T signal detection efficiency unchanged. Care was taken so that as far as possible the different

orientations of the polariser didn't occlude the probe beam as it entered the monochromator. Differences in the response of the sample over its surface would otherwise create signal strength differences that were not related to the polarisation effects under investigation.

There were two light beams in the experiment (pump and probe) and two orientations for each beam (parallel and perpendicular to the direction of chain alignment). This results in four combinations of pump and probe orientation. Spectra were obtained using a thin film of aligned PFO on a glass substrate in helium at 90K. In other respects (pump power and chop rate) the conditions were the same as for the unaligned sample. The spectra are plotted as Figure 43. Referring to the key in Figure 43, the first orientation refers to that of the pump beam with the sample chains, the second to the probe beam. Thus (para-perp) means the pump beam is parallel to the sample chains (i.e. sample oriented such that chains are vertical) and the probe beam is perpendicular (i.e. the polariser at the monochromator entrance slit passes horizontally polarised light).

Unfortunately the magnitudes of the various spectra in Figure 43 cannot be relied upon absolutely. Each spectrum takes a finite amount of time to collect and sample degradation occurs during this time, reducing the signal that would otherwise be obtained within and between spectra. Additionally the data for the perpendicular pump case (perp-para and perp-perp) were collected from a different sample as the original sample was not yielding any useful data at that point. The trend in the photoluminescence signal strength at 2.8 eV is as would be expected; a higher PL signal is observed when pumping parallel rather than perpendicularly. This is due to the higher parallel absorbency of the sample (see Figure 39). When the pump and collection polarisations are crossed the detected PL signal is reduced; this indicates that the dipole moment of the emission is oriented with that of the excitation, as would be expected for a fast photoluminescence process.
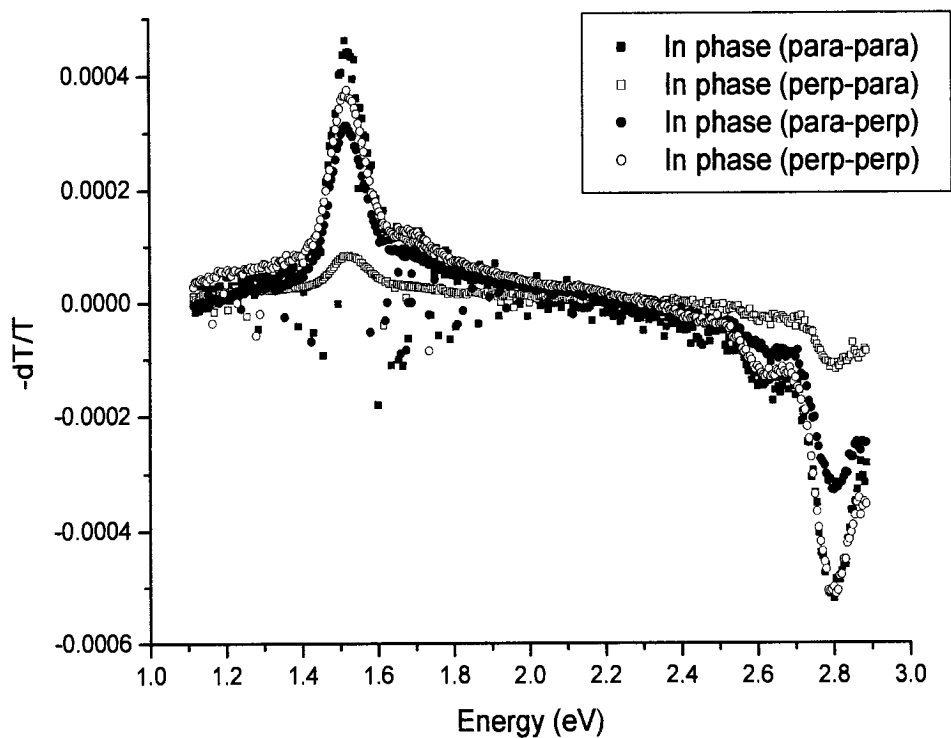
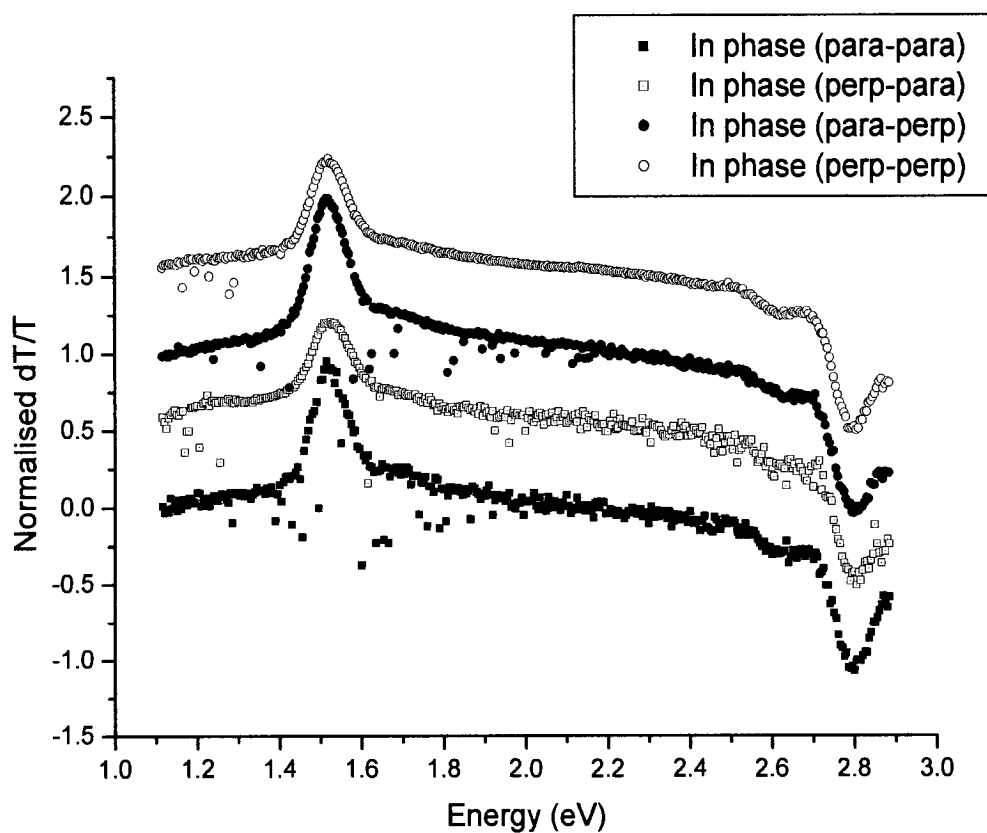**Figure 43. Raw steady state PIA spectra of an oriented PFO sample in He at 90K.**

Figure 44. Normalised PIA spectra of an oriented-PFO sample in He at 90K.

In order to make comparisons between the various aligned spectra it is helpful to normalise the data. Figure 44 shows the normalised in phase component of the photoinduced absorption spectrum for each of the four permutations. Normalisation was performed at the photoluminescence vibronic side band visible in the plot; the spectra are therefore corrected for the difference in absorption due to pump orientation and sample variations. The normalised spectra were displaced by 0.5 for clarity; the plot is to allow comparison of lineshape only, not signal magnitude.

Figure 44 shows that there is no change in the lineshape of the photoinduced feature at 1.52 eV, nor of the photoluminescence features at higher energy. This implies that the same basic photophysical processes are occurring with each different polarisation permutation. The normalised magnitudes of the signals (and therefore the steady state population of the excited state in the case of the photoinduced absorption peak) do vary between orientations. This is shown in Figure 45, which plots a closeup of the normalised data presented in Figure 44 without the displacement. The PIA signal at 1.52 eV is proportionally greater for the parallel pump than for the perpendicular pump, regardless of probe orientation. As can be seen in the inset, normalisation ensures that there is no difference between the orientations in the rest of the photoinduced spectrum. This implies that either the PIA feature has a different dependence on absorbed laser intensity to the photoluminescence feature or that there is some relative enhancement of the parallel (intrachain) generation efficiency of the excited state. Chop rate and accurate signal magnitude data has been obtained at 1.52 eV feature for each of the four permutations. This data is presented in a following section.

The shoulder at approximately 1.7 eV does not show any pump-parallel enhancement, appearing instead only to scale with the photoluminescence signal. This suggests that the shoulder might have a different origin to the 1.52 eV feature as it appears to scale in the same manner as the photoluminescence signal does. However the signal magnitude of the shoulder is (by definition) small and it is difficult to be certain about the conclusions we can draw from the data. This is demonstrated best by the (perp-para) case, where the un-normalised signal strengths are so low that a shoulder is seen at low energy too and therefore is more probably a background signal.
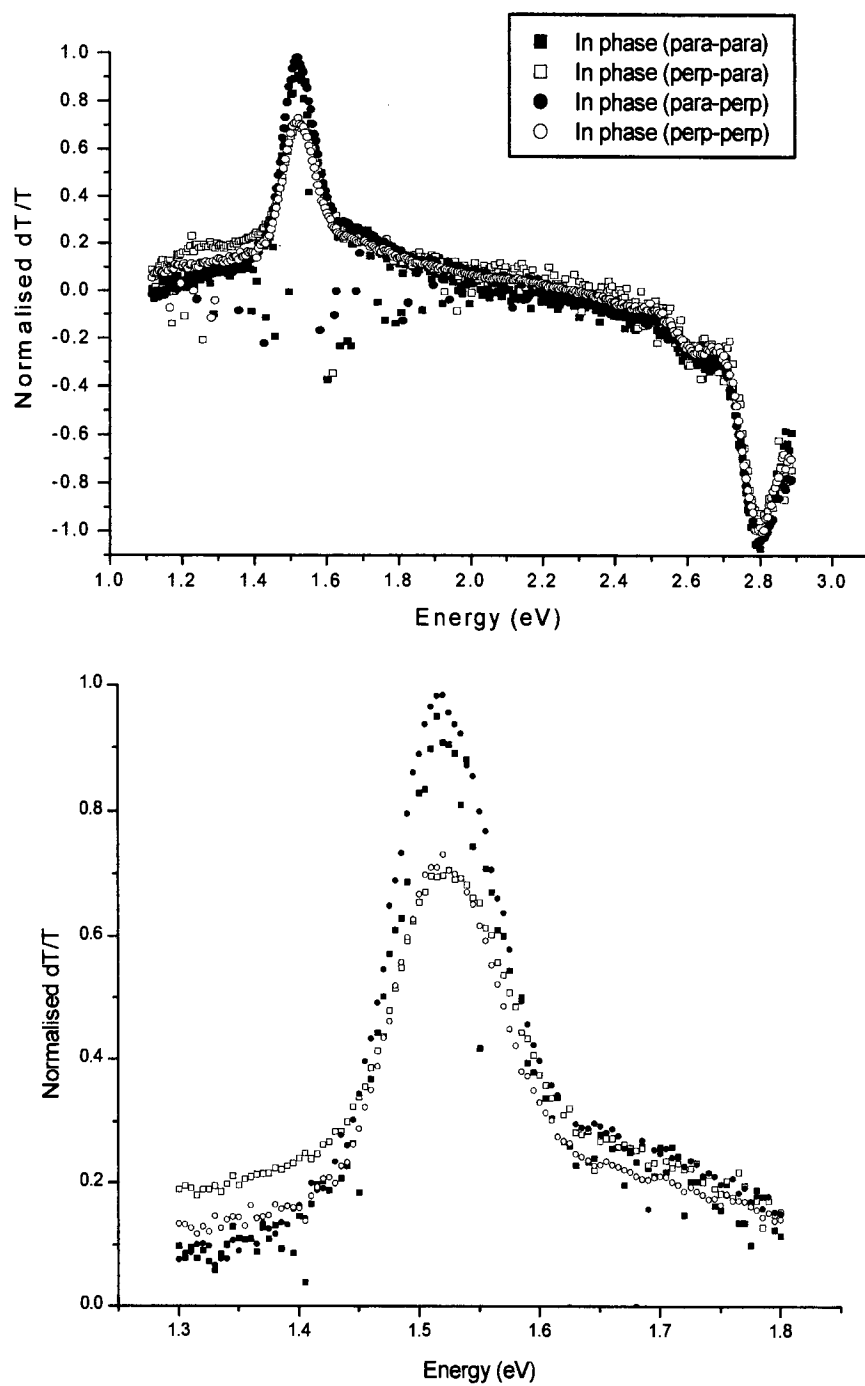
Figure 45. Normalised spectra (top) together with closeup of PIA region (bottom)

Chop rate (lifetime) dependence on orientation for 1.52 eV PIA peak

Chop rate dependencies were measured for each of the four components. Fortunately the PFO samples were more resilient to the laser beam than PPy (section 4.2) and chop rate measurements could be taken with less repetition and sample changing. The laser power was adjusted so that sufficient (but not excessive) signal levels were obtained at the higher chop rates. A pump power of 30 mW was used, yielding 0.38 mW/mm^2 power density. These data are presented in Figure 46 to Figure 49. In each case, the experimental data is plotted as a set of points together with a continuous line that represents the best-fit decay function. As with PPy the data were fitted using the Levenburg-Marquardt functionality of Origin.
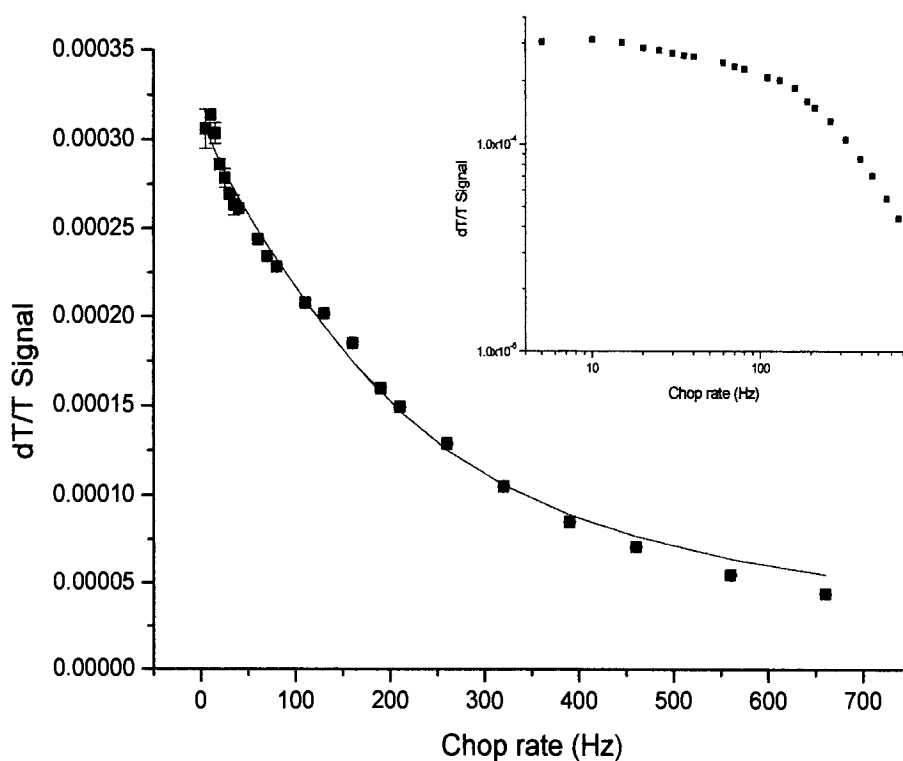
Figure 46. Chop rate plot for parallel-perpendicular configuration. The solid line represents the fit, the inset is a log-log plot of the data.
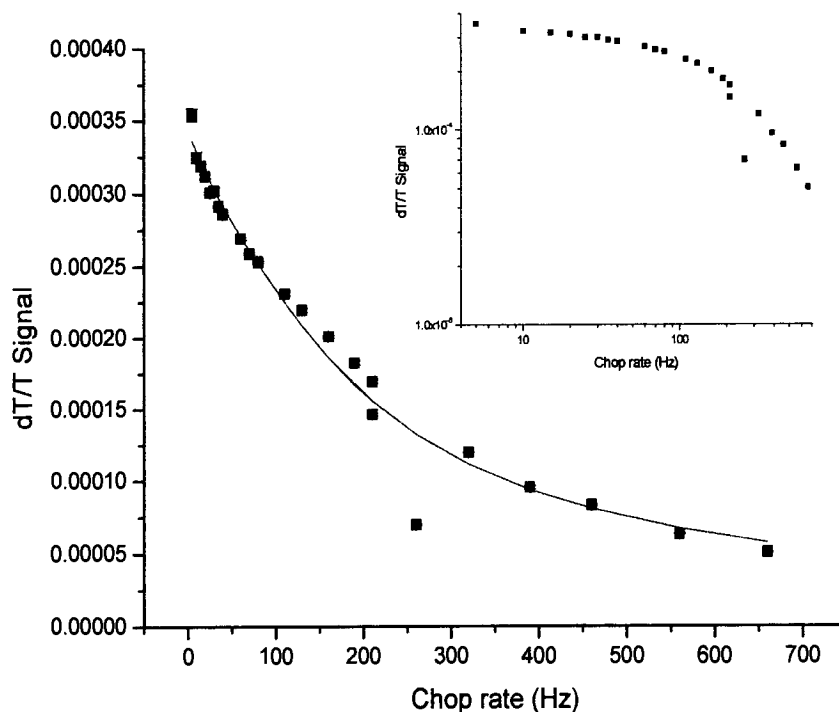
Figure 47. Chop rate plot for parallel-parallel configuration. The solid line represents the fit, the inset is a log-log plot of the data.
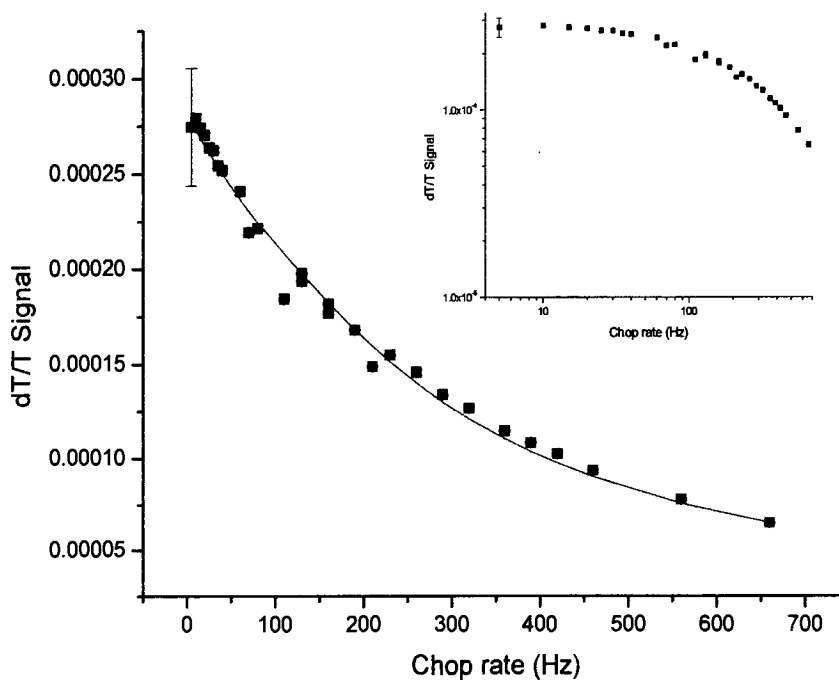
Figure 48. Chop rate plot for perpendicular-perpendicular configuration. The solid line represents the fit, the inset is a log-log plot of the data.
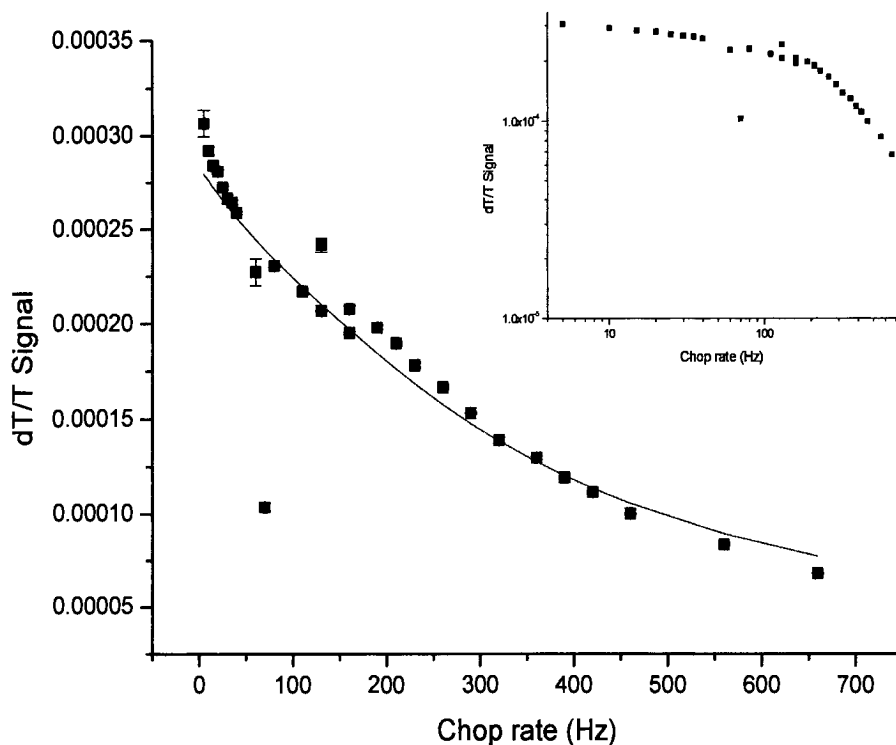
Figure 49. Chop rate plot for perpendicular-parallel configuration. The solid line represents the fit, the inset is a log-log plot of the data.

Figure 46 shows the chop rate dependence of a sample in the (parallel-perpendicular) configuration: that is, where the pump beam is parallel to the chain orientation and the probe beam is perpendicular to it. The log-log plot insert shows that the signal drops continuously, indicating a bimolecular decay. Indeed, the data were best fitted using a bimolecular decay function, yielding a steady state lifetime $\tau_{steadystate}$ = (13.3 ± 0.4) milliseconds.

Figure 47 shows the chop rate dependence for the (parallel-parallel) configuration. The data are best fitted by a bimolecular decay and this gives a steady state lifetime $\tau_{steadystate}$ = (14.0 ± 0.9) milliseconds. Within the experimental error this is identical to the value obtained for the (parallel-perpendicular) configuration.

Figure 48 shows the chop rate dependence for the (perpendicular-perpendicular) configuration. The data are best fitted by a bimolecular decay and this gives a steady

101

state lifetime $\tau_{steadystate}$ = (9.91 ± 0.28) milliseconds. This is shorter than the lifetime established for the 1.52 eV PIA feature when the sample is pumped parallel to the chain orientation.

Figure 49 shows the chop rate dependence for the (perpendicular-parallel) configuration. Again the data are best fit by a bimolecular decay function and in this case the fit yields a steady state lifetime $\tau_{steadystate}$ = (8.3 ± 1.0) milliseconds. Within the errors this value is identical to that established for the (perpendicular-perpendicular) orientation. The relatively poor fit to this data set could be due to sample degradation and/or a change in the alignment of the optics system when the chopper blade is changed at 160 Hz.

Orientation (pump-probe)	Bimolecular lifetime (ms)
Parallel-parallel	14.0 ± 0.90
Parallel-perpendicular	13.3 ± 0.40
Perpendicular-parallel	9.91 ± 0.28
Perpendicular-perpendicular	8.3 ± 1.00

Table 3. Steady state bimolecular lifetimes for polarisation components of 1.52 eV PIA peak.

From these chop rate results (summarised in Table 3), we can see that the excited state responsible for the 1.52 eV PIA feature decays bimolecularly in all orientations. This was expected from the similarity of the feature lineshapes observed in the photoinduced absorption spectra (Figure 44). The orientation of the probe beam does not significantly affect the lifetime of the feature but it is clearly longer when the electric field of the pump beam is parallel to the polymer chains.

Signal strength dependence on orientation for 1.52 eV PIA peak

It is necessary to perform fast signal strength measurements at each orientation permutation in order to accurately compare the steady state population at each combination. The effects of sample degradation during long exposures to the laser required when measuring spectra mean that the peak heights so obtained cannot be relied upon for comparison. The raw dT/T spot single wavelength signals for each

orientation are given in Table 4. The orientation listing follows the format given for Figure 44. These data were obtained using a pump power of 20 mW (0.25 mW/mm^2 at the sample) and a chop rate of 22 Hz. For each orientation 200 data samples were taken and averaged to yield the value and standard deviation errors given in the table.

It is clear from Table 4 that the probe polarisation has a strong effect on the resultant dT/T signal regardless of the pump orientation. When the probe is parallel to the polymer chains a large PIA signal is measured; when it is perpendicular to the chain a small signal is measured. This indicates that the electric dipole of the excited state lies predominantly along the chain axis, which is as expected for a localised triplet exciton.

Orientation (pump-probe)	Raw dT/T signal (x10^{-4})
Parallel-parallel	4.29 ± 0.03
Parallel-perpendicular	0.26 ± 0.04
Perpendicular-parallel	1.97 ± 0.08
Perpendicular-perpendicular	0.18 ± 0.05

Table 4. Signal strength for polarisation components of 1.52 eV PIA peak.

The observed signal dependency on the pump orientation is an extrinsic anisotropy that does not take into account the different absorption of the pump beam at different orientations. The observed signal strength is not necessarily linearly dependent on the pump beam intensity, as indicated in section 3.2 (Equation 11 and Equation 13). A monomolecular decay will have a linear dependence of signal upon pump intensity and a bimolecular decay will have square root dependence. These dependencies are seen again in the limiting cases of the polarisation dependent rate equations describing the population of photoexcited states (Equation 20 and Equation 21). These equations yield a different relationship for the steady state number of long-lived photoexcited states for the linear (monomolecular) and quadratic (bimolecular) decay regimes. The decay mechanism for the 1.52 eV PIA feature has been identified as bimolecular from the chop rate measurements for all polarisation orientations (Figure 46 to Figure 49). The intrinsic anisotropy I is extracted using Equation 21 (Equation 23). However the use of the quadratic (high photoexcitation density) dependence is an assumption and ideally the intensity dependence of the 1.52 eV signal should be measured. It would

then be possible to ensure that the laser intensity is such that the quadratic dependence is justified.
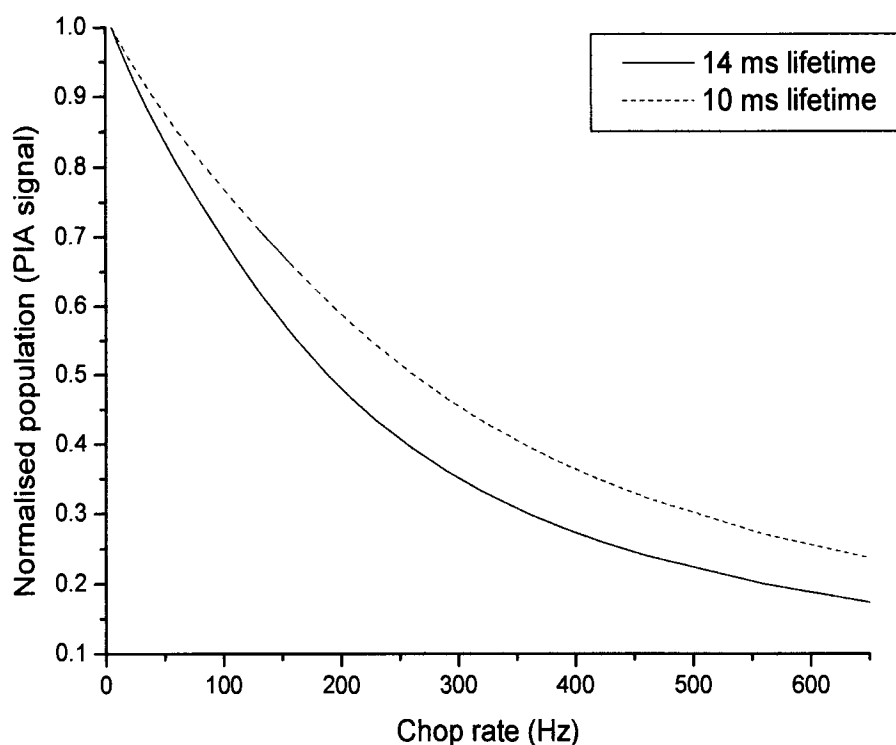
Figure 50. Steady state population verses chop rate for bimolecular decays of different lifetime.

A different lifetime has been measured for the 1.52 eV PIA peak depending on the pump orientation. This different lifetime will yield a different steady state population for the same chop rate if all other experimental parameters are held constant. This is shown in Figure 50, which is essentially a normalised plot of Equation 13 for two different lifetimes. It is necessary to correct the signal magnitudes for this lifetime-chop rate dependency before using the photoinduced signal magnitudes in a quantitative way. The equations from Comoretto[68] that calculate the intrinsic polarisation anisotropy take no account of the slightly different recombination kinetics that are observed in this case. At a chop rate of 22 Hz, taking lifetime values of 14.0 milliseconds and 9.9 milliseconds for the parallel and perpendicular pump respectively, the normalised populations are 0.931 and 0.950. This means that the parallel pump signal magnitudes need to be multiplied by 1.02 in order to be correct with respect to the perpendicular pump signals. The errors on this correction add to the total error that is given with the intrinsic anisotropy value below.

Formally, the derivation of Equation 20 and Equation 21 considers unpolarised probe light and ideally the calculation of I from Equation 23 would use signal magnitude data from an experiment with parallel and perpendicular pump excitation and unpolarised probe. However the results given in Table 4 show that the chain-perpendicular probe configuration makes a negligible contribution to the overall signal. Using the lifetime-corrected chain-parallel probe components for the parallel and perpendicular pump values yields $\left(-\Delta T_{\perp}/-\Delta T_{\parallel}\right) = 0.45 \pm 0.10$.

The argon ion laser outputs two wavelengths whilst running in the UV, at 347 nm and 360 nm. Single line UV emission is achievable from the argon ion laser using appropriate optics but this would reduce the output power too much. Sample absorbencies were therefore measured at 354 nm, the average of the two pump wavelengths. Values of 1.267 for the parallel alignment $\left(A_{\parallel}\right)$ and 0.235 for the perpendicular alignment $\left(A_{\perp}\right)$ were obtained. These values were measured from the same sample as was used for the photoinduced absorption signal strength measurements. Assuming a value of 100 nm for the sample thickness, these absorbency values yield absorption coefficients of $\alpha_{\parallel} = 2.91 \times 10^5$ cm^{-1} and $\alpha_{\perp} = 0.54 \times 10^5$ cm^{-1}.

The same sample was then used to measure the parallel and perpendicular reflectivities of the sample at the laser wavelength. The argon ion laser itself was used to perform this measurement, yielding values of $R_{\perp} = 0.243 \pm 0.05$ and $R_{\parallel} = 0.130 \pm 0.06$.

Using these values a calculation of the intrinsic anisotropy gives I = 0.34 ± 0.15. From the definition of I (Equation 23) we can deduce that $g_{\perp}/g_{\parallel} < 1$; the efficiency of generation of the photoexcited state is greater with the pump polarisation parallel rather than perpendicular to the chain. This confirms the initial assignment of the feature to a triplet exciton state with the wavefunction aligned along the chain axis.

It is possible that the intrinsic anisotropy is higher than calculated here because the perpendicular-perpendicular configuration has a shorter lifetime (10 ms) than the parallel-parallel configuration (14 ms). The shorter lifetime could suppress the photoinduced absorption signal that is detected experimentally. Note that this effect is

due to the experimental efficiency of signal detection and is a different issue to the chop rate / lifetime correction made above. A higher perpendicular-perpendicular signal will yield a higher extrinsic anisotropy fraction $(-\Delta T_{\perp} / -\Delta T_{\parallel})$ and therefore a higher value for I. However, it is not likely that the experimental efficiency of detection varies quite so strongly with this relatively minor change in lifetime.

This level of anisotropy is different to that observed for the orientation spectra shown in Figure 44 and Figure 46 to Figure 49 but those measurements were performed at different times on a different sample. The different samples could have different degrees of absorption anisotropy; that is, different degrees of chain orientation. It is also possible that the level of anisotropy observed here (or relative non-anisotropy seen in the PIA spectra) is partially due to a variation of sample quality / thickness / order across the surface of the substrate. The pump and probe beams illuminate the entire exposed surface of the sample and the post sample optics collect all the probe light that has passed through the sample. Care was taken to keep the same region of the sample in the sample holder window when rotating it. However the detector has a relatively small area and it is possible that the projection of sample image on the detector is such that not all of the probe light impinges on the active area of the detector. If this is the case, and the probe light doesn't come from the centre of the sample then rotation of the sample could bring light from more or less efficient areas of the sample onto the detector. A visual inspection of the samples under the expanded laser beam did reveal a variation in PL efficiency across its surface. The best route to avoid this kind of sample variation is to keep the sample at the same orientation and rotate the plane of polarisation of the laser beam using a wave plate as mentioned earlier. Fortunately, the relative heights of the peaks in the polarised PIA spectra in Figure 44 are still a meaningful quantity in this analysis.

Pulse radiolysis data

PFO was developed to be soluble in common organic solvents and this solubility facilitates investigation using the pulsed radiolysis technique (see section 3.4). Results from triplet and charge energy transfer are shown below.
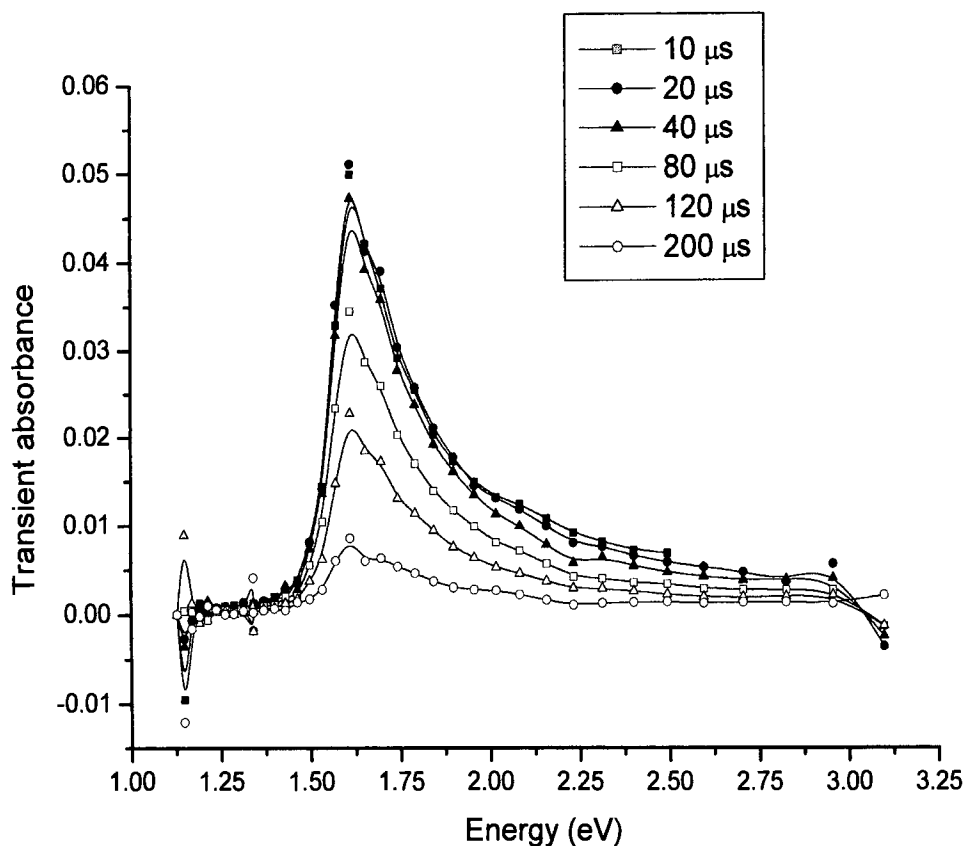
Figure 51. Pulsed radiolysis transient absorption spectrum for PFO following triplet energy transfer[86].

Figure 51 shows a pulsed radiolysis time resolved transient absorption spectrum following triplet energy transfer into a solution of PFO in benzene. A clear transient absorption is seen at 1.625 eV, with a lifetime of 30 µs. By varying the triplet donor, the S_0-T_1 energy was evaluated at 2.30 eV[44].
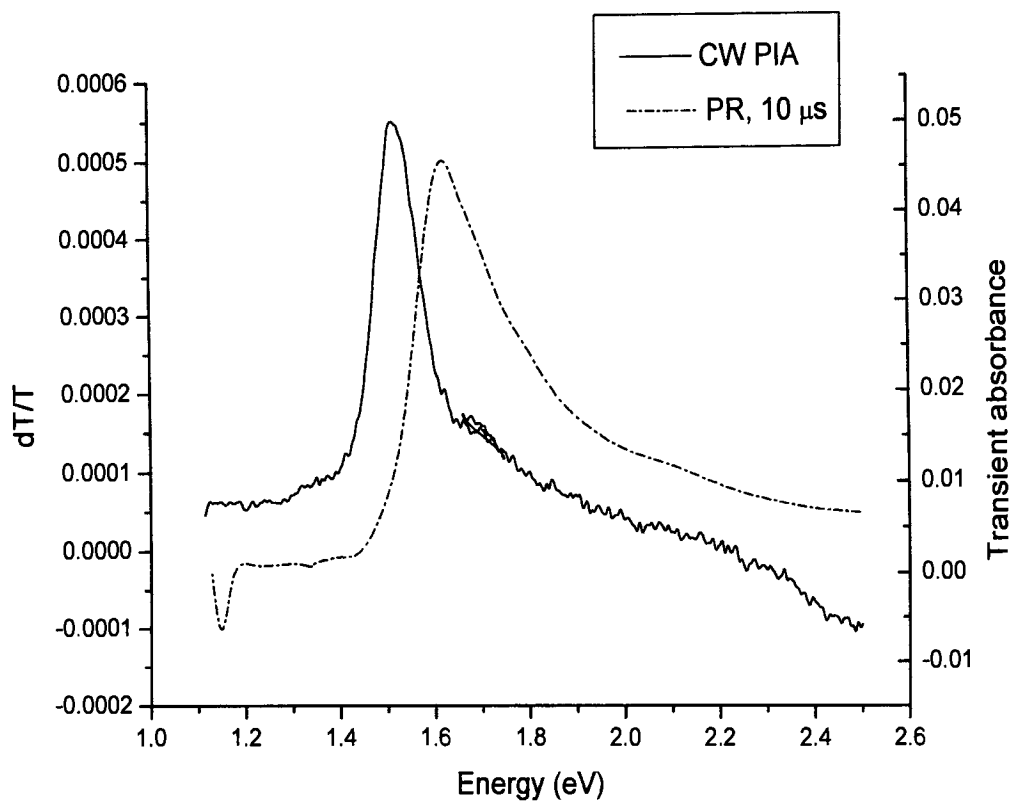
Figure 52. Plot showing photoinduced absorption data for an unaligned sample (left) with pulsed radiolysis (right).

Figure 52 shows a plot of the CW PIA from an unaligned thin film sample of PFO (Figure 40) together with the pulsed radiolysis data for triplet transient absorption 10 µs after irradiation by the electron beam. There is very good correspondence between the thin film photoinduced absorption peak at 1.52 eV and the solution state triplet transient absorption obtained through pulsed radiolysis; the peaks are separated by about 0.1 eV. This further confirms the assignment of the 1.52 eV feature to a triplet-triplet transition. The pulsed radiolysis transient also has the same asymmetric lineshape with a high energy tail; this could be a characteristic of the T_1-T_2 transition or else due to contributions from higher (T_1-T_n) transitions within the triplet manifold.

5.3. Discussion

The interpretation of the photoinduced absorption data is a lot simpler in the case of PFO than it was for PPy. The unpolarised, unoriented 90K quasi steady state PIA spectrum (Figure 40) shows a single photoinduced absorption peak at 1.52 eV. This agrees with CW photoinduced absorption data recently published by Cadby *et al*[7]. The absence of IRAV modes(more) was used in [7] to assign the feature to a transition within the manifold of a triplet exciton. This work has confirmed this assignment by performing polarised PIA analysis on oriented PFO samples together with pulsed radiolysis experiments on PFO solutions.

The spectra from oriented samples show the 1.52 eV peak is seen at all polarisation permutations. As expected there is no detectable change in the lineshape or phase of the PIA features in the normalised spectra (Figure 44), suggesting that the same basic photogeneration process is occurring under all orientations. Normalisation on the photoluminescence signal produces spectra with the magnitude of the photoinduced absorption peak enhanced in the parallel pump case. Different creation and decay kinetics combine to yield these different steady state populations, although sample degradation effects during collection of the spectra mean that signal magnitudes so obtained can be unreliable. Rapid single wavelength signal magnitude measurements were made on the 1.52 eV peak in order that an accurate comparison could be made between the orientations. These results, together with bimolecular lifetimes extracted from a best fit to the chop rate dependencies, are summarised in Table 5.

Orientation (pump-probe)	Bimolecular lifetime (ms)	Raw dT/T signal (x10^{-4})
Unoriented	17.4 ± 0.5	N/A
Parallel-parallel	14.0 ± 0.90	4.29 ± 0.03
Parallel-perpendicular	13.3 ± 0.40	0.26 ± 0.04
Perpendicular-parallel	9.91 ± 0.28	1.97 ± 0.08
Perpendicular-perpendicular	8.3 ± 1.00	0.18 ± 0.05

Table 5. Summary of PIA characterisation from 1.52 eV feature.

It can be clearly seen from the data that there is not much signal when the probe light is polarised perpendicularly to the polymer chains. This shows that the excited states are oriented along the chain; this is as expected. Considering the probe-parallel case, then, there is a clear signal enhancement for the pump-parallel case over the pump-perpendicular one. However the raw signal does not take into account the different steady state lifetimes of the parallel and perpendicular cases. More significantly, the laser absorption is much higher when the pump beam is parallel to the polymer chain, leading to an enhancement of the pump parallel signal. Following an analysis that corrects for these factors, we find a slight enhancement of the parallel generation of the excited state, with the intrinsic anisotropy, I = 0.34 ± 0.15. This confirms the triplet assignment since charged polaron states (the other long-lived candidate) should exhibit an interchain (perpendicular pump) enhancement resulting in a value of I > 1 (see Equation 22). Both the calculated value of the intrinsic anisotropy and the PL-normalised oriented PIA spectra indicate that excitation parallel to the chain produces proportionally more triplet states. The calculation of I depends on an assumption of the film thickness and that the 1.52 eV feature is in the high photoexcitation density regime. This last assumption implies that the state has a bimolecular decay profile and hence a square root dependence of the steady state population upon laser intensity. Bimolecular decay profiles are observed in the chop rate data (Figure 46 to Figure 49) but the intensity dependencies have not been measured directly. The aligned samples have a very high optical absorption anisotropy relatively little anisotropy in the triplet absorption. This implies that the triplet excitons are mobile and lose polarisation quickly.

The pulsed radiolysis data[86] clearly shows a triplet absorption transient which matches up well (Figure 52) with the photoinduced absorption peak. The asymmetric shape of the triplet transient suggests that the asymmetry of the photoinduced feature is not due to a partially buried feature: either the T_1-T_2 transition has the high energy tail or contributions from higher transitions within the triplet manifold (T_1-T_n) are responsible. Furthermore, the pulsed radiolysis data shows that absorptions due to the charged state would be submerged under the photoluminescence signal.

The 10-14 ms bimolecular decay profile of the triplet state suggests that triplet-triplet and singlet-triplet annihilation is the dominant pathway for reducing the triplet

population at the photoexcitation densities generated in these experiments. Thus the triplet radiative decay lifetime must be long, which we know is the case independently from the triplet lifetime obtained through the pulsed radiolysis experiments (30 μs) in solution. Photoinduced absorption results from Cadby *et al* show a monomolecular dependence; the discrepancy is probably due to a different steady state population being created in the two samples. Monomolecular decay routes will be more dominant at lower photoexcitation densities, where the probability of a singlet-triplet or triplet-triplet interaction is lower. It is possible that a monomolecular decay could be measured by reducing the pump intensity; a measurement of the peak signal dependence on pump intensity would help to illustrate this effect.

Triplets are highly mobile even at 77K and so they will migrate through the polymer. On-chain they are free so if two triplet excitons are present on a chain (as will increasingly be the case for higher photoexcitation regimes/large triplet populations) then they will annihilate. Therefore in 10 ms or so there is little phosphorescent decay but lots of triplet migration and non-radiative decay through TTA.

We now consider the different triplet lifetimes. The lifetime of the triplet excitons is longer for unoriented samples, but a bimolecular decay profile is still observed. This means that triplet migration must be easier in the aligned samples, allowing for more triplet exciton collisions and thus more TTA. The lifetime of the triplets is shortest with perpendicular pumping. This may be because perpendicular pumping promotes TTA as it is more likely to get more than 1 triplet per chain.

5.4. Summary

Polarised and unpolarised photoinduced absorption experiments have been performed on aligned and unaligned samples of PFO, provided by Sony. Using the photoinduced absorption data, together with pulse radiolysis data taken from the literature, the origin of the one observed photoinduced feature, at 1.52 eV in the solid state, has been unambiguously determined. The PR triplet transient, quasi steady state photoinduced absorption enhanced intrachain lifetime and generation rate clearly indicate that triplet exciton states are responsible for the peak. It is clear that TTA is the dominant mechanism for depopulating the triplet state, certainly at the higher triplet densities found in these experiments.

Chapter 6. Experimental Study of Polyaniline

6.1. Introduction

Polyaniline is one of the oldest known conjugated, organic polymers. It was first prepared in 1834 to give a black, amorphous powder known as aniline black[87]. Polyaniline is one of the conducting polymers with the greatest scope for low cost fabrication and good levels of electrical conductivity[88]. It also has high proven stability against dedoping or other mechanisms for damage[89]. Additionally the material exhibits interesting optical properties in that long-lived states are generated upon photoexcitation[8].

<u>Chemical structure</u>

Polyaniline has a greater range of possible forms than any other conjugated polymer since, in addition to supporting different oxidation states, different amounts of protonation at the nitrogen are possible[81]. At least four phases are established, as shown in Figure 53.

Polyaniline is not readily soluble in convenient solvents, though the emeraldine base form will dissolve in N-methyl pyrrolidinone (NMP), and EB thin films can be made by spinning from an NMP solution. The emeraldine base (EB) form needs to be protonated to get the conductive emeraldine salt form. The EB form is studied in this work because it has the most interesting optical properties. The conductive emeraldine phase can be processed from solution in strong acids like sulphuric acid, or can be processed from solution in meta-cresol if a sulfonic acid like camphor sulfonic acid is used to provide the counter-ion.

Leuco emeraldine
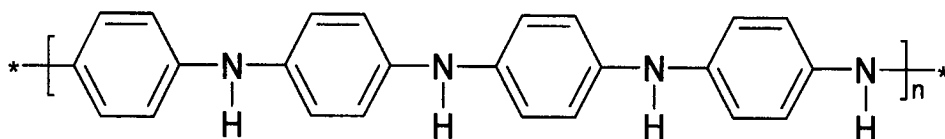
Emeraldine base
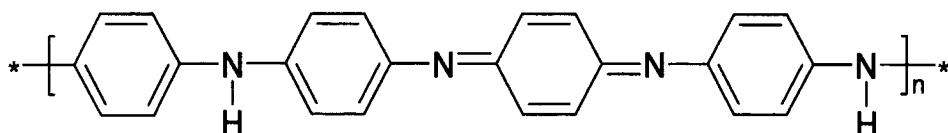
Pernigraniline
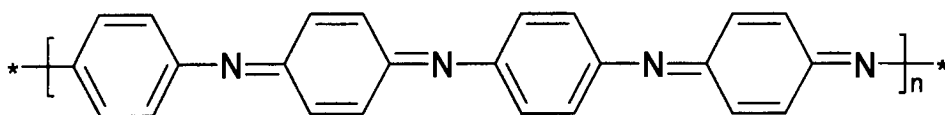
Emeraldine salt
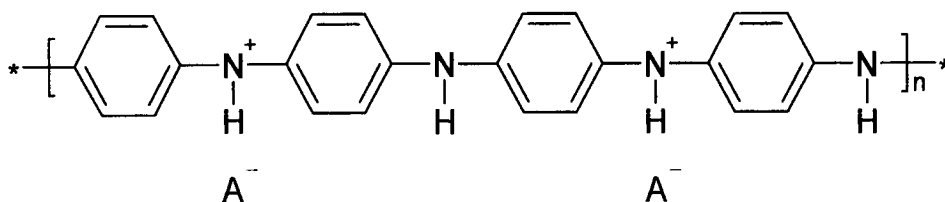
Figure 53. Chemical structures of polyaniline at different stages of oxidation and protonation. The anions A⁻ in the conducting emeraldine salt form are selected to achieve stability or processibility in solution.

The emeraldine base is considered a semi-conjugated polymer. This conjugation extends over the quinoid ring to the neighbouring two benzenoid rings through the imine nitrogen atoms. The central quinoid ring and the neighbouring nitrogen atoms are often taken together and called a quinoidimine unit. EB contains neighbouring oxidised and reduced units and this leads to the possibility of charge transfer states being generated about these structures.

Ground and Excited States

The charge carriers and the role of chain distortions are more complicated in polyaniline than for other nondegenerate ground state polymers. Generation of charge carriers causes the imine rings to change their geometry, altering the bond lengths and allowing the ring to rotate to new positions. This new rotational degree of freedom is thought to play a dominant role on the physical properties of the polymer.

An absorption spectrum[90,91] of a thin film of the emeraldine base (see Figure 54) shows absorption bands at 2.0 eV, 3.9 eV and 4.4 eV. The latter two absorptions have been attributed to excitations within the benezenoid rings [92,93]. The 2.0 eV absorption has been shown[92,97] to create self-trapped CT excitons. In this case, an electron is promoted to the LUMO of the quinoid ring from HOMO levels of the two neighbouring benzenoid rings. The quinoid ring then twists away from its ground state orientation, trapping the exciton to that site and stabilising it. This process is illustrated in Figure 55.
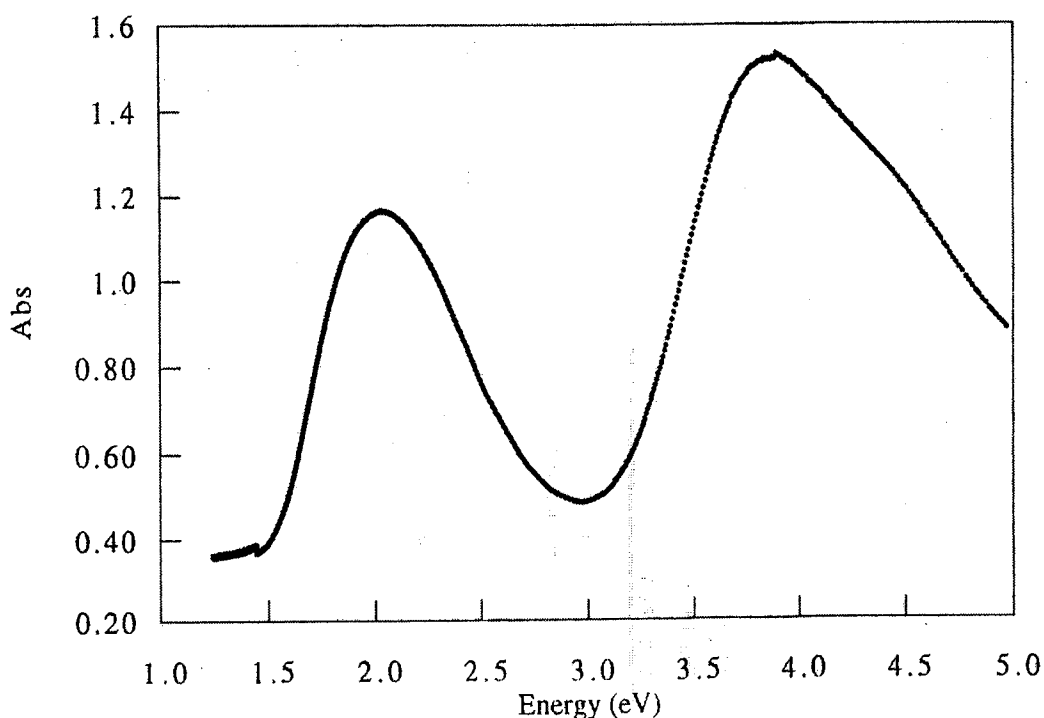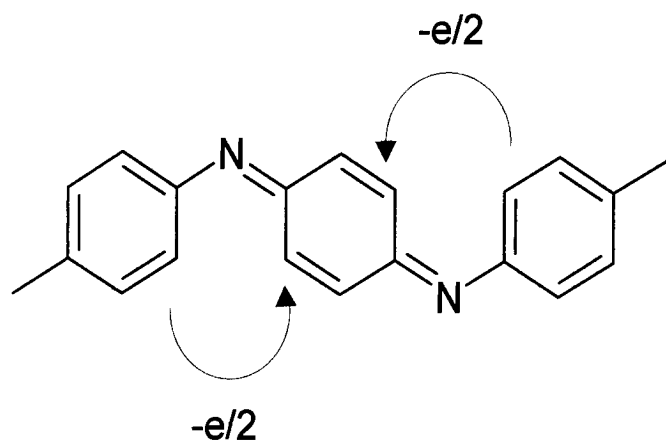

Figure 54. Absorption spectrum of EB[90].

Figure 55. Schematic of CT exciton formed upon 2 eV photoexcitation[90].

Other workers[8,89] have performed quasi steady state PIA experiments on the emeraldine base form of polyaniline and detected PIA bands at 0.9 eV, 1.5 eV and 3.1 eV. Chop rate characterisations performed by these groups reveal that the 1.5 eV and 3.1 eV features have the same chop rate (and thus origin) and that the 0.8 eV feature has a weaker chop frequency dependence and thus shorter lifetime and separate origin. Based on this data, Sariciftci et al[89] assign the 0.8 eV feature to a intrachain polaron (P^+ and P^- pair) and the two longer lived 1.4 eV / 3.1 eV features as an interchain polaron pair. However they also note that triplet excitons are observed in oligomers of aniline and emphasise that the possibility of features arising from long lived triplet excitons cannot be ruled out from their experiments.

Photoinduced absorption does not give any information on the spatial extent of generated excited states. The technique of electroabsorption[90] (EA) does give such data. In EA the absorption spectrum of a material is modulated by an applied electric field. The excited states generated can be thought of as an electric dipole that interacts with the electric field; the extent of the interaction gives the size of the dipole. For a charge transfer excitation the EA lineshape changes as the second derivative of the absorption, and there is a quadratic dependence of signal on applied field. This excitation type is observed[94] in emeraldine base upon pumping into the 2 eV band. Assuming the excited state generated to be an electron-hole pair the separation of the charges can be determined, and a value of 4 Å is obtained. This means that the state generated upon photoexcitation into the 2 eV band is extended over a distance larger than one ring, but less than two. This strong localisation implies that the CT exciton is self-trapped, as proposed by Duke[92].

6.2. Results

Thin film PIA

Experimental characterisation of EB is difficult because strong hydrogen bonding between EB chains makes the material difficult to dissolve in anything but NMP. NMP itself is not a good solvent to spin thin films from because of its low volatility (high boiling point). This results in poor quality thin films that have a low optical absorbance, leading to low photoinduced absorption signal magnitudes. However, although the signals from thin films are lower in the case of EB, the reduced absorption means that the samples last longer under the laser beam than those of other materials. This means that to some extent taking more optical samples to reduce the noise can compensate for the reduced signal level.

The quasi steady-state PIA spectrum from a thin film of emeraldine base PANi is shown in Figure 56. The data were obtained from a sample at room temperature, in air. A pump power of 120 mW was used with a beam diameter of 2mm, yielding a power density at the sample of ~ 12 mWmm^{-2}. Three clear features are shown, photoinduced absorptions at 0.8 eV and 1.4 eV, together with a strong photobleaching at around 2 eV. As can be seen, the signal magnitudes in this experiment are two orders of magnitude below the signals seen in the PFO and PPy experiments. This low signal magnitude prevented effective chop rate characterisation being obtained. In fact these experiments on EB were performed first, and it is possible that later refinements in the experimental apparatus and techniques used may have resulted in more efficient signal collection in the cases of PFO and PPy. It is difficult to be absolutely certain from the spectra, but Figure 56 suggests a phase difference between the 0.8 eV and 1.4 eV features, and thus that a different excited state is responsible for each.
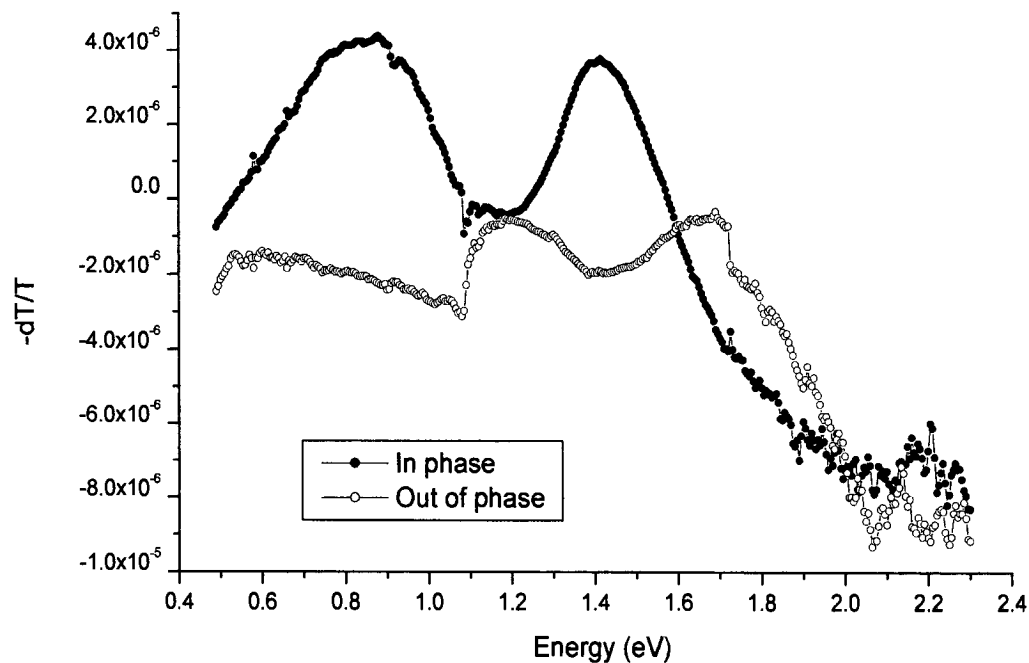
Figure 56. Quasi steady state PIA of an EB thin film in air at 300 K.

Attempts were made to extend the range of the photoinduced absorption experiment in order to access the 3.1 eV peak observed by other groups. Extension of the range requires the use of a light source with a stronger UV output to punch enough signal through the absorption bands. A Xe arc lamp was chosen for this application but the light output was too noisy. The AC noise in the probe light was orders of magnitude above the dT signal strengths observed for PANi and would have swamped any real dT signal over the range of chop rates available to the experiment.

Solution state PIA

Photoinduced absorption experiments were performed on solutions of emeraldine base in NMP in an attempt to separate out inter and intra chain effects. Unfortunately NMP (the only available solvent) has strong absorption bands in the near-IR region that prevents any data being obtained on the 0.8 eV peak in the solution state. A reduced range solution state photoinduced absorption spectrum is shown in Figure 57.

This experiment was performed on a solution of 0.05 % by weight emeraldine base in NMP. Any dissolved oxygen in the solution was removed through the use of a sealed freeze-thaw cell that incorporated a quartz cuvette for spectroscopic analysis. The

removal of oxygen from the solution does two things. Firstly it prevents the oxidation of emeraldine base to pernigraniline (a conversion that is fortunately accompanied by a clearly noticeable colour transition of the deep blue of emeraldine base to the purple of pernigraniline). Secondly it eliminates possible triplet quenching.
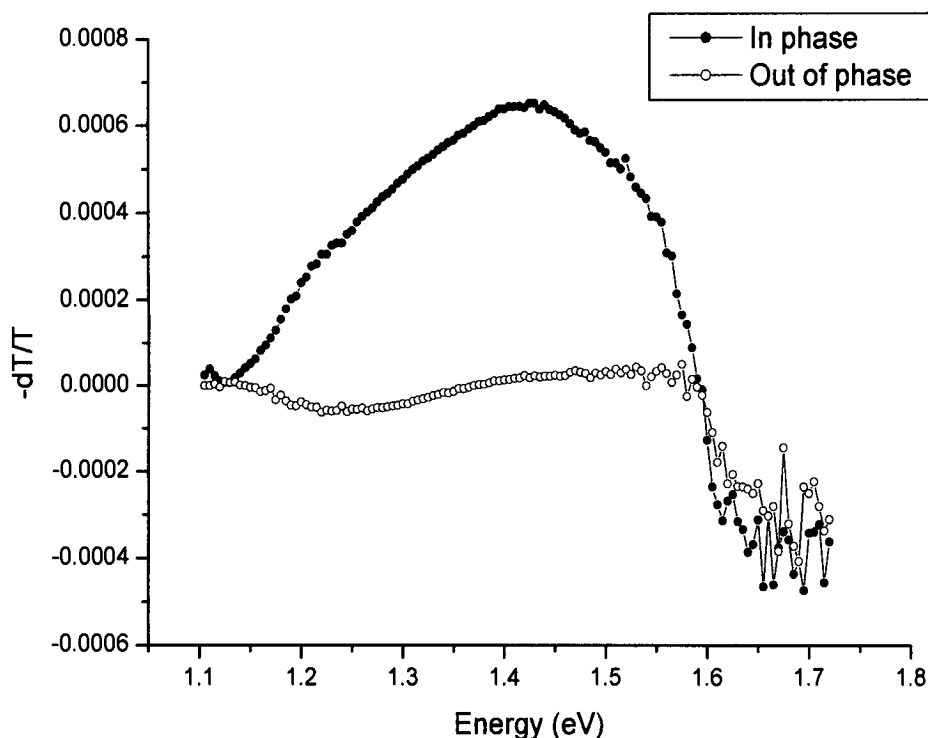
Figure 57. Quasi steady state photoinduced absorption spectrum of an EB solution at room temperature.

Two features are clearly visible in Figure 57, a photoinduced absorption feature and a photobleaching signal. Thus the solid state and solution state experiments reveal identical results within the experimental range accessible to the solution state experiment. The fact that the 1.45 eV signal is seen in the solution indicates that it is due to an intra-chain species as the distance between chains in solution should be enough to eliminate inter-chain interactions. To verify the intra-chain nature of the feature, measurements were made of the 1.45 eV peak strength for various concentrations of solution. These data are plotted in Figure 58. The plot shows a linear relationship between photoinduced absorption peak strength and solution concentration. At these concentration levels, there is a linear relationship between solution concentration and optical absorbance. Thus Figure 58 confirms that the species responsible for the 1.45 eV absorption is intra-chain in nature.
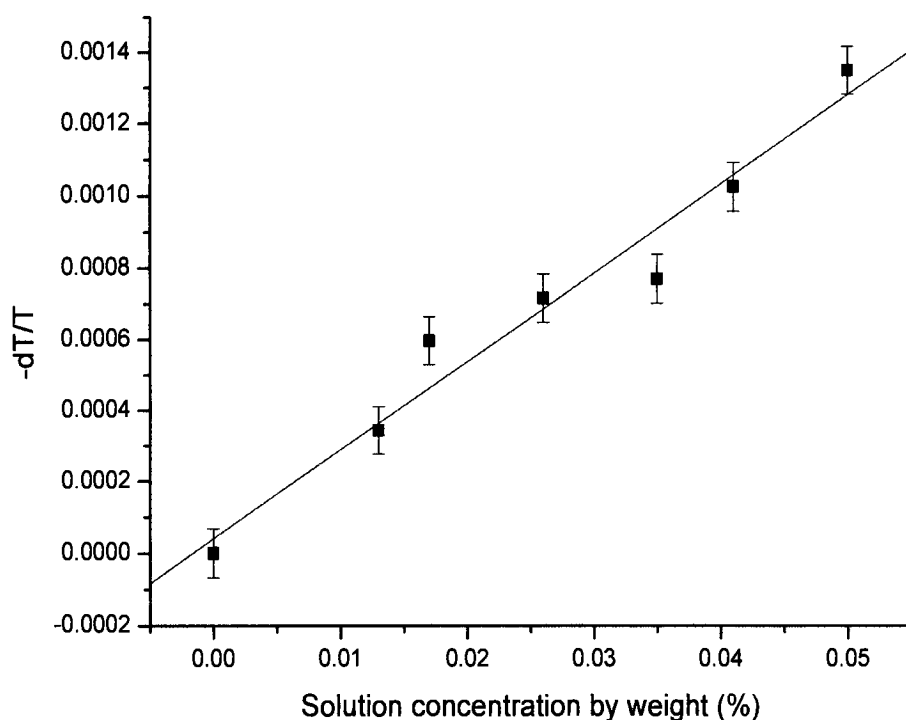
Figure 58. Concentration dependence of 1.45 eV photoinduced absorption feature

Pulse radiolysis

The standard pulse radiolysis experiments (see section 3.4) were applied to emeraldine base at the Paterson Institute for Cancer Free Radical Research Facility in Manchester UK. Both triplet and charged state energy donors were used, with varying success. The negative charged state energy transfer experiment is shown in Figure 59. Three features are visible on the plot, two transient absorptions at 1.57 eV and 3.11 eV and a photobleaching at 2.16 eV. Figure 60 shows the normalised signal as a function of time for both transient absorption features. It appears that both the 1.57 eV and 3.11 eV features have the same decay kinetics, although a proper fast time-resolved pulse radiolysis experiment would help confirm this.
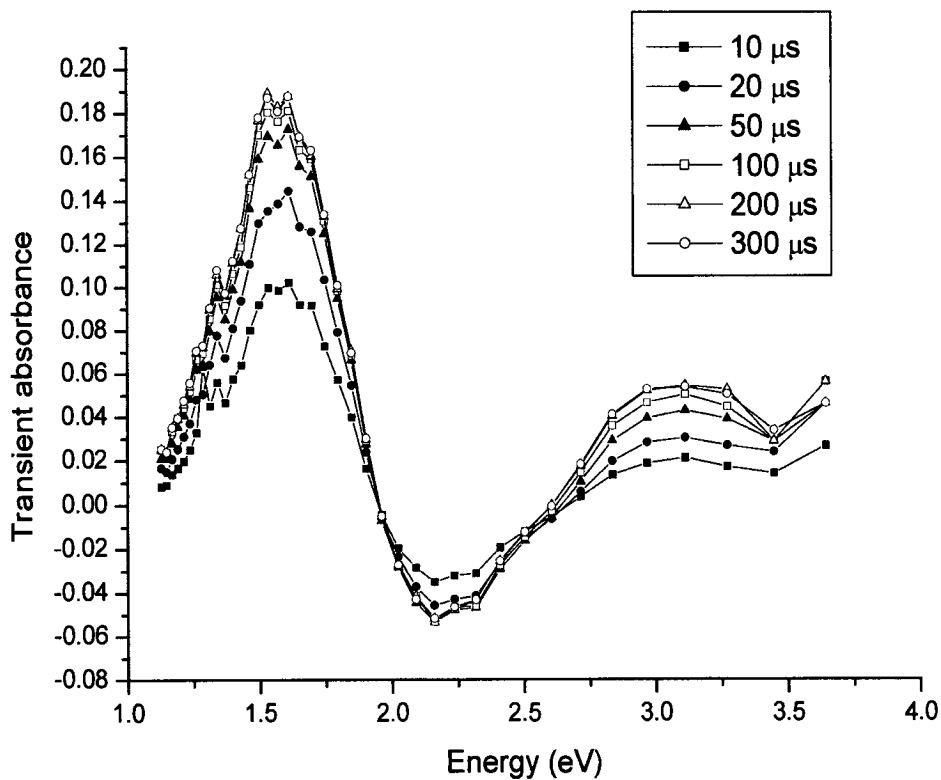
Figure 59. Pulse radiolysis showing introduction of charged states to EB.
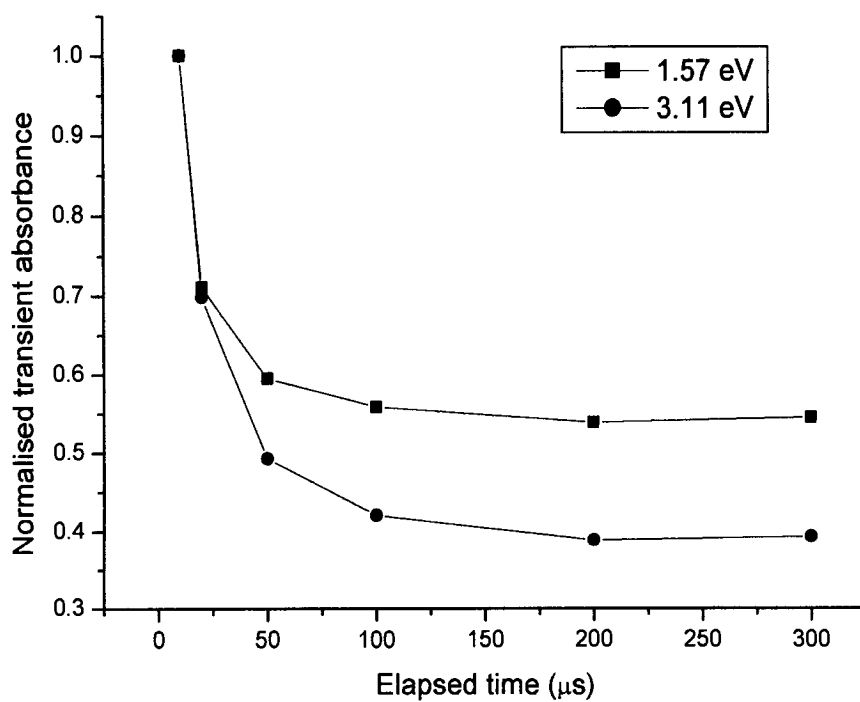
Figure 60. Time dependence of normalised signal at 1.57 eV and 3.11 eV.
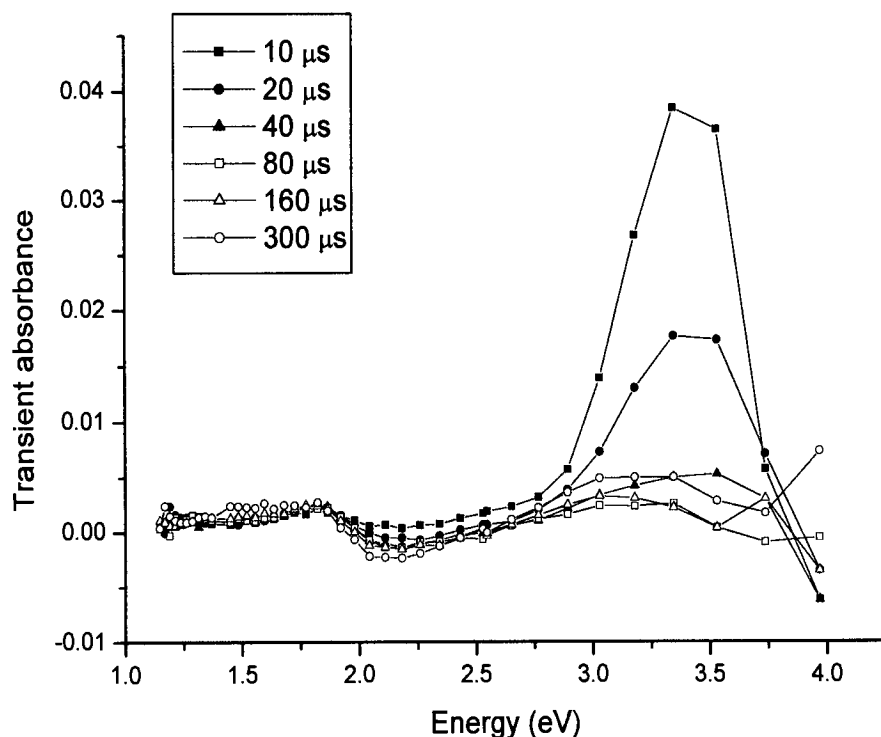
Figure 61. Pulse radiolysis showing triplet energy transfer.

Figure 61 shows the transient absorption following triplet energy transfer. The feature at 3.4 eV is due to the benzene donor excited state. This feature quickly dies away to reveal a residual, low-level signal. This signal is very similar to that for the charged state transfer (Figure 59), although it is much lower in intensity. It is clear that no large polymer triplet signal is available over the experimental range. However the residual triplet signal seen was not quenched by oxygen. From this it was determined that the T_1 energy must be less than 0.9 eV[44].

6.3. Discussion

Two photoinduced absorption features are seen following photoexcitation of a solid state sample (Figure 56). From the phase difference seen in Figure 56 and from the different chop rate dependences measured by other groups, it is clear that these two photoinduced absorption features arise from different excited state species. This section will identify these species.

<u>1.4 eV PIA feature</u>

The 1.4 eV feature is seen both in the thin film (Figure 56) and solution state (Figure 57) photoinduced absorption experiments. There is also a linear relationship between the signal strength at 1.4 eV in solution and the solution concentration. This means that the excited state responsible for this feature is intra-chain in nature, which rules out the classic polaron (separated charge state) mechanism suggested by Sacriciftci *et al* that requires photoexcited charge pairs to be separated across adjacent polymer chains in order to generate a quasi stable excitation in polymers with a non-degenerate ground state like emeraldine base.

Turning now to the results from pulse radiolysis, there is excellent agreement between the transient absorption following negative charge state energy transfer (Figure 59) and the 1.4 eV photoinduced absorption; indeed, the 3.1 eV transient absorption is also in agreement with the extended range emeraldine base photoinduced absorption spectra reported by other groups. Both these features have similar decay kinetics. Applying the principle of conservation of oscillator strength to Figure 59, would suggest that the 1.4 eV and 3.1 eV photoinduced features are in fact one broad photoinduced band with a narrow bleaching effect at around 2 eV superimposed on the top. Thus it seems clear from the pulse radiolysis results that the excited state is somehow charged in nature, even if we know from the photoinduced absorption results that the state is intra-chain. Since the recovery of the photobleaching is slower than the decay of the 1.4 eV and 3.1 eV induced peaks, we know there must be a band below the experimental limit of 1 eV.

This all fits well with the electroabsorption results[90], which show that a charge-transfer exciton is formed following photoexcitation. This species is a stable intra-chain excitation in emeraldine base because, unlike the two other polymers studied in this research, it has adjacent oxidised (quinoid) and reduced (benzenoid) units. Thus the photoexcited electron is promoted to a quinoid ring from the two neighbouring benzenoid rings. The charge then stays localised at the quinoid ring due to a self-trapping mechanism whereby the quinoid unit twists out of the plane of the polymer, decoupling itself from the rest of the chain[94]. This is also consistent with the adding of charge to the polymer, as in the pulse radiolysis experiment.

0.8 eV PIA feature

The low energy feature seen in the solid state photoinduced absorption experiments is outside the energy range of the pulse radiolysis experiment and of the solution state PIA. From other solid state PIA experiments[8,89] it is known that the feature has a shorter lifetime and therefore different origin to the 1.4 eV feature. From the triplet energy transfer experiments we know that the S^0-T^1 energy separation is < 0.9 eV. It is reasonable to assume that a transition within the triplet manifold (T^1-T^n) would be lower in energy, and this feature is therefore assigned to such a transition within a long-lived triplet state.

6.4. Summary

Photoinduced absorption experiments were performed on solid state and solution state samples of the emeraldine base form of polyaniline. In the solid state peaks are observed at 0.8 eV and 1.5 eV, in line with previously reported results. The solution state experiment shows a peak at 1.5 eV that disproves the previous assignment of this feature to an inter-chain polaron pair. Furthermore this conclusion is consistent with data obtained from electroabsorption and pulse radiolysis. The origin of the 0.8 eV peak is less ambiguously resolved because of the lack of solution state and pulse radiolysis data in the IR spectral region. However from the results obtained on other materials, and due to the established S^0 to T^1 energy separation of 0.9 eV, it seems reasonable to assign the 0.8 eV band to a transition within the manifold of a long lived triplet exciton.

Further work to be performed on the long-lived photophysics of this material should focus on the origin of the 0.8 eV peak. Through the use of solid state solutions or alkyl substituted polyaniline it may be possible to perform quasi steady state PIA experiments on polymer chains that are in isolation.

Chapter 7. Conclusions

The thesis has reported quasi stead state photoinduced absorption measurements from three materials: polypyridine (PPy), polyfluorene (PFO) and the emeraldine base (EB) form of polyaniline.

To this end, a dedicated photoinduced absorption spectrometer was developed, and new control and analysis software written. Modifications were required to the apparatus and data collection methodology in order to collect data from these different samples as each sample provided slightly different challenges. Polarisation data was collected from aligned samples of PFO. The data collection speed had to be increased for PPy due to its rapid photodegradation. The emeraldine base samples were fortunately resistant to the laser beam but the PIA signal strengths were weak, which required the apparatus to achieve a signal resolution of 5×10^{-7}. In addition, solution state experiments were conducted on EB.

Once the experimental apparatus has been optimised for each particular material and good data obtained, there is still a question as to how the data are to be interpreted. Quasi steady state photoinduced absorption yields information on the long-lived descendents of the initial singlet exciton population, and it is the nature of these states that has to be determined. Reference was made to published results obtained using the technique of pulse radiolysis. Together the photoinduced absorption and pulse radiolysis techniques allow the nature of the photoexcited states to be assigned with a high degree of confidence.

The polarisation dependency of the photoinduced absorption results in PFO was used to assign the PIA to triplet excitons, based on the interchain enhancement of the state generation efficiency. In PPy the temperature and oxygen dependence of the emission and photoinduced absorption spectra was used to determine the triplet and charged state features. In both cases the assignment of the excited states is completely consistent with the complementary data from the pulse radiolysis experiments. For the EB work the use of results from electroabsorption studies and pulse radiolysis were required to completely explain the observed photoinduced absorption features. Additionally the ability of pulse radiolysis to determine the S_0-T_1 energy is of particular importance in assigning phosphorescent signals (in the case of PPy) and in

128

providing an energy value below which all triplet-triplet photoinduced absorption signals must lie. This was used explicitly in order to identify the triplet-triplet absorption within EB, but the PPy and PFO triplet-triplet assignments are also consistent with this rule.

Photoinduced absorption features and assignments are given in Table 6.

Material	PIA band peaks (eV)	Assignment
PPy	2.29	Triplet exciton
	1.5	Polaron
	0.8	Polaron
PFO	1.52	Triplet exciton
	1.7	Triplet exciton
EB	1.4	Self-trapped CT exciton
	0.8	Triplet exciton

Table 6. Summary of results

Chapter 8. Appendix A

Instrument control software

A custom Windows NT application was designed and written in order to collect and analyse the quasi steady-state data presented in this thesis. The application interface is based around the windows multi-document interface (MDI) architecture, similar to that found in Microsoft Word 97. Each document in the application was a data record, corresponding to photoinduced absorption spectral data over a particular range, plotted into its in phase and out of phase components. The main application window is shown in Figure 62, and shows visible range scans for PFO.
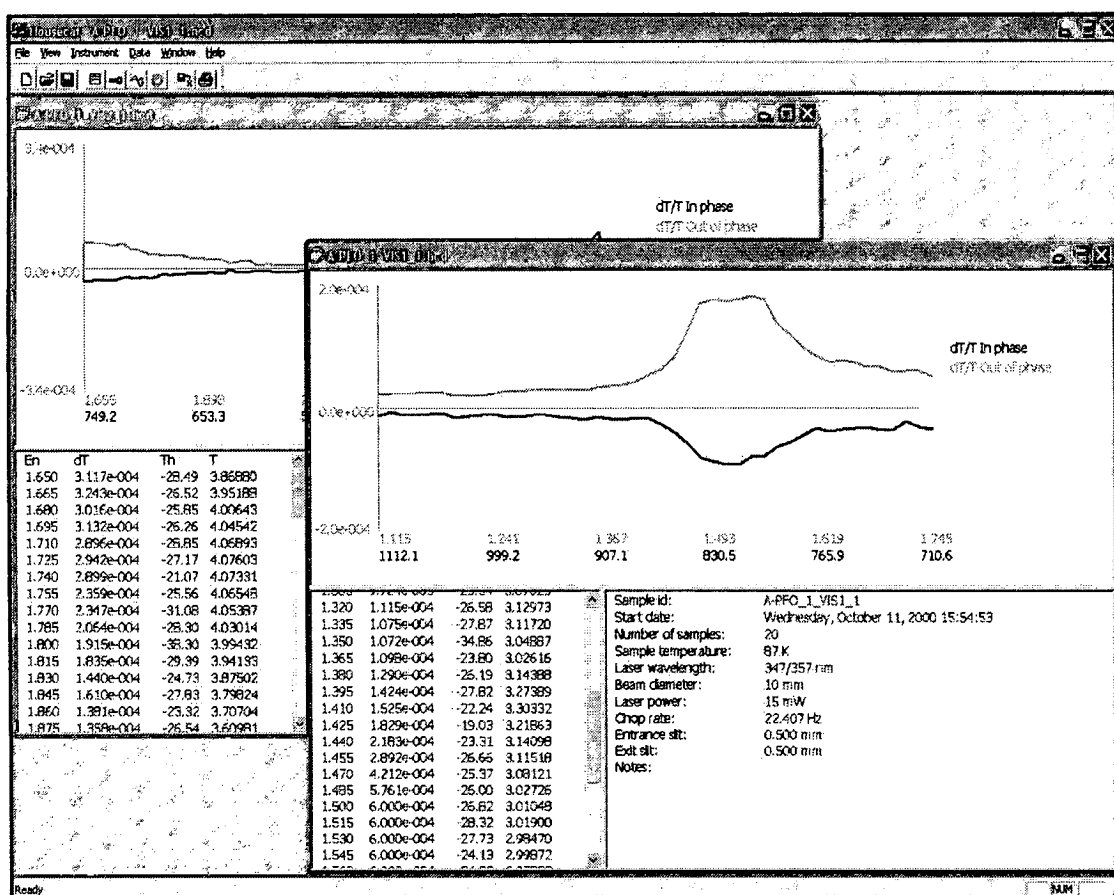
En	dT	Th	T
1.650	3.117e-004	-28.49	3.86880
1.665	3.243e-004	-26.52	3.95188
1.680	3.016e-004	-25.85	4.00643
1.695	3.132e-004	-26.26	4.04542
1.710	2.896e-004	-26.85	4.06893
1.725	2.942e-004	-27.17	4.07603
1.740	2.899e-004	-21.07	4.07331
1.755	2.359e-004	-25.56	4.06548
1.770	2.347e-004	-31.08	4.05387
1.785	2.054e-004	-28.30	4.03014
1.800	1.915e-004	-36.30	3.99432
1.815	1.835e-004	-29.39	3.94193
1.830	1.440e-004	-24.73	3.87502
1.845	1.610e-004	-27.83	3.79824
1.860	1.391e-004	-23.32	3.70704
1.875	1.358e-004	-26.54	3.60981

1.320	1.115e-004	-26.58	3.12573
1.335	1.075e-004	-27.87	3.11720
1.350	1.072e-004	-34.86	3.04887
1.365	1.098e-004	-23.80	3.02616
1.380	1.290e-004	-26.19	3.14388
1.395	1.424e-004	-27.82	3.27389
1.410	1.525e-004	-22.24	3.30332
1.425	1.829e-004	-19.03	3.21863
1.440	2.183e-004	-23.31	3.14098
1.455	2.892e-004	-26.66	3.11518
1.470	4.212e-004	-25.37	3.08121
1.485	5.761e-004	-25.00	3.02726
1.500	6.000e-004	-26.62	3.01048
1.515	6.000e-004	-28.32	3.01900
1.530	6.000e-004	-27.73	2.98470
1.545	6.000e-004	-24.13	2.99872

Sample id: A-PFO_1_VIS1_1
Start date: Wednesday, October 11, 2000 15:54:53
Number of samples: 20
Sample temperature: 87 K
Laser wavelength: 347/357 nm
Beam diameter: 10 mm
Laser power: 15 mW
Chop rate: 22.407 Hz
Entrance slit: 0.500 mm
Exit slit: 0.500 mm
Notes:

Figure 62. Application main window showing two open documents comprising quasi-cw PIA data from PFO

An individual data record is show in more detail as Figure 63. The top region of the record shows the in phase and out of phase components of the PIA data. Optionally the DC (T) level can also be plotted. It's often important to monitor the strength of the DC level to avoid detector saturation. The bottom left region of the record shows the

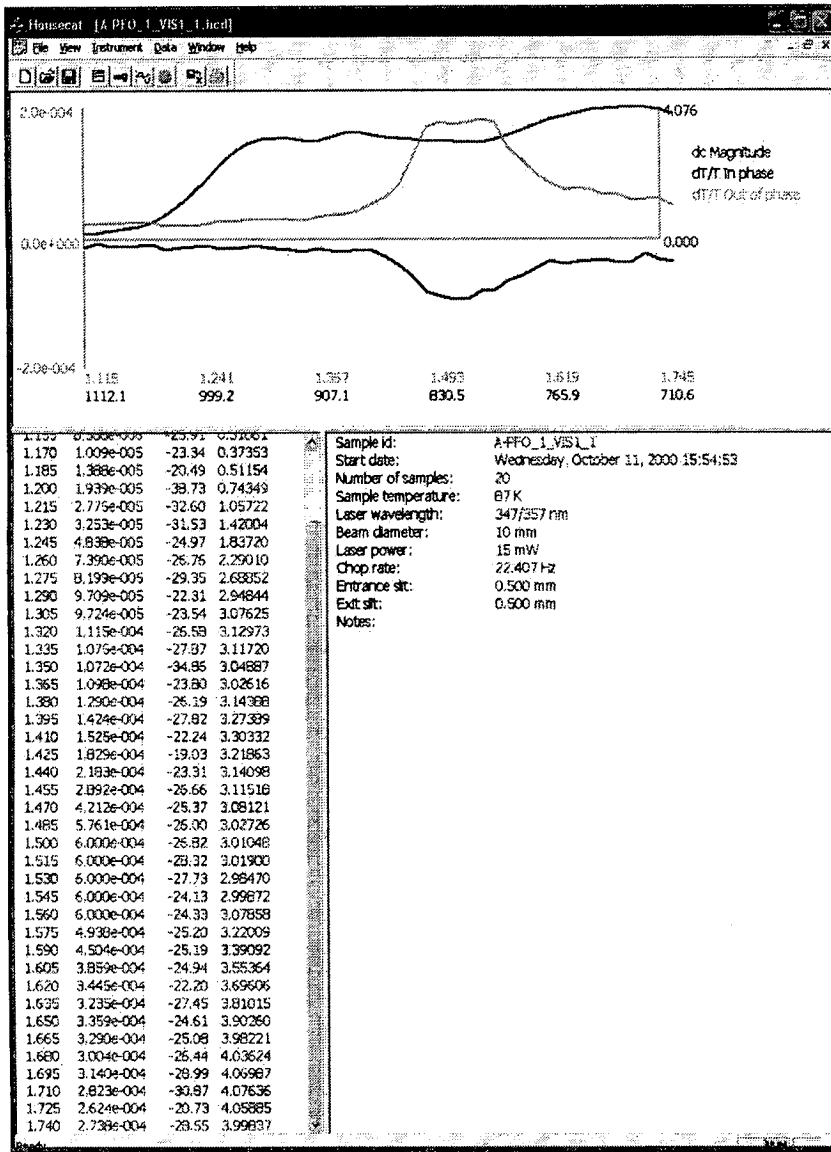actual data points measured, and the bottom right region shows information on the experimental conditions.

Figure 63. An individual data record

The main window also contains controls that activate new dialogs from which the instrument can be configured (Figure 64), manually directed to a certain wavelength in order to collect spot measurements (Figure 65), and set-up and execute scans (Figure 66, Figure 67).
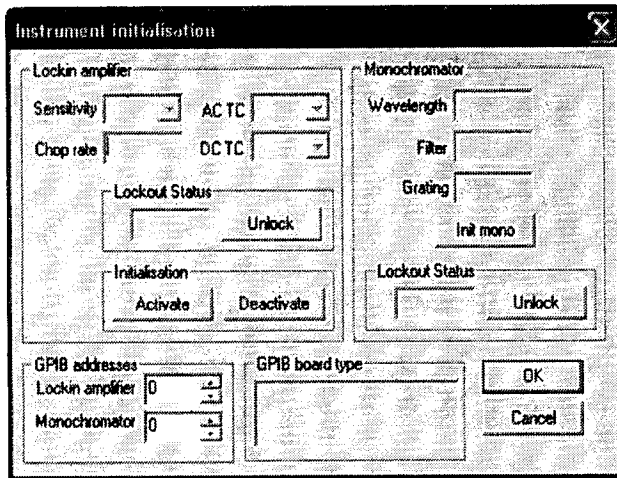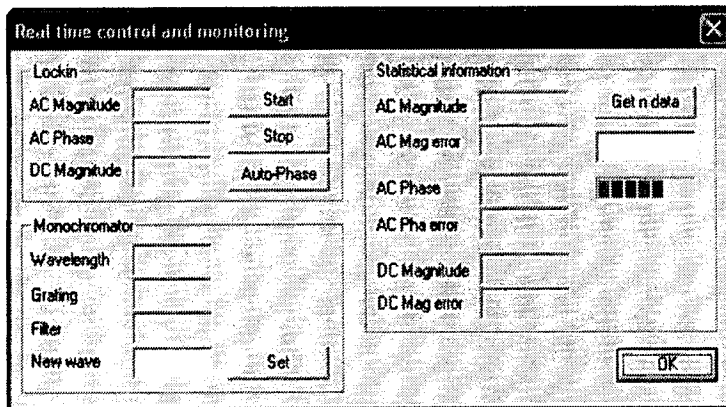
Figure 64. Instrument initialisation.
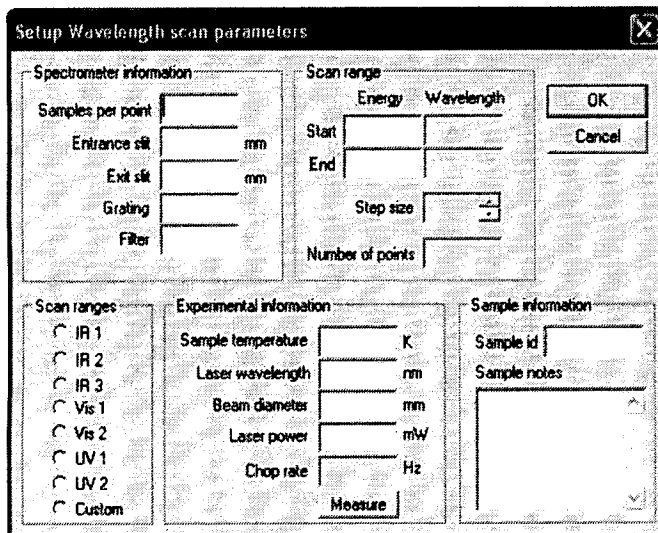

Figure 65. Real time control and monitoring.
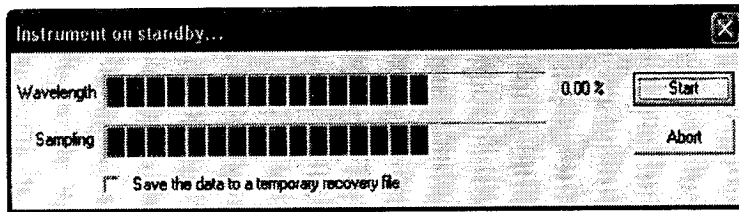

Figure 66. Scan setup.

Figure 67. Scan execution.

Chapter 9. References

135

References

1   L. de Bernieres, *The War of Don Emmanuel's Nether Parts,* Minerva (1991)

2   J. H. Burroughes *et al, Nature,* **347,** 539 (1990)

3   R. J. Visser, *Phillips Journal of Research,* **51,** 463 (1998)

4   R. H. Friend *et al, Nature,* **397,** 121 (1999)

5   R. H. Friend *et al, Physics World,* **12,** 35 (1999)

6   V. Dyakonov, *Chem. Phys.,* **227,** 203 (1998)

7   A. J. Cadby *et al, Synth. Met.,* **111,** 515 (2000)

8   M.G. Roe *et al, Phys. Rev. Let.,* **60,** 2789 (1988)

9   T. W. G Solomons, *Organic Chemistry,* 5th Ed; John Wiley and Sons, Inc

10   P. W. Atkins, *Molecular Quantum Mechanics,* Oxford University Press (1983)

11   C. H. J. Wells, *Introduction to Molecular Chemistry,* Chapman and Hall (1978)

12   E. F. H. Brittain *et al, Introduction to Molecular Spectroscopy; theory and experiment,* Academic Press (1970)

13   S. C. J. Meskers *et al, Chem. Phys. Lett.,* **339** 223 (2001)

14   Y. V. Romanovskii, *Physical Review Letters,* **84,** 1027 (2000)

15   C Rothe *et al, J. Chem. Phys.* **115,** 9557 (2001)

16   W. P. Su *et al, Phys. Rev. Lett,* **42** 1698 (1979)

17   W. P Su *et al, Phys. Rev. B,* **22,** 2099 (1980)

18   W. P Su and J. R. Schrieffer, *Proc. Natl. Acad. Sci. USA,* **77,** 5626 (1980)

19   J. Orenstein, *Handbook of Conducting Polymers,* T A. Skotheim, Editor. Marcel Decker (1986)

20   N. F. Colarneri *et al, Phys. Rev. B,* **38,** 3960, (1988)

21   H. Bassler *et al, Synth. Met.,* **49** 341 (1992)

22   B. Schweitzer, H. Bassler, *Synth. Met.,* **109,** 1 (2000)

23   W. P Su, *Handbook of Conducting Polymers,* T A. Skotheim, Editor. Marcel Decker (1986)

24   U. Rauscher *et al, Phys. Rev. B,* **42,** 9830 (1990)

25   S. Barth and H. Bassler, *Phys. Rev. Lett,* **79,** 4445 (1997)

26   S. A. Bagnich and A. V. Konash, *Chem. Phys.,* **263,** 101 (2001)

27   M. Pope, C.E Swenberg, *Electronic Processes in Organic Crystals and Polymers,* 2nd Ed; Oxford Science Publications (2000)

28	C. M. Hertel *et al*, *Synth. Met.* **116**, 139-143 (2001)
29	S. F. Alvarado *et al*, *Appl. Phys. Lett*, **77**, 904 (2000)
30	C. M. Heller *et al*, *Phys. Rev. B.*, **54**, 5516 (1996)
31	C. H. Lee *et al*, *Phys. Rev. B.*, **49**, 2396 (1994)
32	J. M. Leng *et al*, *Phys. Rev. Lett.*, **72**, 156 (1994)
33	P. G. Dacosta and E. M. Conwell, *Phys. Rev. B.*, **48**, 1993 (1993)
34	J. W. van der Horst *et al*, *J. Chem. Phys.*, **114**, 6950 (2001)
35	B. Schweitzer *et al*, *Chem. Phys. Lett.*, **313**, 57 (1999)
36	S. Barth *et al*, *Chem. Phys. Lett*, **774**, 165 (1997)
37	R. Chance *et al*, *Handbook of Conducting Polymers*, T A. Skotheim, Editor. Marcel Decker (1986)
38	S. Dailey, *A Study of Conjugated Polymers and their Applications in Light Emitting Diodes*. PhD thesis, University Of Durham (1998)
39	E. M. Conwell and M. W. Wu, *Appl. Phys. Lett.*, **70**, 1867 (1997)
40	M. Wohlgenannt *et al*, *Nature*, **409**, 494 (2001)
41	T. M. Hong and H. F. Meng, *Phys. Rev. B.* **6307**, 5206 (2001)
42	A. P Monkman *et al*, *Chem. Phys Lett*, **307**, 303 (1999)
43	L. P. Candeias *et al*, *J. Phys. Chem. B* **104**, 8366 (2000)
44	A. P Monkman and H. D. Burrows, *Light Emitting Polymers*, Sheats and Shinar Editors. J. Wiley Series on Polymer Science, to be published.
45	D. A. dos Santos *et al*, *Chem. Phys.*, **227**, 1 (1998)
46	M. A. Baldo *et al*, *Nature*, **403**, 750 (2000)
47	T. Virgili *et al*, *Synth. Met*, **111**, 203 (2000)
48	Th. Forster, *Discusss. Faraday Soc.* **27**, 7 (1959)
49	D.L. Dexter, *J. Chem. Phys* **21**, 836, (1953)
50	J. B. Birks, *Phys. Let.* **24A**, 479 (1967)
51	A. P. Monkman *et al*, *Chem. Phys. Lett.* **340**, 467 (2001)
52	P O'Connor and J. Tauc, *Phys. Rev. B*, **25**, 2748 (1982)
53	D. Comoretto *et al*, *Phys. Rev. B*, **53**, 15653 (1996)
54	D Comoretto *et al*, *Phys Rev B*, **56**, 10264 (1997)
55	G Dellepiane *et al*, *Phys. Rev. B*, **48** 7850 (1993)
56	W. H. Press *et al*, *Numerical Recipes in C*, 2nd *Ed*, Cambridge University Press (1996)
57	OriginLab Corporation

58	M. Wormington *et al, Phil. Trans. R. Soc. Lond. A* **357** 2827 (1999)
57	A. P. Monkman *et al, Synth. Met.,* **116**, 75 (2001)
60	J. H. Baxendale and M. Fiti, *J. Chem. Soc Faraday Trans.2* **68**, 218 (1972)
61	R. Cooper and J. K. Thomas, *J. Chem. Phys* **48**, 5097 (1968)
62	J. K. Thomas, *Ann. Rev. Phys. Chem.* **21**, 17 (1970)
63	E. J. Land, *Proc. Roy. Soc.* **A305**, 457 (1968)
64	R Bensasson and E. J. Land, *Trans. Faraday Soc.* **67**, 1904 (1971)
65	A. P. Monkman *et al, Proc. SPIE* **3797**, 109 (1999)
66	R. H. Friend *et al, J. Phys. D: Appl. Phys.,* **20**, 1367 (1987)
67	T. Yamamoto *et al, J. Am. Chem. Soc.* **116** 4832 (1994)
68	J. W. Blatchford *et al, Phys. Rev. Lett.,* **76** 1513 (1996)
69	A. J. Epstein *et al, Macromol. Symp.,* **116**, 27 (1997)
70	M. Halim *et al, Synth. Met.* **84** 951 (1997)
71	A. P. Monkman *et al, Proc. SPIE* **3148**, 82 (1997)
72	D. D. Gebler *et al, Poly. Mat. Sci. and Eng.,* **73**, 473 (1995)
73	Y. Z. Wang *et al., Proc. SPIE,* **2528**, 54 (1995)
74	M. A. El-Sayed, *J. Chem. Phys.,* **38**, 2834 (1963)
75	H. D. Burrows *et al, J. Chem. Phys.,* **112**, 3082 (2000)
76	R. B. Fletcher *et al, Synth. Met.,* **111**, 151 (2000)
77	M. Grell *et al, Adv. Mater.,* **9**, 798 (1997)
78	K. S. Whitehead *et al, Synth. Met.,* **111**, 181 (2000)
79	M. Grell *et al, Adv. Mater.,* **11**, 671 (1999)
80	P. D. Townsend and R. H. Friend, *Synth. Met.,* **17**, 361 (1987)
81	J. W. P Hsu *et al, Phys. Rev. B.,* **49**, 712 (1994)
82	J. Orenstein *et al, Phys. Rev. B,* **30**, 786 (1984)
83	D. Comoretto *et al, Phys. Rev. B.,* **46**, 10041 (1992)
84	D. Marsitzky and K. Mullen, *Advances in Synthetic Metals: Twenty Years of Progress in Science and Technology,* P. Bernier *et al* Editors. Elsevier. (1999)
85	D. D. C. Bradley *et al, Proc. SPIE,* 3145 (1997)
86	A. P. Monkman *et al, Phys. Rev. Lett.,* **86**, 1358 (2001)
87	E. M. Genies *et al, Synth. Met.,* **36** 139 (1990)
88	S. J. Pomfret *et al, Polymer,* **41**, 2265 (2000)

| 89 | N. S. Sariciftci *et al*, *J. Chem. Phys.*, **98**, 2664 (1993) |

90   S. J. Pomfret, *Electroabsorption Measurements of Conjugated Organic Materials*, PhD thesis, University of Durham (1995)

91   A. P. Monkman *et al*, *Synth. Met.* **14** 87 (1991)

92   C.B Duke, *et al*, *Chem Phys Lett.*, **131**, 82 (1986)

93   Y. Cao *et al*, *Synth. Met.*, **29** E285 (1989)

94   S. J. Pomfret *et al*, *Synth. Met.*, **76** 19 (1996)